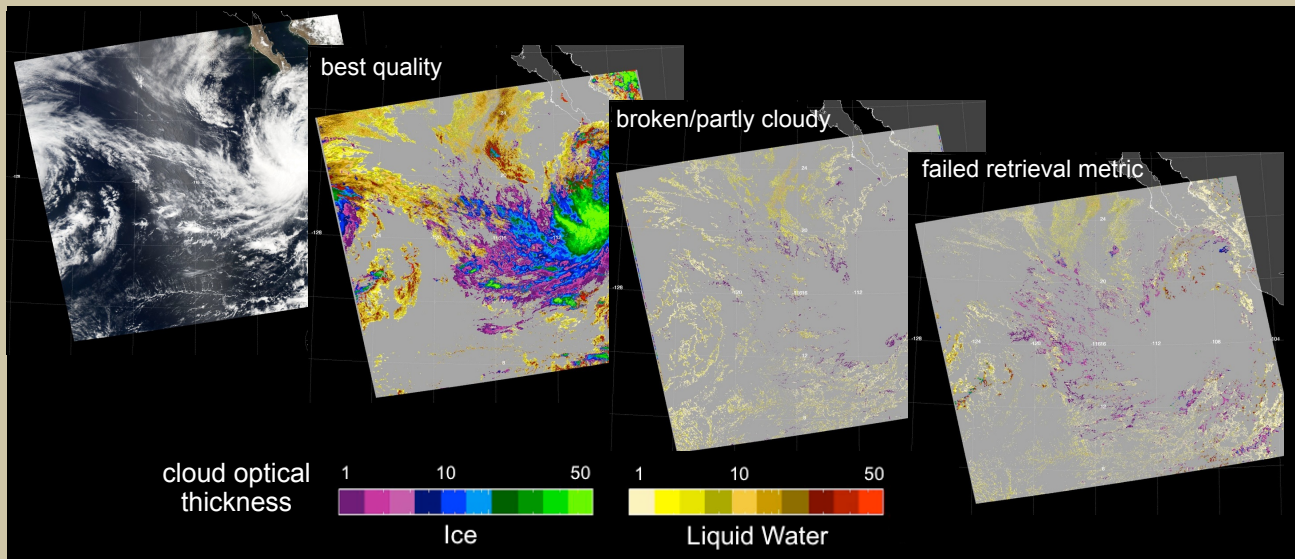


MODIS Cloud Optical Properties: User Guide for the Collection 6 Level-2 MOD06/MYD06 Product and Associated Level-3 Datasets



Version 0.9 (beta)
17 September 2014

STEVEN PLATNICK¹, MICHAEL D. KING², KERRY G. MEYER^{3,1}, GALA WIND^{4,1},
NANDANA AMARASINGHE^{4,1}, BENJAMIN MARCHANT^{3,1}, G. THOMAS ARNOLD^{4,1},
ZHIBO ZHANG⁵, PAUL A. HUBANKS^{6,1}, BILL RIDGWAY^{4,1}, JEROME RIEDI⁷

¹ Earth Sciences Division, NASA Goddard Space Flight Center, Greenbelt, MD

² Laboratory for Atmospheric and Space Physics, University of Colorado, Boulder, CO

³ Science Systems and Applications, Inc., Lanham, MD

⁴ Universities Space Research Association (USRA), Columbia, MD

⁵ University of Maryland Baltimore County, Baltimore, MD

⁶ ADNET Systems, Inc., Lanham, MD

⁷ Laboratoire d'Optique Atmosphérique, Université des Sciences et Technologies de Lille/CNRS, Villeneuve d'Ascq, France

TABLE OF CONTENTS

1. Introduction.....	1
1.1. The MODIS Cloud Product.....	3
1.1.1. <i>Cloud-top properties overview</i>	3
1.1.2. <i>Cloud optical and microphysical properties overview</i>	4
1.2. Theoretical Basis of Cloud Optical Retrievals	6
1.2.1. <i>Theoretical basis of primary cloud optical properties algorithm</i>	6
1.2.2. <i>Theoretical basis of 1.6 and 2.1 μm cloud optical properties algorithm</i>	7
2. Level-2 Collection 6 Changes	9
2.1. New Ice Cloud Models.....	11
2.2. Wind-speed Interpolated Ocean Bidirectional Reflectance Properties.....	15
2.3. New Gap-filled Spectral Surface Albedo Dataset	19
2.4. Improved Shortwave-Derived Cloud Thermodynamic Phase	21
2.4.1. <i>Phase retrieval algorithm overview</i>	22
2.4.2. <i>C6 changes</i>	22
2.4.2. <i>Phase algorithm evaluation</i>	24
2.4.3. <i>Known issues</i>	26
2.5. Separate Cloud Effective Radius Retrievals at 1.6, 2.1, and 3.7 μm	29
2.6. Retrieval Failure Metrics (RFM)	34
2.7. Improved Pixel-level Uncertainties	40
2.8. Clear Sky Restoral and Processing of Pixels Flagged as Partly Cloudy.....	46
2.9. New Cloud Radiative Transfer Look-up Tables (LUTs)	57
2.10. Miscellaneous Changes	65
2.10.1. <i>Multilayer cloud detection updates</i>	65
2.10.2. <i>Cloud model single scattering properties vs. CER</i>	68
2.10.3. <i>Ancillary data sources</i>	68
2.10.4. <i>Increased vertical resolution of NCEP temperature and moisture profiles</i>	70
2.10.5. <i>Improved spatial interpolation of surface temperature</i>	70
2.10.6. <i>Spatially and temporally interpolated column ozone from GDAS</i>	70
2.10.7. <i>Adjust low cloud top temperature retrievals for non-unity emissivity</i>	70
2.10.8. <i>Improved surface albedo at 3.7 μm</i>	71
2.10.9. <i>Other 3.7μm updates: above-cloud emission and solar irradiance</i>	71

2.10.10. <i>Maximum retrievable cloud optical thickness extended to 150</i>	72
2.10.11. <i>Use of new 1km cloud-top property retrievals</i>	72
2.10.12. <i>Statistics_1km and Statistics_1km_sds</i>	73
3. Level-3 Cloud Optical/Microphysical Dataset Overview	74
4. MODIS-Atmosphere Team Web Site and Browse Imagery	77
5. MOD06 Optical Properties Data: Frequently Asked Questions	78
6. References	80
Appendix A. Scientific Data Sets (SDSs) in the L2 Cloud Product File	85
Appendix B. Summary SDS and Quality Assurance (QA) Assignments	87
Appendix C. Key Acronyms	93
Appendix D. Cloud Model LUT Scattering Properties	95
Appendix E. Cloud Retrieval Phase Flow chart	101
Appendix F. Cloud Optical/Microphysical Level-3 Statistics	106
Appendix G. Summary of High-Level MOD06 Collection 6 Efforts	111

1. Introduction

One of the primary atmospheric products produced from the MODIS sensor on the Terra and Aqua satellites is the cloud product. This product (Earth Science Data Set names **MOD06** and **MYD06** for Terra and Aqua MODIS, respectively) contains pixel-level retrievals of cloud-top properties (pressure, temperature, and height—both day and night), and cloud optical properties (optical thickness, effective particle radius, and water path for both liquid water and ice cloud thermodynamic phases—daytime only). For conciseness, we will typically abbreviate cloud optical thickness, effective radius, and water path as **COT**, **CER**, and **CWP**, respectively. Unless otherwise noted, further mention of MOD06 also includes the Aqua MODIS products as the algorithms are mostly identical.

The original pre-launch cloud optical retrieval algorithm was described in an Algorithm Theoretical Basis Document (**ATBD**), c.f. modis-atmos.gsfc.nasa.gov/reference_atbd.html. While this was useful for communicating algorithm details to the retrieval community and providing a mechanism for community review, the ATBD has been superseded by NASA ROSES solicitation reviews, publications, and our focus on web-delivered “user guides”.

This document describes the physical basis and algorithm updates for the optical property datasets, focusing on changes in the Collection 6 (**C6**) version vs. Collection 5 (**C5**), the structure and content of the MODIS cloud product (including the science data sets, metadata, and quality assurance), and frequently asked questions. The document is intended as an essential resource for all users of the C6 MODIS cloud optical products. While the emphasis is on the cloud optical properties component, overall MOD06 cloud product information will be provided when relevant.

The “Level” terminology is used to denote broad categories of NASA data products: Level 0 (**L0**) denotes raw spectral channel counts, Level 1B (**L1B**) denotes calibrated and geolocated reflectances and/or radiances, Level 2 (**L2**) denotes orbital-swath science (geophysical) products, and finally Level 3 (**L3**) denotes gridded spatial/temporal aggregations of the L2 products.

The MODIS cloud product is a L2 product, and is archived in version 4 of a self-described Hierarchical Data Format (**HDF4**) file based upon the platform (Terra or Aqua) and temporal period of collection (every 5 minutes along the orbit track). One 5 min file, or **data granule**, contains data from roughly 2330 km cross-track (1354 1 km pixels) to 2000 km along-track of Earth located data. Thus, a data granule is comprised of approximately 2.7M 1 km pixels. The Terra overpass time at the equator is around 1030 local solar time in its descending (daytime) mode and 2230 local solar time in its ascending (nighttime) mode. The Aqua overpass time is around 1330 local solar time in ascending (daytime) mode and 0130 local solar time in descending (nighttime) mode.

Each L2 cloud parameter is retrieved at a spatial resolution determined by the sensitivity of the retrieval, not necessarily on a native single field of view (**FOV**) basis for the MODIS

spectral band used in the retrieval. Resolutions of L2 cloud products are at 1×1 km (nadir) for all cloud optical properties, and either 5×5 km or 1×1 km (new in C6) for cloud-top properties.

MODIS Level-2 HDF product files have standardized filenames, described below.

Terra MODIS: **MOD06_L2.AYYYYDDD.HHMM.VVV.YYYYDDDHMMSS.hdf**

Aqua MODIS: **MYD06_L2.AYYYYDDD.HHMM.VVV.YYYYDDDHMMSS.hdf**

The definition of the highlighted text is as follows:

MOD06 = Earth Science Data Type name

L2 = Denotes a Level-2 product

A = indicates following date/time information is for the acquisition (observation)

YYYYDDD = acquisition year and day-of-year

HHMM = acquisition hour and minute start time

VVV = collection (e.g., '006' for Collection 6)

YYYYDDDHMMSS = production data and time

hdf = denotes HDF file format

Note that: (a) all times are UTC times, not local, and (b) the MOD prefix represents a L2 Terra platform file. Aqua platform files (data granules) have the prefix MYD.

MODIS (re)processing streams are referred to as data “Collections”. An increment in the Collection number (or version) denotes comprehensive changes (additions and/or updates) to the science algorithms. Collection 5 was completed in calendar year 2006 (and a reprocessing to C5.1 was completed in calendar year 2010). Atmosphere Team C6 Aqua L2 reprocessing began in December 2013 and was completed in early May 2014 (4 July 2002 through 31 December 2013); Aqua forward processing began on January 1, 2014. Atmosphere Team L3 and Terra (re)processing is expected to begin in early summer 2014.

Details on the changes implemented in each Collection are available in the “products” section of the MODIS-Atmosphere web site (modis-atmos.gsfc.nasa.gov). Occasionally significant updates are implemented in the middle of a Collection. This is only done when an operational algorithm software bug is discovered that seriously impacts one or more of the **Scientific Data Sets (SDSs)** contained within a L2 (or L3) file. Scientists working with MODIS data should always be aware of updates applied to the operational software (especially those applied in the middle of a collection) by visiting the ‘Known Problems’ page (modis-atmos.gsfc.nasa.gov/products_knownproblems.html) in the “products” section of the MODIS-Atmosphere web site, or by checking the Data Processing Calendar (modis-atmos.gsfc.nasa.gov/products_calendar.html).

In addition to the separate suite of MODIS Atmosphere Team data product files (cloud, aerosol, clear sky profiles, and precipitable water products), the team provides a L2 Joint Atmosphere Team Product (**MODATML2/MYDATML2**) for users interested in selected atmosphere parameters, e.g., for climate studies, trend analysis, aggregation sensitivity studies, or correlative studies requiring more than one atmosphere L2 file. MODATML2 is generated by subsetting key science parameters from each atmosphere product and combining them into a single L2 file with a resolution of 10 km (aerosol) or 5 km (profiles, cloud-top properties, subsampled native 1 km cloud datasets). The sampling of 1 km fields is consistent with the Atmosphere Team L3 sampling approach (filename **MOD08/MYD08**), ensuring that MODATML2 can serve as a basis for research-level aggregation efforts in a manner that is fully consistent with the pixels used in the existing MOD08 product. The relatively small ATML2 file size (depending on cloud fraction) is more practical for downloading large time periods and has a significant number of users. Format and content information for the C6 ATML2 product are at modis-atmos.gsfc.nasa.gov/docs/ATML2_C6_SDS.pdf.

All team products are distributed by the NASA GSFC Land and Atmospheres Archive and Distribution System (**LAADS**, ladsweb.nascom.nasa.gov/data/) and are available via search interface or direct ftp download. Production is done by the MODIS Adaptive Processing System (**MODAPS**), also located at GSFC.

1.1. The MODIS Cloud Product

MODIS on Terra and Aqua provides unique spectral and spatial capability for retrieving cloud optical properties. Relative to previous generation global imagers (e.g., AVHRR), MODIS has a number of additional spectral channels, including 1.6 and 2.1 μm window channels that, in addition to an AVHRR heritage 3.7 μm channel, provide cloud microphysical information. CO₂-slicing bands (13 μm spectral region) and the related cloud-top algorithm have heritage with the HIRS instrument [e.g., *Wyle and Menzel*, 1999]. Native spatial resolution is at 250 m (0.66 and 0.86 μm channels), 500 m (five channels including 3 shortwave-infrared), and 1 km (all others).

1.1.1. Cloud-top properties overview

The cloud top properties (cloud top pressure, temperature, and effective cloud amount) are produced for the cloudy portion of the 5×5 pixel arrays wherein the cloud pixels (identified by the probably cloudy and cloudy bits of the cloud mask) are averaged to reduce noise. The MODIS science team utilizes an extended suite of bands, in particular bands in the CO₂ absorption region from 13.3 to 14.2 μm . These so-called CO₂-slicing bands have a long history of use in identifying cloud top pressure for high clouds due to the opacity of CO₂, a uniformly mixed (but temporally changing) gas in the Earth's atmosphere [*Chahine*, 1974; *King et al.*, 1992]. They are, however, less capable of determining cloud top pressure (or altitude) for low

boundary-layer clouds. In MODIS, the CO₂-slicing bands are supplemented with an infrared window band at 11 μm for optically thicker and lower-level clouds.

C6 improvements in the cloud top properties algorithm and changes in the product datasets have been described in the updated ATBD (modis-atmos.gsfc.nasa.gov/docs/MOD06_ATB-D_2013_03_06.pdf) and Baum *et al.* [2012], and include: (i) improved knowledge of the spectral response function of the thermal infrared bands, based largely on comparison with corresponding hyperspectral measurements from the collocated AIRS (Atmosphere Infrared Sounder) observations on Aqua, (ii) restrictions to the CO₂-slicing method based on the infrared phase retrieval information, (iii) introduction of surface emissivity maps, (iv) introducing a latitude dependent 11 μm brightness temperature lapse rate over the ocean, (v) improvements to the thermal infrared-derived thermodynamic phase, and (vi) introduction of cloud top properties using 1 km spatial resolution.

1.1.2. Cloud optical and microphysical properties overview

Multispectral reflectances are used to simultaneously retrieve cloud optical thickness (**COT**), effective radius (**CER**), and derived cloud water path (**CWP**) globally during the daytime for liquid and ice phases. The optical/microphysical algorithm makes primary use of six visible (**VIS**), near-infrared (**NIR**), shortwave-infrared (**SWIR**) and midwave-infrared (**MWIR**) MODIS bands, as well as several thermal bands. In addition to the 1 km MODIS Level-1B data, the optical property algorithm requires as input: the MODIS cloud mask (**MOD35**), the cloud-top pressure portion of MOD06 [Ackerman *et al.*, 2008; Holz *et al.*, 2008], and a variety of ancillary datasets including gap-filled MODIS land and snow/ice surface spectral albedos, snow/ice data (Near-real-time Ice and Snow Extent, NISE), and forecast analysis fields (NCEP GDAS).

Cloud optical properties (COT, CER, and integrated CWP of both liquid water and ice clouds) are produced for pixels identified as probably cloudy or cloudy by the cloud mask during the daytime portions of each orbit. The basic physical principle behind the simultaneous retrieval of COT and CER is the bispectral solar reflectance method first described by Nakajima and King [1990] and applied to airborne data. MOD06-specific heritage work also includes Platnick and Twomey [1994] and Platnick and Valero [1995] (microphysical retrievals using the AVHRR 3.7 μm channel), Platnick *et al.* [2001] (retrievals over snow/ice surfaces), and thermodynamic phase retrievals [King *et al.*, 2004]. Basic algorithm details are described in the C5 Algorithm Theoretical Basis Document (ATBD) addendum ([link](#)) and original ATBD [King *et al.*, 1997]. An overview of the MODIS cloud product algorithms (at the time of Collection 4) along with example results is provided in Platnick *et al.* [2003] and King *et al.* [2003]. Collection 5 algorithm-related publications include ice models [Baum *et al.*, 2005; Yang *et al.*, 2007], multilayer detection [Wind *et al.*, 2010; Joiner *et al.*, 2010], Clear Sky Restoral filtering [Zhang and Platnick, 2011; Pincus *et al.*, 2012], pixel-level uncertainties [Platnick *et al.*, 2004], and L3 statistics [King *et al.*, 2013]. Evaluation-specific publications include phase [King *et al.*, 2010; Riedi *et al.*, 2010], view angle biases [Liang *et*

al., 2009; Maddux *et al.*, 2010], and the impacts of non-plane-parallel clouds [Zhang *et al.*, 2010; Zhang and Platnick, 2011; Zhang *et al.*, 2012].

The more significant updates for the C5 processing stream [Platnick *et al.*, 2003; King *et al.*, 2003] included: (i) new ice crystal size/habit distribution models and the corresponding ice reflectance library calculations [Baum *et al.*, 2005], (ii) a clear sky restoral algorithm that attempts to identify pixels that are poor retrieval candidates due to sunglint, edges of clouds, heavy dust or smoke contamination, or spatially variable (partly cloudy) pixels, in which case these ‘cloudy’ pixels are *restored* to clear sky and no cloud optical property retrievals are attempted, (iii) improved snow-free surface albedo maps [Moody *et al.*, 2005, 2008], and (iv) spectral sea ice and snow-covered land surface albedo characteristics by ecosystem [Moody *et al.*, 2007].

Major C6 improvements in the cloud optical properties algorithm include (i) improving the ice cloud optical properties, based in part on comparison with CALIOP as well as thermal IR retrievals of COT, (ii) improved surface albedo maps, (iii) enhancements of the shortwave-derived cloud thermodynamic phase, (iv) incorporation of wind-speed interpolated bidirectional reflectance properties over the ocean, especially important for optically thin clouds, (v) separate CER retrievals at 1.6, 2.1, and 3.7 μm , (vi) improvements to pixel-level retrieval uncertainty calculations, and (vii) new cloud radiative transfer code and lookup table (**LUT**) approaches.

C6 cloud optical property algorithm changes have been extensive. The code is numerically intensive, depending on explicit forward radiative calculations for cloud, gases and surface interactions. The Collection 6 L2 MODIS Cloud Product contains nearly **X?** statistical SDSs. Uncertainties for each retrieved L2 pixel are provided for many non-3-D error sources and include error correlations across the retrieval spectral channels. Estimates of uncertainty in aggregated means are also provided in the joint atmosphere team L3 product. **Quality Assessment (QA)** information now includes separate retrievals of pixels unlikely to meet plane-parallel model assumptions, multiple effective particle radii derived from various spectral channel combinations whose differences are symptomatic of forward model failures, sub-pixel spatial heterogeneity, and additional multilayer/phase detection tests. New ancillary datasets have been incorporated. Recent ice particle radiative transfer calculations [Yang *et al.*, 2013] enabled studies of habit and surface roughness sensitivity across the MODIS spectral and particle size domain, leading to new ice models that provide closure with infrared (**IR**) and next-version Cloud-Aerosol Lidar with Orthogonal Polarization (**CALIOP**) retrievals. The lines of core science code have doubled since C5. Processing requirements are viable only because MODAPS technical capabilities have increased in tandem.

C6 updates are representative of evolving passive imager cloud retrieval science as spectral information from MODIS and other capable sensors is explored. For example, A-Train studies have provided important constraints on ice particle radiative models [Holz *et al.*, 2014]. The climate modeling community continues to improve its ability to exploit the product, e.g., MODIS CFMIP COSP simulator [Pincus *et al.*, 2012] and NASA Working Group for

Observations for Modeling Intercomparison Studies (obs4MIPs). Cloud assessment reports (e.g., GEWEX, *Stubenrauch et al.* [2013]; VIIRS/MODIS, *Platnick et al.* [2013]) acknowledge the challenges in establishing cloud climate data records.

1.2. Theoretical Basis of Cloud Optical Retrievals

1.2.1. Theoretical basis of primary cloud optical properties algorithm

The simultaneous retrieval of cloud optical thickness and effective radius is best achieved by simultaneously measuring the reflection function in a non-absorbing and absorbing spectral channel (e.g., VIS/NIR and SWIR, respectively), and comparing the resulting measurements with theoretical forward model calculations, as demonstrated with airborne data by *Nakajima and King* [1990] (also see historical papers on airborne/spaceborne observations and retrievals by *Twomey and Cocks* [1982, 1987], *Curran and Wu* [1982], *Rawlins and Foot* [1990], *Nakajima et al.* [1991], *Han et al.* [1994], *Platnick and Twomey* [1994], *Platnick and Valero* [1995], *Minnis et al.* [1997]). The technique is especially accurate over dark ocean surfaces because the reflection function of the earth–atmosphere system arises primarily from light scattering by the cloud layer, with little influence from the underlying surface. In comparing measurements with theory, however, it is essential that the light-scattering properties of the cloud are modeled realistically, and that the cloud is properly ascribed to either a liquid water or ice cloud with corresponding optical properties. For applications of this technique to global observations, involving clouds over snow and sea ice surfaces, or various land surfaces, it is further necessary to estimate realistic values of the underlying surface reflectance in the appropriate channels.

Figure 1.2-1 illustrates the underlying principle behind the simultaneous retrieval of COT and CER from reflected solar radiation measurements for (a) liquid water clouds and (b) ice clouds, shown here for clouds over snow and sea ice surfaces. The minimum values of the reflection function at 1.24 and 2.13 μm correspond to the reflection functions of the underlying surface at those wavelengths in the absence of an atmosphere. The dashed curves represent reflection function contours for fixed COT, and the solid curved contours are for fixed CER. Over snow and sea ice surfaces, as shown here, the reflection function of liquid water clouds at 1.24 μm decreases as COT increases from 0 to about 2, where it begins to increase; over land and ocean surfaces where 0.87 μm is used instead, the reflection function is small and this would not be the case. The data points superimposed on the theoretical curves of Fig. 1.2-1 correspond to Aqua MODIS observations over Greenland, acquired at the observational solar and viewing directions specified in the figures on July 28 (1345 UTC) and 29 (1250 UTC) 2008 for ice and liquid water clouds, respectively.

Other channel pairs can be used to retrieve COT and CER. While the primary or standard channel pair uses the 2.13 μm channel for microphysical information, the 1.62 μm and 3.7 μm MODIS channels can also be used as described in Sect. 2. The next subsection describes an

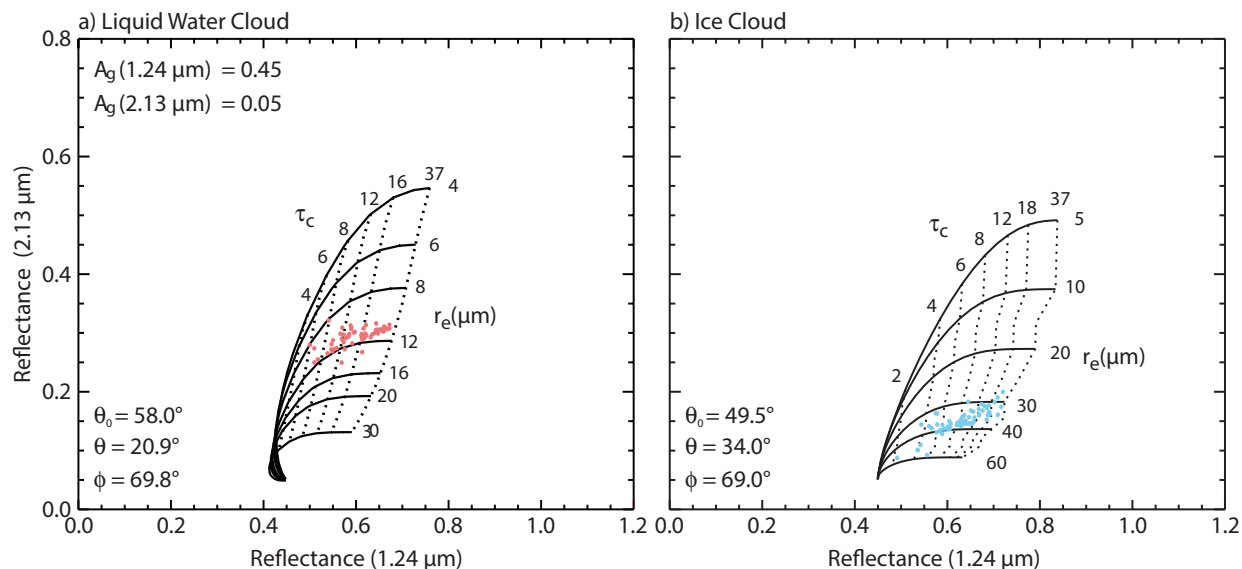


Figure 1.2-1. Theoretical relationship between the reflection function at 1.24 μm and 2.13 μm for (a) liquid water and (b) ice clouds for various values of COT (dashed lines) and CER (solid lines) for specified values of surface albedo and solar/view geometry. Data from measurements above arctic liquid water and ice clouds are superimposed on the figure.

alternate retrieval using two SWIR channels to minimize errors over snow and ice surfaces that was first implemented in C5 processing.

1.2.2. Theoretical basis of 1.6 and 2.1 μm cloud optical properties algorithm

Due to the relatively high surface albedo at 0.87 μm or 1.2 μm (used in standard retrievals) over snow and sea ice surfaces, *Platnick et al.* [2001] proposed an alternative method for simultaneously retrieving COT and CER from reflectance measurements. This method takes advantage of the fact that the surface albedo of snow and sea ice is quite low at 1.62 μm (cf. *Moody et al.* [2007]). **Figure 1.2-2** illustrates the theoretical relationship and corresponding data points of the simultaneous retrieval of COT and CER using measurements at 1.62 and 2.13 μm , where it is assumed that the surface albedo of sea ice is 0.03 at both wavelengths. Although the solution space loses the near-orthogonality of the COT and CER retrievals using standard channel pairs, and therefore is more sensitive to calibration uncertainties in the measurements, the sensitivity to COT is generally better than the standard method because of decreased uncertainty in the value of the surface albedo. This technique is noticeably more robust for liquid water clouds (Fig. 1.2-2a) than for ice clouds, however, where the more appreciable lack of orthogonality is apparent (Fig. 1.2-2b).

MODIS applies this supplemental cloud optical properties retrieval for COT and CER over the ocean as well as snow and sea ice surfaces, in addition to the standard algorithm, a feature that was first implemented in C5.

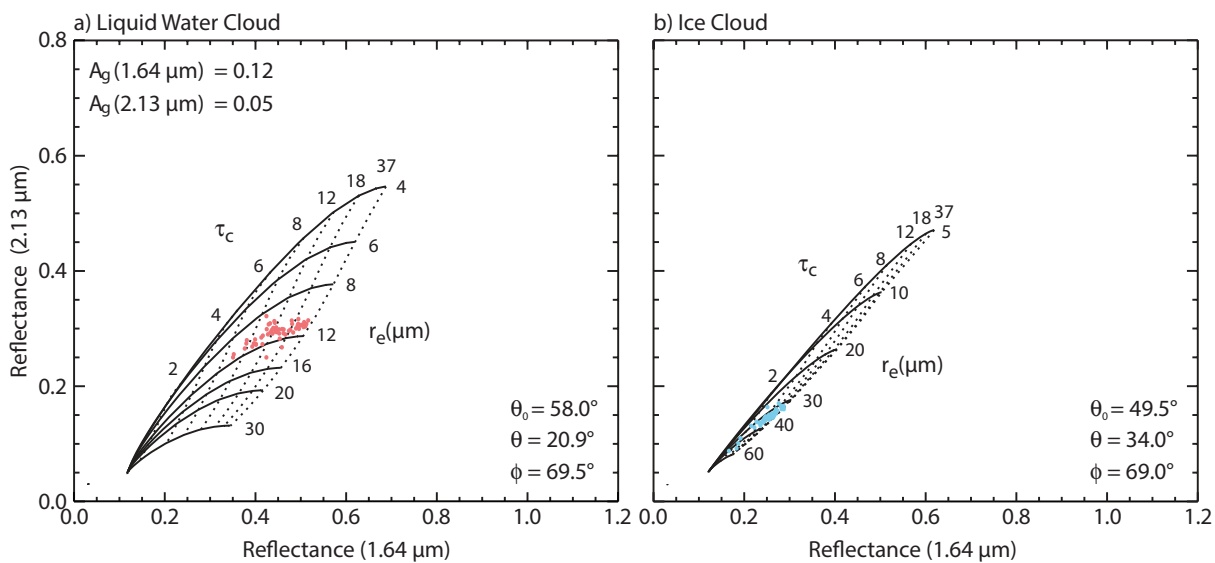


Figure 1.2-2. Theoretical relationship between the reflection function at 1.62 μm and 2.13 μm for (a) liquid water and (b) ice clouds for various values of COT (τ_c , dashed lines) and CER (r_e , solid lines) for specified values of surface albedo and solar/view geometry. Data from measurements above arctic liquid water and ice clouds are superimposed on the figure.

2. Level-2 Collection 6 Changes

Recent Collection Overview

The C6 algorithm development and testing efforts have been extensive. The major algorithm efforts are also summarized in the **Appendix G** table. Highlights include:

- **Radiative transfer/Look-up Tables (LUTs):** Eliminated the use of asymptotic parameter radiative transfer code (reduces code complexity/maintenance); generated precomputed LUTs with separate single and multiple scattering components to reduce the number of angular grid points and linear interpolation errors (median errors are typically $\ll 1\%$ across the solution domain).
- **Thermodynamic retrieval phase:** Improved algorithm using a variety of separate tests with assigned weights (MOD06 IR phase product [Baum *et al.*, 2012], microphysical retrievals for each phase, cloud-top temperature, and the $1.38\ \mu\text{m}$ channel reflectance). Comparisons against CALIOP and POLDER phase products show a substantial improvement in the overall global skill.
- **Ice radiative models:** Severely roughened aggregated columns [Yang *et al.*, 2013] provide closure with global cirrus COT from IR methods and new CALIOP lidar ratios [Holz *et al.*, 2012].
- **Spectral retrievals:** In C5, the 1.6 and $3.7\ \mu\text{m}$ CER retrievals were provided as differences with respect to the $2.1\ \mu\text{m}$ CER retrieval. In C6, all spectral retrievals are now reported in separate SDSs (i.e., separate absolute COT, CER, and WP retrievals for band combinations that include the 1.6 , 2.1 , and $3.7\ \mu\text{m}$ channels). The 1.6 and $3.7\ \mu\text{m}$ retrievals are found in SDS names *<parameter name>_16* and *<parameter name>_37*, respectively; the legacy $2.1\ \mu\text{m}$ C5 retrieval SDS is not appended with a band designation qualifier.
- **Retrieval failure metrics:** Provided for those pixels where the observations fall outside the LUT solution space (Retrieval_Failure_Metric SDS).
- **Quality Assessment (QA):** Now includes separate SDSs for lower quality scenes derived from C5-like Clear Sky Restoral algorithms [e.g., Zhang and Platnick, 2011] that flag pixels not expected to be overcast (referred to as ‘Partly Cloudy’ retrievals and found in SDSs *<parameter name>_PCL*), a $1\ \text{km}$ sub-pixel $250\ \text{m}$ reflectance heterogeneity index SDS (Cloud_Mask_SPI), and an updated multilayer detection scheme [Pavolonis and Heidinger, 2004; Wind *et al.*, 2010; Joiner *et al.*, 2010].
- **Quantitative pixel-level uncertainty:** Provided for all spectral optical/microphysical retrievals [Platnick *et al.*, 2004] and updated to include scene-dependent LIB uncertainties [Sun *et al.*, 2012], cloud model and surface albedo error sources (cloud effective variance, ocean surface wind speed and direction), and $3.7\ \mu\text{m}$ emission error sources. Does not include estimates of 3D radiative transfer biases or ice habit model error sources. Provided in SDS names *<parameter name>_Uncertainty_<band channel/pair designation>* (if appropriate).
- **Water surfaces:** Wind-speed interpolated bidirectional reflectance properties (Cox-Munk model) of water surfaces.

- **Surface ancillary datasets:** New dynamic 8-day sampling surface spectral albedo dataset derived from gap-filled C5 Aqua+Terra MODIS data (MCD43B3, *Schaaf et al.* [2011]), and adoption of land spectral emissivities consistent with cloud-top property code [*Seemann et al.*, 2008].

Details on individual C6 science tests and accompanying browse imagery are available at modis-atmos.gsfc.nasa.gov/team/pge06_test_details.html; algorithm enhancement details are at modis-atmos.gsfc.nasa.gov/products_C006update.html.

2.1. New Ice Cloud Models

Comparisons of forward RT calculations (using new ice crystal light scattering models) with satellite remote sensing using polarization of reflected sunlight from Polarization and Directionality of the Earth's Reflectances (POLDER) suggest that severely-roughened ice crystals significantly outperform their counterparts assuming smooth ice crystals [Yang *et al.*, 2013]. Moreover, reflectance-based cloud optical property retrievals using a single habit, namely severely-roughened compact aggregates composed of eight solid columns (hereafter referred to as simply *aggregated columns*), were found to provide closure with thermal IR-based retrievals and are in better agreement with CALIOP [Holz *et al.*, 2014]. Consequently, the smooth ice crystal size/habit distribution cloud models used in C5 [Baum *et al.*, 2005] have been replaced with a gamma particle size distribution consisting of these severely-roughened aggregated columns.

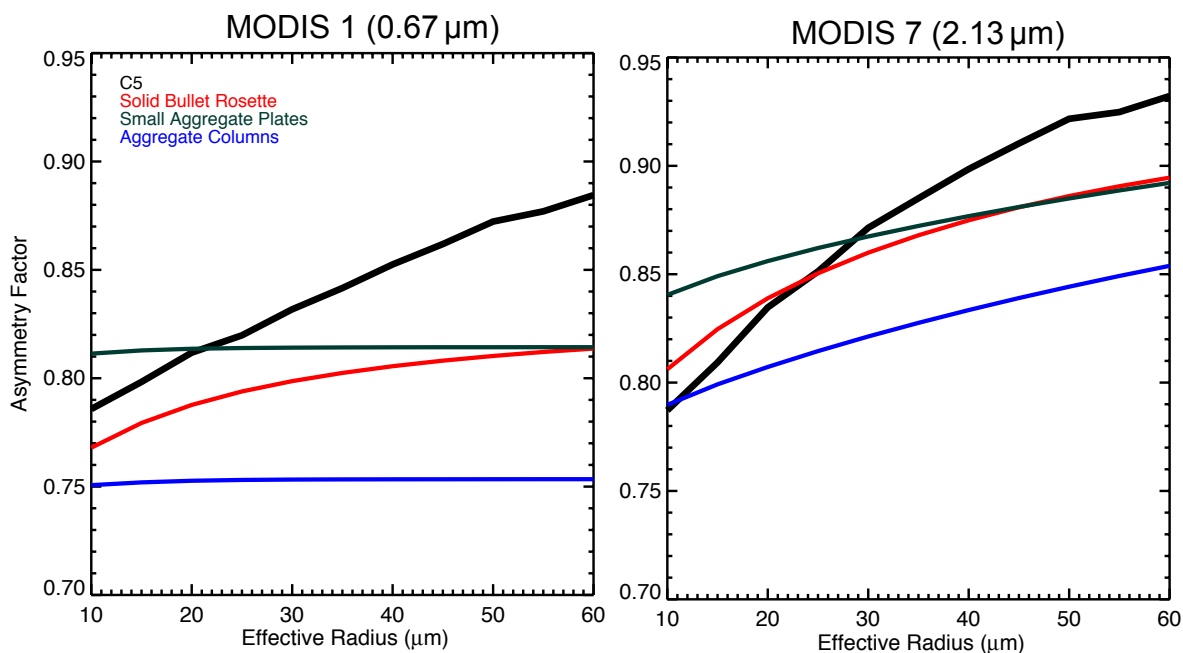


Figure 2.1-1. Asymmetry factor as a function of effective radius for ice crystals having the size/habit distribution used in C5 (black line), and gamma distribution of roughened solid bullet rosettes (red), solid aggregate plates (green), and the aggregate columns used in C6 (blue). Panel (a) applies to $0.67\ \mu\text{m}$ and panel (b) to $2.13\ \mu\text{m}$. Note that ice crystals having severely roughened surfaces have significantly lower asymmetry factors than those assumed in C5.

Figure 2.1-1 shows the effect of using severely roughened ice crystals on calculations of the asymmetry factor (g). In all cases considered (solid bullet rosettes, solid aggregate plates, and aggregate columns), the roughened particles yield substantially smaller asymmetry factors than the C5 models. Since cloud reflectance at a non-absorbing wavelength is largely a function of scaled optical thickness $(1 - g)\tau$, where τ denotes COT, it follows that differences between C5 COT retrievals and those using roughened particles (C6) can be approximated by

$$\frac{\tau^{C6}}{\tau^{C5}} \cong \frac{1 - g^{C5}(r_e)}{1 - g^{C6}(r_e)} \quad (2.1-1)$$

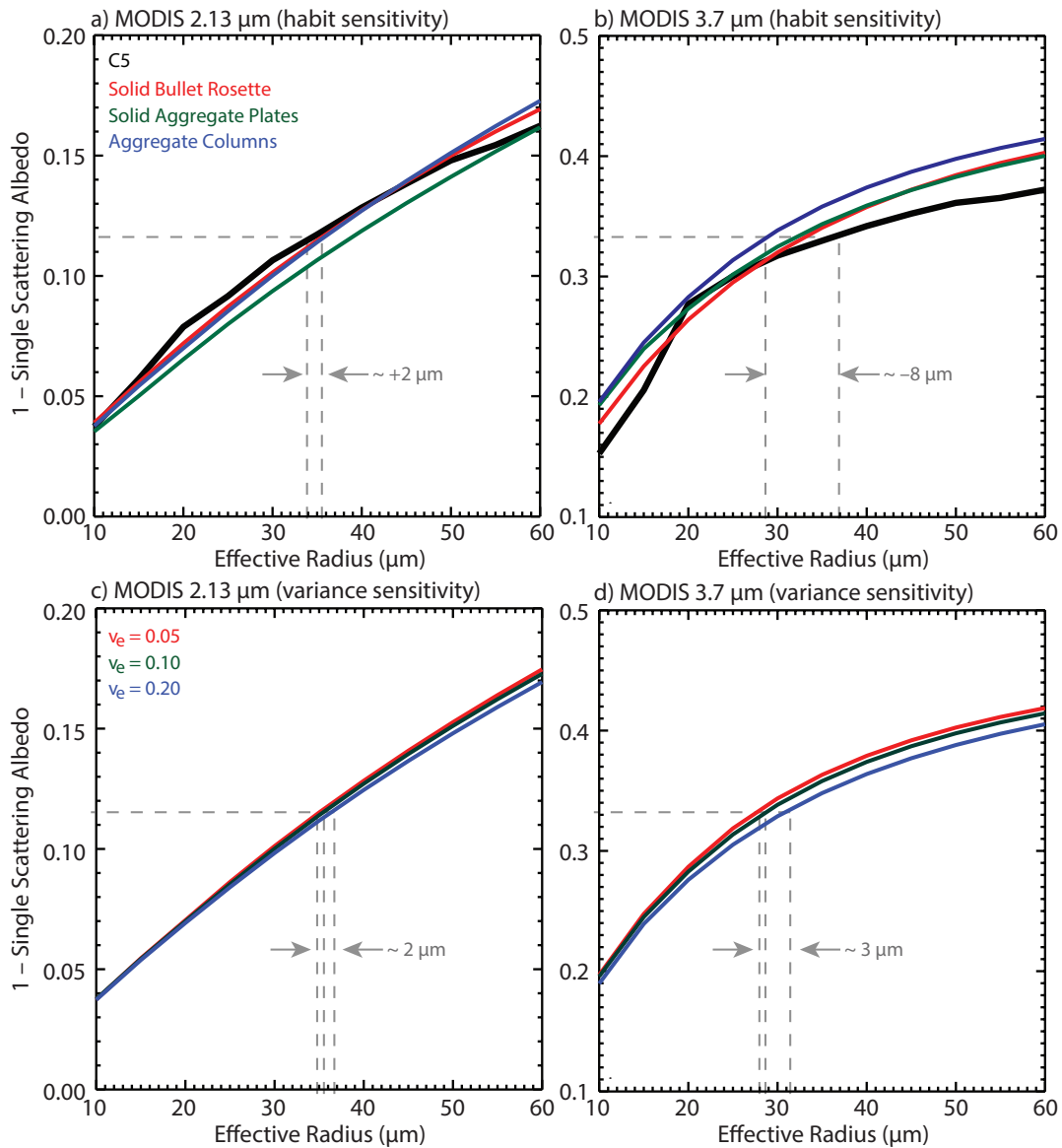


Figure 2.1-2. Simulations of co-albedo as a function of CER for crystals having the size/habit distribution used in C5 (black line), and gamma distribution of roughened solid bullet rosettes (red), solid aggregate plates (green), and the aggregated columns used in C6 (blue). Panel a) applies to the 2.13 μm MODIS channel and panel (b) to 3.7 μm. Ice crystals having severely roughened surfaces have smaller (larger) absorption than those assumed in Collection 5 at 2.13 μm (3.7 μm), which can potentially lead to larger (smaller) values of the effective radius in C6. Panels c) and d) are calculations of co-albedo for aggregate columns at various values of effective variance, as shown in panels c) and d).

Thus assuming roughened ice crystals will yield smaller COT retrievals than those of C5. This result provides better closure with CALIOP and thermal IR retrievals of COT than does C5 [Holz *et al.*, 2014], which has been shown to be biased large in the case of COT retrievals of optically thin clouds (i.e., those that can be retrieved by CALIOP).

In addition to cloud asymmetry factor, the cloud single scattering albedo (ω_0) derived from the new roughened ice crystal models is also generally larger at the absorbing SWIR wavelengths, as shown in **Figure 2.1-2** by the smaller values of co-albedo $1-\omega_0$ for the 2.13 μm MODIS channel. In the MWIR, namely 3.7 μm , $1-\omega_0$ is larger than that found in C5. Because the SWIR and MWIR wavelength channels are primarily used to infer particle size, assuming roughened ice crystals will often lead to larger values of CER at 2.13 μm than the smooth ice crystal models of C5, and smaller values of CER at 3.7 μm .

We have also examined the impact of effective variance of the gamma size distribution on the single scattering albedo of roughened aggregate columns (cf. Figure 2.1-2c and 2.1-2d for

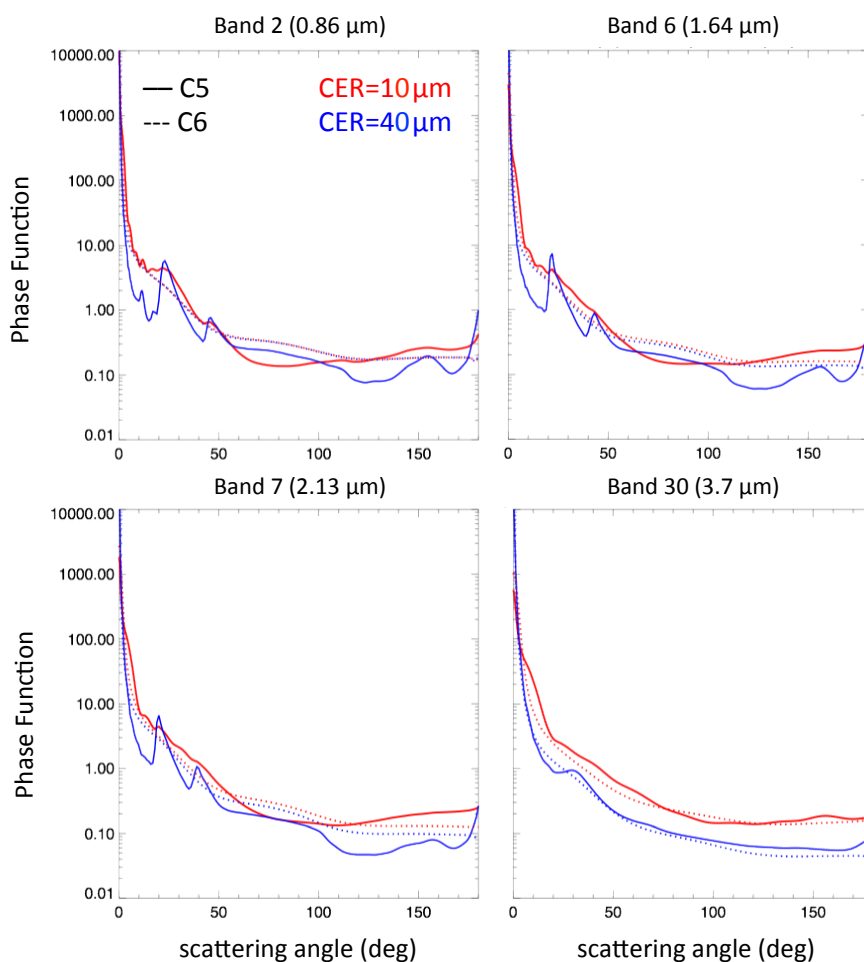


Figure 2.1-3. C5 (solid line) vs. C6 (dotted) ice model phase functions for two effective radii (red: 10 μm ; blue: 40 μm).

2.13 and 3.7 μm , respectively). Although the true effective variance of ice clouds is not known, we have chosen to use an effective variance (v_e) of 0.10 in the C6 models (consistent with liquid water gamma distribution models). Note the sensitivity to this assumption is considered in calculating the retrieval uncertainty estimates (Sect. 2.7).

Ice and liquid water scattering parameters (asymmetry parameter, single scattering albedo, and extinction efficiency) used in the C6 LUTs are provided in the MOD06 L2 data file. The parameters, given in **Appendix D**, are provided for seven MODIS spectral channels and 18 and 12 CERs for liquid and ice phase, respectively. The 2-D parameter SDSs for ice phase are named *Asymmetry_Paramter_Ice*, *Single_Scatter_Albedo_Ice*, and *Extinction_Efficiency_Ice*. An example of the C6 ice model phase functions for four MODIS channels are shown in **Fig. 2.1-3** along with the corresponding C5 phase functions.

2.2. Wind-speed Interpolated Ocean Bidirectional Reflectance Properties

Over the ocean, look-up-tables (LUTs) for the reflection function of clouds overlying an ocean surface subject to non-isotropic reflection are now used. The ocean bidirectional reflectance model uses the wind speed and direction-dependent Cox-Munk wave-slope distribution [Cox and Munk, 1954]. Separate LUTs were calculated for three different wind speeds (3, 7, and 15 m s^{-1}), each one averaged over four vector wind directions (0, 90, 180, and 270° relative azimuth). Pigment concentration and salinity are set to 0.15 $\text{mg}\cdot\text{m}^{-3}$ and 34 parts-per-thousand, respectively. A parameterization for white cap (foam) reflectance is taken from Koepke [1984]. Consequently, the LUTs now more accurately model the reflectance of opti-

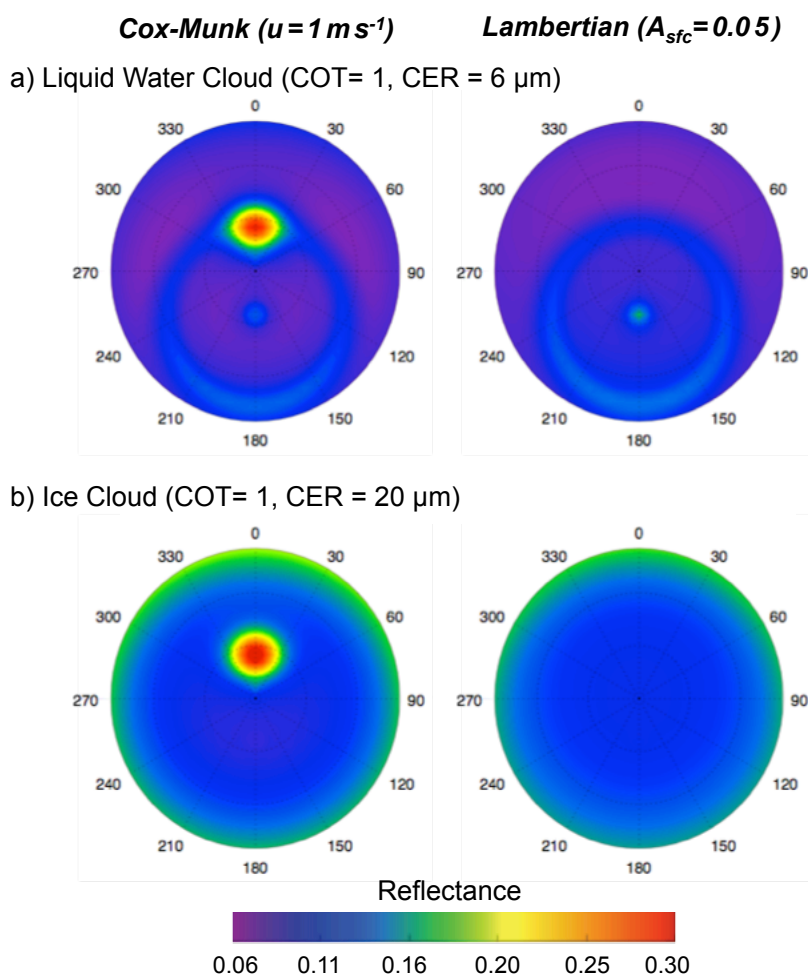


Figure 2.2-1. The angular cloud-top distribution of reflectance in MODIS channel 1 (0.65 μm) for $\text{COT}=1.0$ overlying the ocean surface for (a) liquid water clouds ($\text{CER}=10 \mu\text{m}$) and (b) C6 ice cloud model ($\text{CER}=20 \mu\text{m}$). The column on the left applies to a Cox-Munk surface reflectance model with a wind speed of 1.0 m s^{-1} ; the column on the right refers to a Lambertian surface reflectance model with a surface albedo of 0.05 (used in C5). The glory and rainbow scattering pattern for water clouds is evident.

cally thin clouds over the ocean that are sensitive to the non-isotropic sunglint distribution. In C5 (and earlier collections), all reflectance of the underlying surface (both land and ocean) were modeled as Lambertian (isotropic), with an ocean surface albedo $A_g=0.05$ that is characteristic of diffuse illumination. While the Lambertian ocean surface assumption is appropriate for sufficiently optically thick clouds, it is especially prone to errors for thin clouds near and away from sunglint. Our analysis shows that once COT becomes less than about 2, large differences are observed in above-cloud reflectance between a Cox-Munk surface and a Lambertian surface with $A_g=0.05$. The 10 m altitude wind speed over the ocean is now a required ancillary field and is obtained from the NCEP GDAS model.

Figure 2.2-1 shows calculations of the cloud-top bidirectional reflectance distribution function for both (a) liquid water and (b) ice clouds overlying an ocean surface. The left-hand column applies to the Cox-Munk wave-slope distribution model and the right-hand column

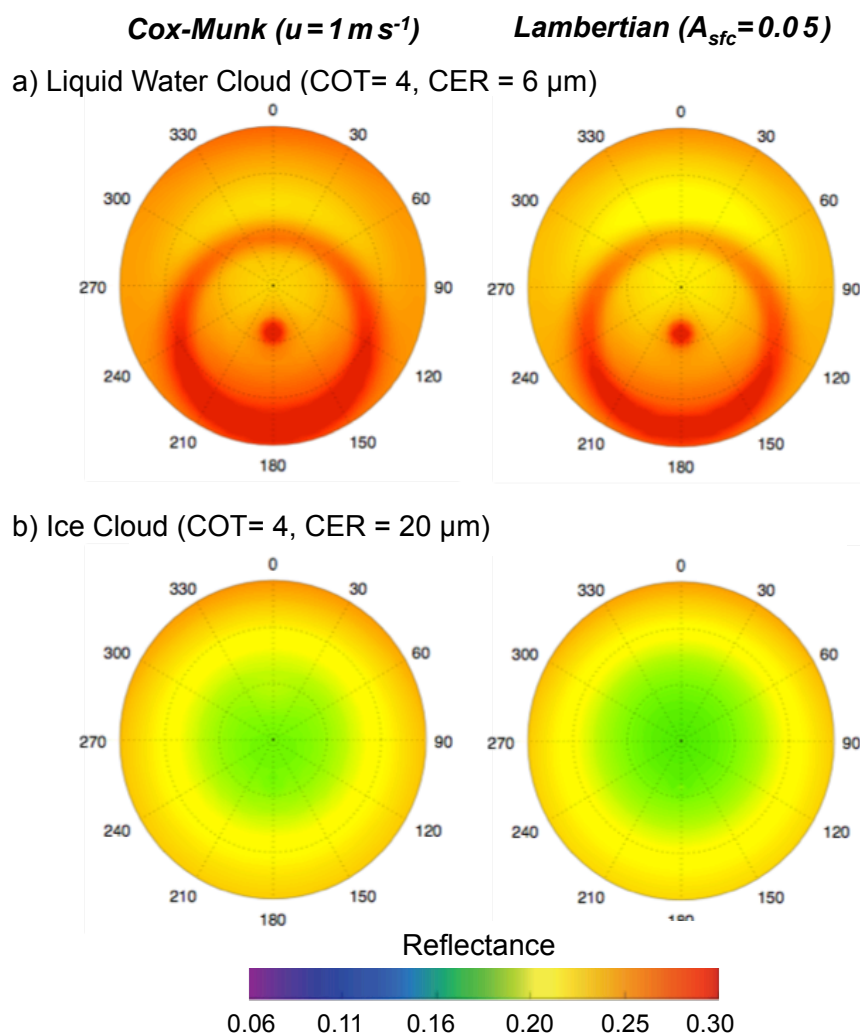


Figure 2.2-2. Same as Fig. 2.2-1 except COT=4.0.

applies to a Lambertian ocean surface. The calculations are for a solar zenith angle $\theta_0=18.2^\circ$ and $COT=1.0$, with a wind speed of 1 m s^{-1} for the Cox-Munk model. With the Lambertian model, the cloud top reflectance is more isotropic, and generally much brighter away from sunglint, whereas for a more realistic Cox-Munk distribution the ocean reflectance is darker away from the sunglint angles. For optically thin clouds where sunglint and the ocean reflectance is more apparent, this modification to the surface scattering model leads to more accurate COT (and CER) retrievals, and generally fewer failed retrievals. **Fig. 2.2-2** shows the same cloud-top reflectance distribution function but for $COT=4.0$. At this optical thickness, there is little distinction between the two surface models.

However, the accuracy of the Cox-Munk reflectance distribution for this application is not obvious given the practical need for ancillary ocean surface wind speed data (course resolu-

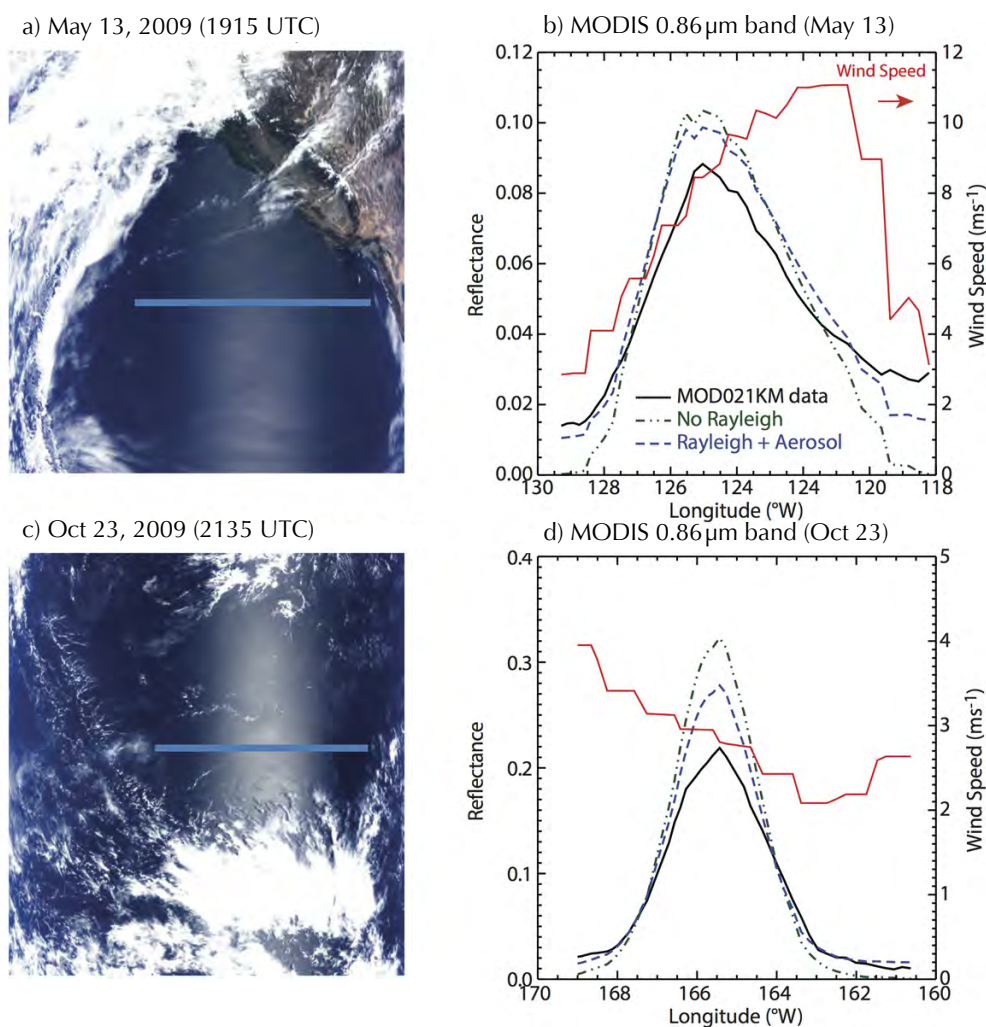


Figure 2.2-3. Cross section (blue rectangle) of the observed and calculated clear sky reflectances with the Cox-Munk surface bidirectional reflectance model in band 2 for two MODIS Terra sunglint scenes. Ocean surface wind speeds are taken from NCEP analysis.

tion) over large geographic regions. An empirical evaluation is shown in **Figure 2.2-3**. The figure shows MODIS 0.86 μm clear sky reflectances calculated for two MODIS Terra sunglint scenes. To understand the sensitivity to the clear sky atmospheric constituents, calculations are made with no Rayleigh scattering (green line) and Rayleigh scattering plus a coarse-mode sea-salt boundary layer aerosol model of optical thickness 0.1 (blue line). Here we have taken the average of five individual pixel scan lines (taken every 10th line) to compute mean reflectance and azimuth and zenith angles. Ocean surface wind speeds are temporally interpolated from the 1° NCEP GDAS 10 m wind data for that day/location. Calculated reflectance compares well with the observations away from the glint, but there is a significant difference near the glint peak, especially for the October scene. A default pristine aerosol optical depth (AOD) of 0.1 is used in calculating the ocean LUTs; it was found that the MOD04 AOD was nominally around 0.1 in the non-glint regions of these granules and therefore would not explain the differences. However, a fairly good match was able to be obtained in both the glint peak and tail regions if the wind speed was increased by about 4 $\text{m}\cdot\text{s}^{-1}$ and 1 $\text{m}\cdot\text{s}^{-1}$ for the May and October granules, respectively. This suggests caution in using thin cirrus and other small COT retrievals in sun glint, though surface sensitivity may be accounted for to some extent in the retrieval uncertainties that include a wind speed/direction error source (Sect. 2.7).

2.3. New Gap-filled Spectral Surface Albedo Dataset

A recently developed high-resolution spatially complete snow-free surface albedo dataset was implemented that builds on the pioneering work of *Moody et al.* [2005, 2008] that was, in turn, based on a 5 year climatology of Terra Collection 4 land surface albedo data (MOD43B3 product). The new dataset (i) utilizes a combination of both Terra and Aqua MODIS data (Collection 5) that increases the number of angular samples needed to characterize the surface bidirectional reflectance distribution function (BRDF), (ii) has enhanced spatial resolution of 30 arc sec (~ 1 km), (iii) increases the time sampling to an 8-day periodicity (based on 16-days of observation), (iv) uses 20 months of data to establish seasonal phenology, (v) does gap-filling based on the RossThickLiSparse reciprocal BRDF model, rather than on the white-sky albedo, and (vi) has data available for each calendar year from 2000 to 2013.

Figure 2.3-1 shows a comparison between the new high-resolution MODIS-derived gap-filled surface albedo at $0.65 \mu\text{m}$ (the wavelength used for cloud optical thickness retrievals over land) on (a) January 1-8, 2006 and (c) May 27-June 3, 2007, with (b) and (d) showing the difference between these new surface albedos and those used previously in C5 (based on *Moody et al.* [2008]). As was the case in Collection 5, the surface albedo of snow-covered regions was overlain on these figures using the ecosystem-dependent spectral albedo of snow

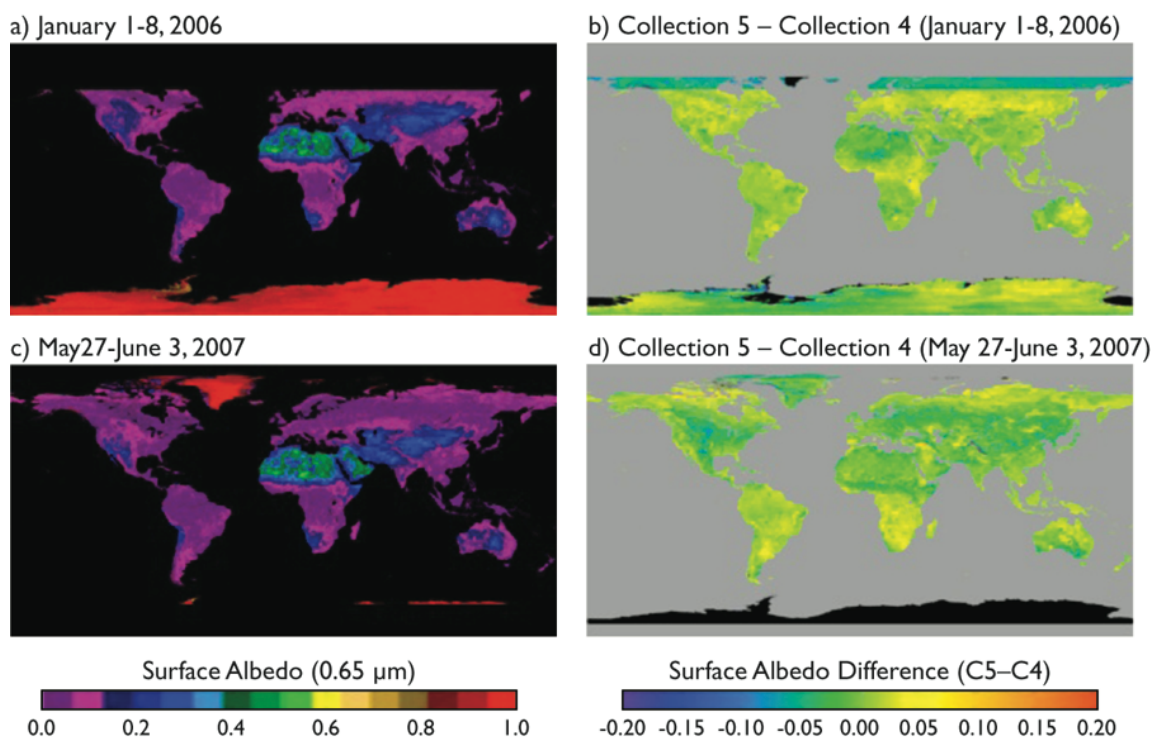


Figure 2.3-1. Spatially complete white-sky albedo at $0.65 \mu\text{m}$ after the temporal interpolation technique was applied to the 8-day periods of (a) January 1-8, 2006 and (c) May 27-June 3, 2007, with (b) and (d) showing the difference between these new surface albedos (based on C5 land processing) and the corresponding values from *Moody et al.* [2008] that were based on C4 land processing.

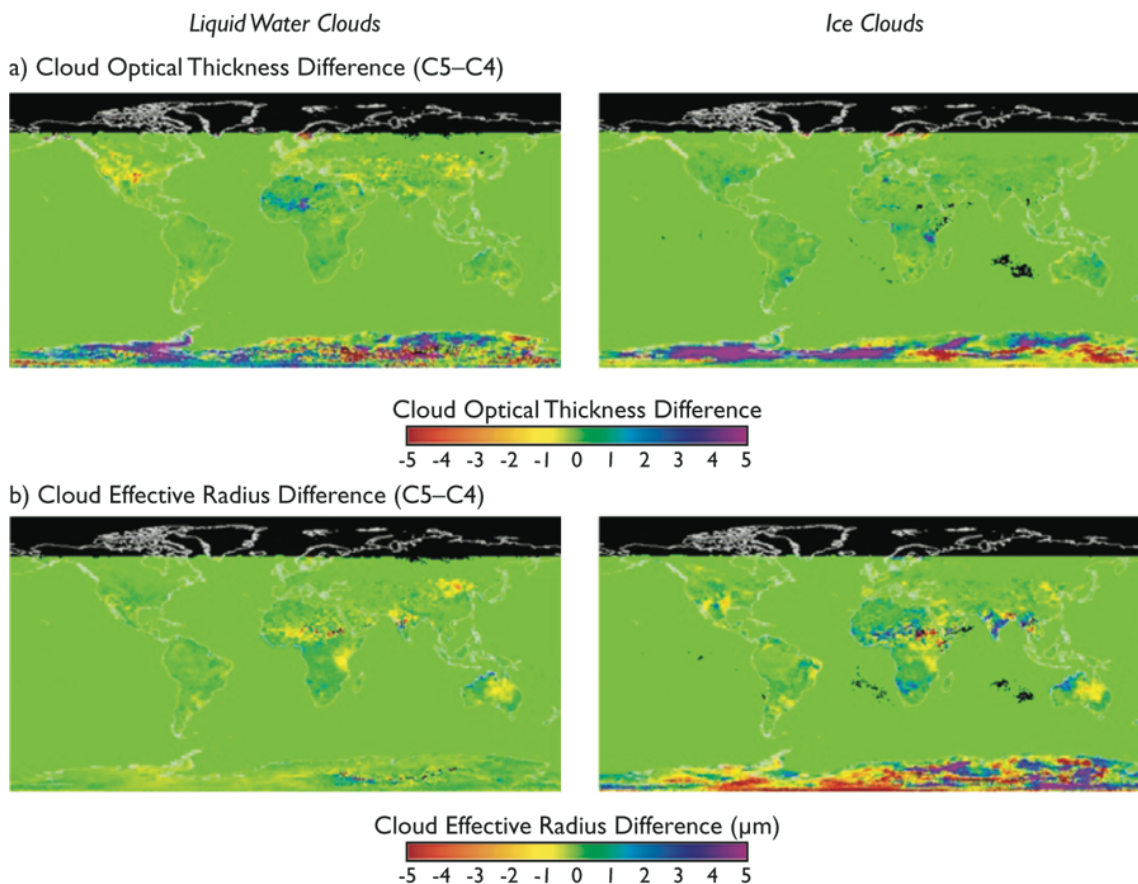


Figure 2.3-2. Differences in (a) cloud optical thickness and (b) cloud effective radius for liquid water (left column) and ice (right column) for January 2006, where we have run the identical algorithm using either the new (C5) or previous (C4) spectral white-sky surface albedos. Large differences are most noticeable in polar regions.

derived from 5 years of Terra data [Moody *et al.*, 2007], except for permanent snow regions, where the new C5-derived surface albedo data set (e.g., Figures 2.3-1a and 2.3-1b) is used.

Figure 2.3-2 shows a comparison of (a) cloud optical thickness and (b) cloud effective radius retrievals using the new (C5 land processing) and old (C4) surface albedos, where the left hand column applies to liquid water clouds and the right hand column to ice clouds. This test run was performed for January 2006. Aside from differences in the polar region, the effects of the ancillary surface albedo change are overall quite small. Note, however, while the old albedo dataset was a 5-year climatology, the new dataset is dynamic up through 2013 (the 2014+ forward processing stream uses equivalent time periods from 2013). So any significant changes to the land cover status in any particular year will likely affect the cloud retrievals over those areas, particularly for optically thinner clouds.

2.4. Improved Shortwave-Derived Cloud Thermodynamic Phase

Cloud thermodynamic phase classification is an important initial step in the MOD06 retrievals process. Because ice and liquid phase clouds have very different scattering and absorbing properties, an incorrect cloud phase decision can lead to substantial errors in COT, CER, and CWP. For C6, the cloud thermodynamic phase algorithm has been completely redesigned. Changes include: (1) a new cloud phase discrimination logic, (2) removal of the use of cloud mask tests (see [MODIS C5 Cloud Phase flowchart](#)), and (3) replacement of the C5 SWIR/NIR reflectance ratio tests with logic utilizing separate ice and liquid phase spectral CER retrievals (though the ratio tests are retained for thin clouds over snow and ice surfaces).

The new algorithm has been optimized via extensive global and regional comparisons between Aqua MODIS and the A-Train CALIPSO lidar (CALIOP), yielding improved skill over C5, particularly for broken clouds as well as optically thin ice cloud edges previously misidentified as liquid cloud phase; similar improvement is observed with respect to collocated polarimetric observations from the POLDER instrument (on the PARASOL mission, also in the A-Train). As in C5, cloud phase results are reported independently as an SDS (see **Table 2.4-1**) as well as in heritage QA bit values in *Quality_Assurance_1km SDS*.

Table 2.4-1: SDS name for the cloud thermodynamic phase algorithm used to determine the phase reported by the optical retrieval algorithm.

Dataset	SDS Name
Cloud Thermodynamic Phase used in Optical Retrievals	Cloud_Phase_Optical_Properties

Table 2.4-2: Summary of reported values in Cloud_Phase_Optical_Properties SDS and C5-heritage QA bits.

SDS (or QA Bit) Value	Phase Result
0	Cloud Mask unavailable, missing data, etc.: <i>No Phase Result</i>
1	Cloud Mask Clear or Probably Clear, or Pixel Restored to Clear Sky: <i>No Phase Result</i>
2	Liquid Water
3	<i>Ice</i>
4	Undetermined

2.4.1. Phase retrieval algorithm overview

All MOD/MYD35 “Cloudy or Probably Cloudy” pixels, excluding those identified as not cloudy by the Clear Sky Restoral (CSR) algorithm (see **Section 2.8**), pass through the cloud thermodynamic phase classification logic shown in **Figure 2.4-1**. The C6 logic includes a tri-spectral IR phase test [Baum *et al.*, 2012] that is separately reported in the SDSs *Cloud_Phase_Infrared_1km* and *Cloud_Phase_Infrared* (5km dataset), cloud top temperature (CTT) tests, and ice and liquid spectral CER retrieval tests; all tests provide a signed integer result (positive for liquid, negative for ice, 0 for undetermined) with the total sum determining the phase. Final phase results are reported in the *Cloud_Phase_Optical_Properties* SDS as integer values as described in **Table 2.4-2**.

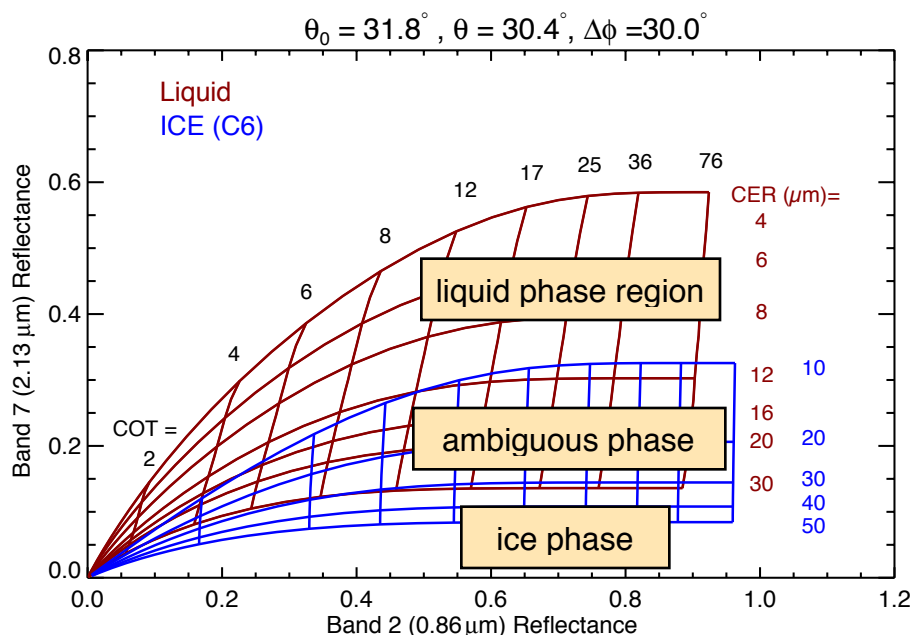


Figure 2.4-1. Theoretical relationship between the reflection function in the 0.86 and 2.13 μm MODIS channels for liquid water (red) and the C6 ice cloud models (blue) for various values of optical thickness and effective radius. Reflectances can occur in regions of the solution space that are unambiguously liquid or ice, but may also lie in regions that are ambiguous regarding phase.

It is important to understand that, similar to C5, pixels having undetermined phase are processed as liquid phase, though they are excluded from the liquid retrieval population in L3 aggregations (and are in fact aggregated separately). Note also that cloud phase is reported for all cloudy pixels having successful or partially successful optical/microphysical retrievals, including those identified as partly cloudy by the CSR algorithm (see **Section 2.8**) or those lying outside the retrieval solution space (see **Section 2.6**).

2.4.2. C6 changes

For C6, the NIR-SWIR cloud thermodynamic phase algorithm has been completely rewritten in an effort to improve the phase discrimination skill for a variety of cloudy scenes

(e.g., thin/thick clouds, over ocean/land/desert/snow/ice surface, etc). While the C5 phase algorithm used a linear sequential logic structure, which makes it difficult to improve and adapt to a large variety of cloud scenes, the new C6 phase algorithm uses a voting discrimination logic that includes several tests providing signed integer votes of different weights. The voting weights have been optimized through extensive comparisons between Aqua MODIS and collocated CALIOP observations, with further evaluation using POLDER.

Four main categories of cloud phase tests comprise the C6 phase algorithm as follows (see the flowchart in **Appendix E** for details):

1. *Tri-Spectral IR Tests*: These tests (actually including a 4th IR water vapor channel) use the 1 km IR cloud thermodynamic phase algorithm of *Baum et al.* [2012] that is run as part of the MOD06 Cloud Top Properties algorithm.
2. *Cloud Top Temperature Tests*: These tests use the MOD06 1 km CTT retrievals. Note the C5 warm cloud sanity check, in which the phase is forced to liquid when $CTT > 270$ K, was retained in modified form for C6 (mainly as a larger liquid phase vote), though only when retrieved liquid phase COT is greater than 2.
3. *1.38 μm Channel Test*: This test uses the 1.38 μm high cloud flag from the MOD35 cloud mask product. The capacity of this test to discriminate high-altitude ice clouds from low-altitude liquid clouds is based on the strong water vapor absorption at 1.38 μm [*Gao et al.*, 1993]. Note this test is applied only when sufficient water vapor is present (roughly 1 cm perceptible water) and ice phase COT is smaller than 2 (to avoid spurious ice votes in the case of optically thick liquid clouds). In C5 this test was used only when the bi-spectral IR cloud phase decision was undetermined.
4. *Spectral Cloud Effective Radii Tests*: These tests replace the C5 SWIR/NIR reflectance ratio tests. While it is difficult to define linear reflectance ratio thresholds to discriminate ice and liquid phase pixels, since reflectance ratios might depend on COT, viewing geometries, etc, CER retrievals implicitly account for such dependencies. **Figure 2.4-1** shows an example of the retrieval solution space for cloud optical thickness and effective radius over a dark surface for the geometry specified in the caption. The red and blue curves are computations for liquid and ice phase clouds, respectively. Some of the solution space is unambiguously liquid water and some unambiguously ice, but there are overlapping regions in which either thermodynamic phase leads to a viable physical solution. However, comparison of retrievals using all three SWIR wavelengths can further reduce ambiguity in the choice of thermodynamic phase. The approach to using this information is described in the flow chart in Appendix E (see panel AE-2). To implement this approach, the C6 algorithm needs to attempt CER retrievals twice, once for each phase, thereby doubling the processing time devoted to the retrieval solution logic.

Evaluation over a wide variety of granules show an overall improvement of the thermodynamic phase determination as compared with C5, especially for optically thin clouds on the

edge of cloud fields that were otherwise misidentified as liquid water clouds. The evaluation methodology and results are described in the following section (2.4.2).

2.4.2. Phase algorithm evaluation

To evaluate the performance of the C6 cloud thermodynamic phase algorithm, extensive granule-level and global comparisons have been conducted against the heritage C5 algorithm, CALIOP, and POLDER. A wholesale improvement is seen for C6 compared to C5.

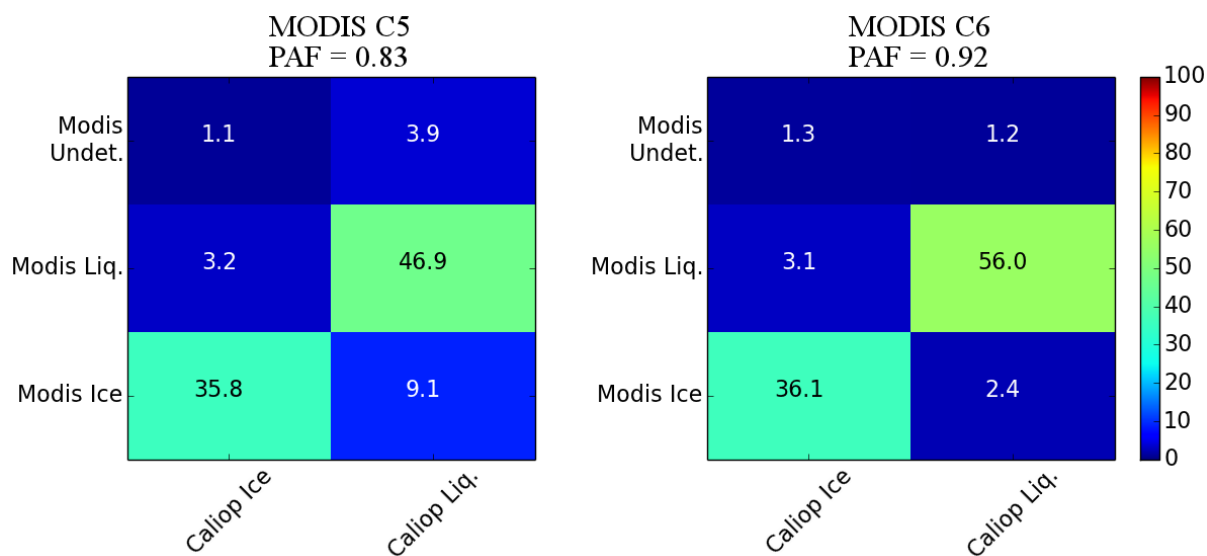


Figure 2.4-2. Global thermodynamic phase evaluation of the MODIS Aqua C5 and C6 algorithms vs. CALIOP over all surface types during January 2008. The population is from all collocations where CALIOP observed a single phase in the column. The overall Probability of Phase Agreement (PAF) skill score increases by ~10% for C6.

Figure 2.4-2 shows a summary skill table comparing Aqua MODIS C6 phase results to the collocated CALIOP v3 Cloud Layer product for global scenes (all surface types) where CALIOP identified a single phase in the column during January 2008. Both 1 km and 5 km CALIOP cloud layer detection datasets are used. The 5 km dataset (more sensitive to thin cirrus) is subsampled to 1 km and merged with the native 1 km dataset. When only one of the datasets detects a cloud in a particular layer of 1 km horizontal scale, that result is used; when they both detect a cloud but the phase is inconsistent, that detection is removed and not used in the skill assessment. Assuming CALIOP as “truth,” the skill of the phase algorithm can be defined as the number of collocated cloudy pixels with the same phase divided by the total number of collocated cloudy pixels (including undetermined MODIS phase retrievals). We refer to this skill definition as the **Phase Agreement Fraction (PAF)**. The C6 PAF is 0.92 for all global collocations. This is a marked improvement over the C5 PAF of 0.83. The global PAF for single-phase cloud layers over different surface types and for optically thin (non-opaque for CALIOP) and opaque cloudy columns is shown in **Figure 2.4-3** where dark and light shading corresponds to the C5 and C6 phase algorithms, respectively. For all surface types, the C6 algorithm has a higher PAF score than C5. The greatest improvements are seen

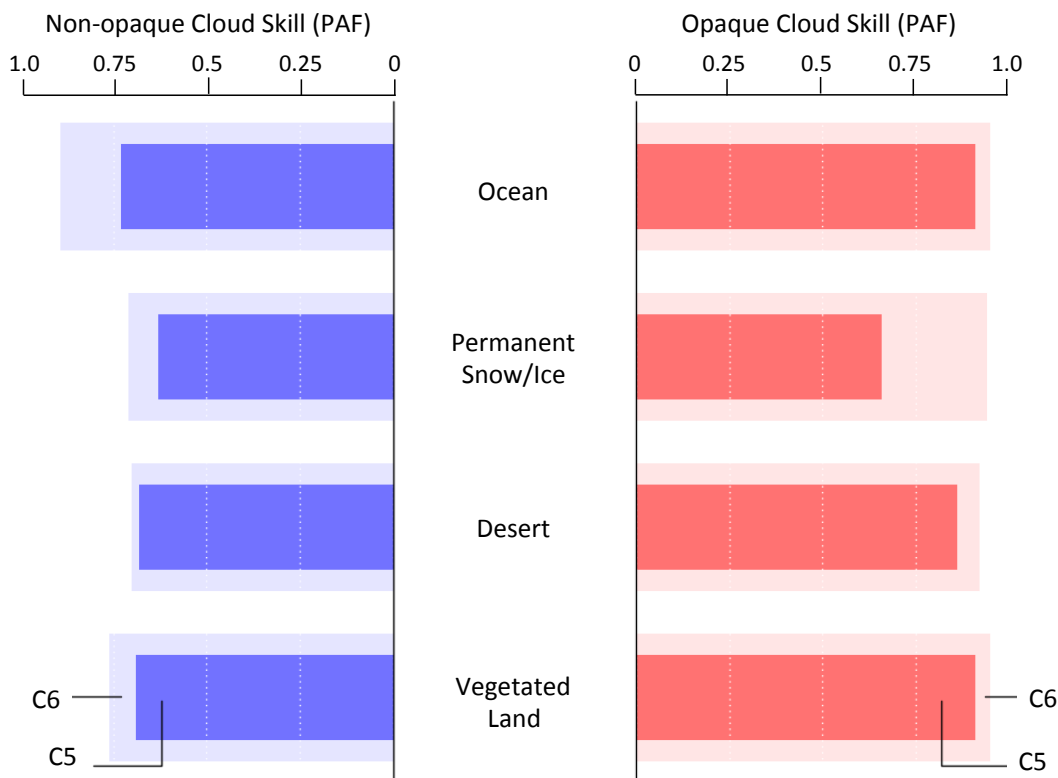


Figure 2.4-3. Global thermodynamic phase evaluation of the MODIS Aqua C5 and C6 algorithms vs. CALIOP for a variety of surface types during January 2008. The population is from all collocations where CALIOP observed a single cloud phase throughout the column. The bar plots to the left are for scenes where the lidar was not completely attenuated by the cloud layers (COT less than about 3); bars to the right are for scenes where the lidar was completely attenuated (no ground return).

for opaque clouds over permanent snow/ice (Greenland, Antarctica) and thin clouds over the ocean; more minor differences are found for thin clouds over non-polar desert regions and opaque clouds over vegetation.

Figure 2.4-4 shows global gridded maps of C5 and C6 phase fractions for January 2008. For C5, fractions only include those pixels for which successful retrievals were obtained and the CSR algorithm reported that the pixel was not “partly cloudy” (see Sect. 2.8). However, the C6 phase pixel population includes successful “partly cloudy” pixels as well as failed retrievals; no retrievals were attempted on this pixel class in C5. Therefore the figure shows C6 results with a C5-equivalent filtering (CSR=0, middle panels) along with the full population (lower panels). Several differences are worth noting. Most obvious is that the C6 algorithm yields an increase in liquid phase in the southern oceans, along with a corresponding decrease in ice phase. There is also an increase in liquid phase over many non-polar vegetated land areas, though there is a notable decrease in south America.

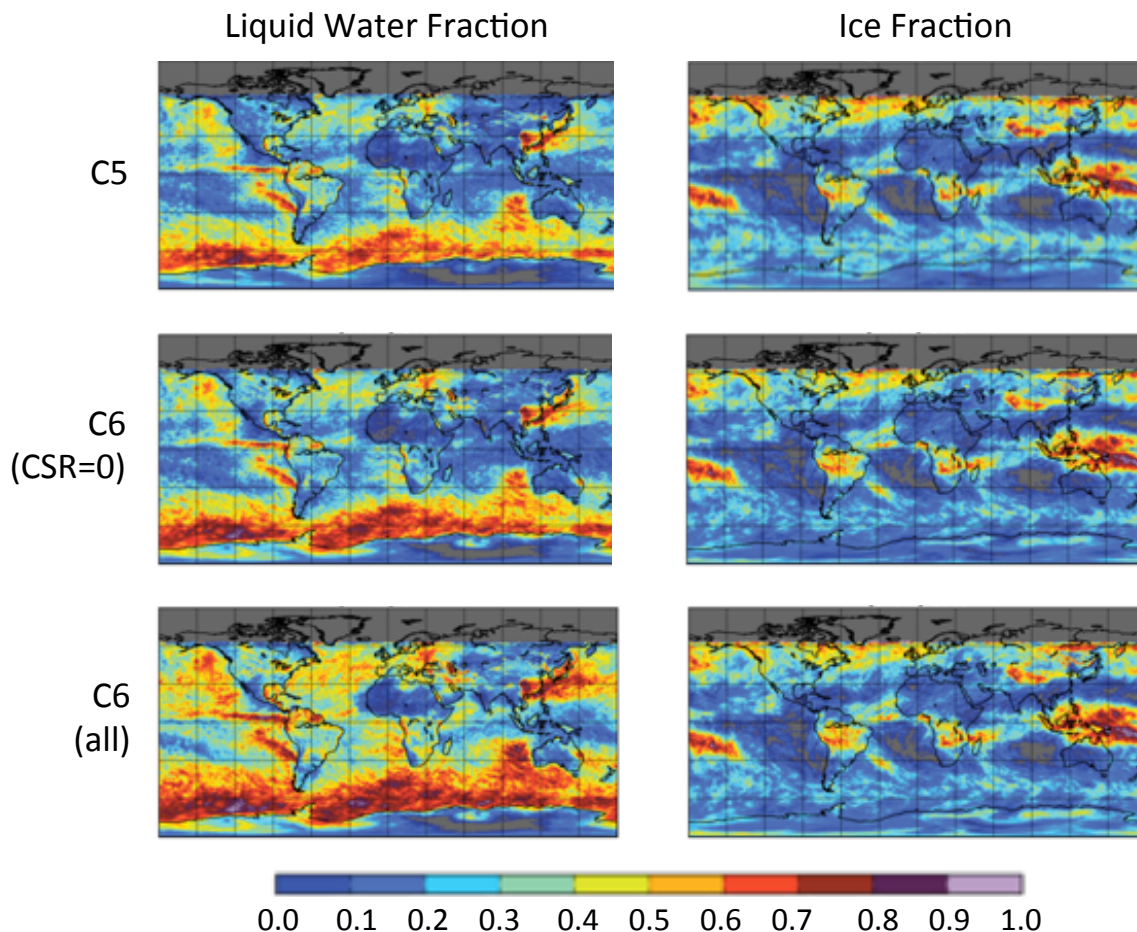


Figure 2.4-4. Global cloud thermodynamic phase comparisons between C5 and C6 for January 2008 (Aqua). Note that cloud phase in C6 is reported for all cloudy pixels having successful or partially successful optical/microphysical retrievals, including those identified as partly cloudy (see Sect. 2.8) as well as those lying outside the retrieval solution space (Sect. 2.6).

Figure 2.4-5 shows an example thermodynamic phase comparison between C5 and C6 for a selected Aqua granule. Panel (a) is a true color image showing optically thin cirrus clouds and low marine boundary layer clouds off of North Africa. Panel (b) shows the cloud-top temperature retrievals, and panels (c) and (d) show the retrieved phase of this granule using the C5 and C6 algorithms. Note the improved identification of ice phase clouds on the edge of optically thin cirrus clouds (especially over the desert) and liquid water clouds in the low boundary layer.

2.4.3. Known issues

Although the C6 cloud phase discrimination algorithm is significantly improved over C5, some situations continue to be problematic. Examples include:

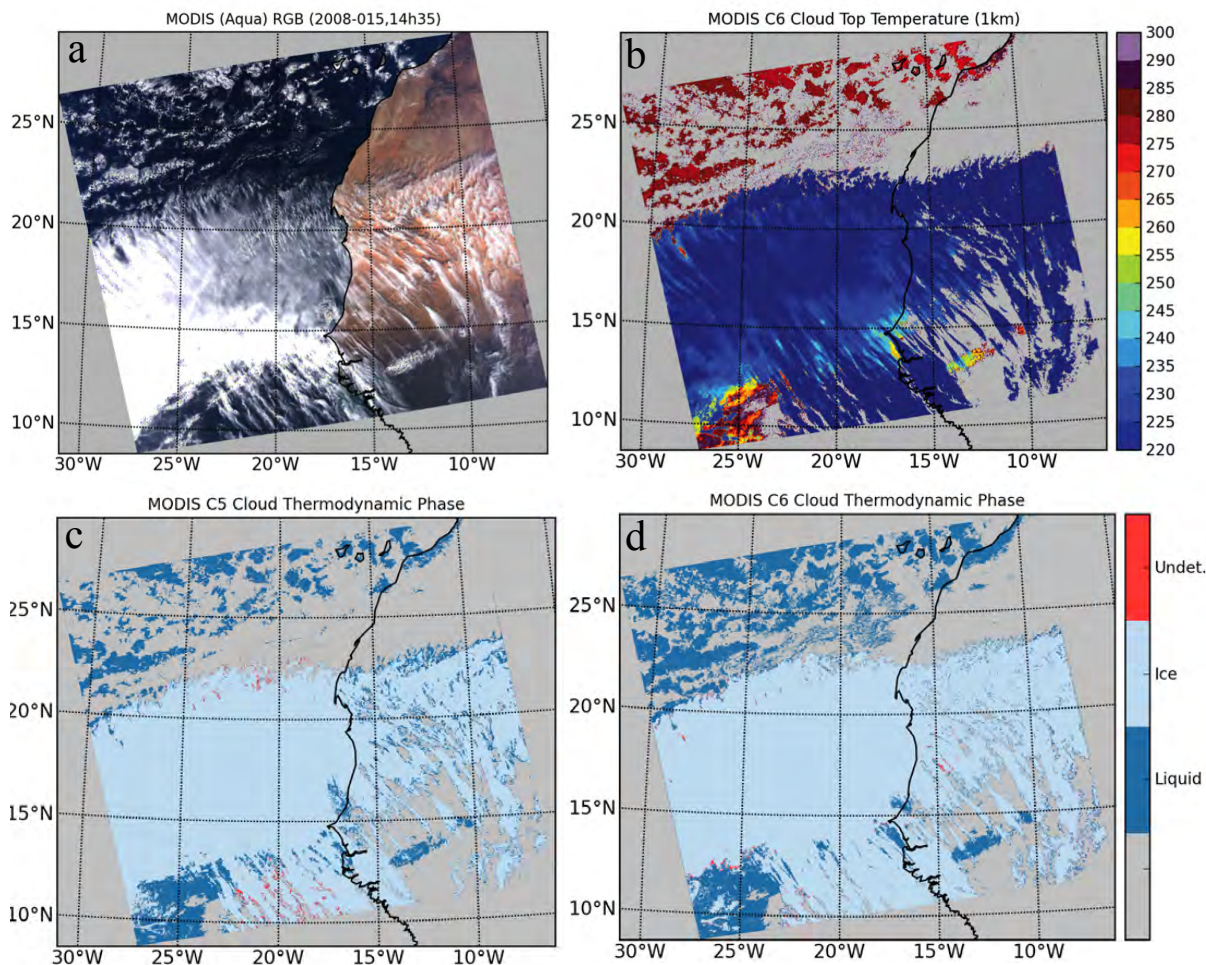


Figure 2.4-5. Example C5 and C6 phase retrievals for an Aqua data granule centered off the coast of north Africa containing a combination of high clouds and marine boundary layer clouds (RGB composite in panel a). Cloud-top temperatures from MYD06 are shown in panel b, while C5 and C6 phase results are in panel c and d, respectively.

- *Optically thin cirrus over warm surfaces*: A particularly acute problem in C5, some thin cirrus may continue to be incorrectly identified as liquid phase over warm surfaces, though C6 provides better skill in such circumstances.

- *Broken liquid phase clouds*: False ice phase discrimination is greatly improved in low maritime broken cloudy scenes, though still evident. However, these pixels are often associated with partly cloudy scenes as identified by the CSR algorithm and are thereby provided in separate *_PCL SDSs (see Sect. 2.8). An example is shown in **Fig. 2.4-7**. Note the better identification of liquid phase clouds in the low boundary layer (verified by CALIOP and cloud-top temperatures) with fewer occurrences of ice phase in the center of small cells in the eastern part of the granule (see zoomed panels). In addition to C6 having fewer spurious

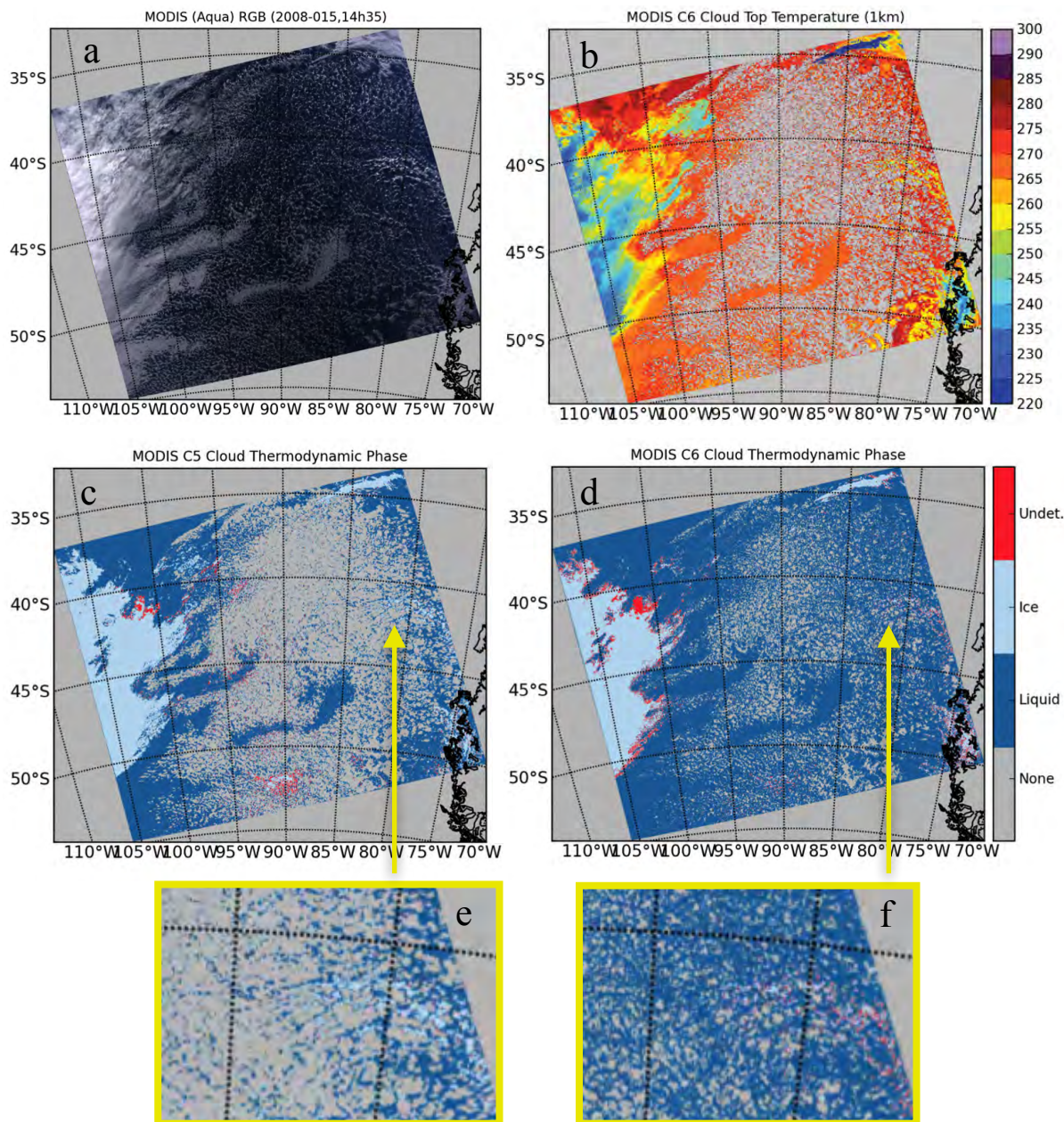


Figure 2.4-7 Example C5 and C6 phase retrievals for an Aqua data granule showing low marine clouds through much of the central/eastern portion of the image (RGB composite in panel a). Cloud-top temperatures from MYD06 are shown in panel b, while C5 and C6 phase are in panel c and d, respectively. An area with substantial broken clouds is shown in the bottom two panels (e and f) indicating less ice cloud retrievals for the C6 phase algorithm.

ice results, many of the broken cloud edges are identified as ‘undetermined’ which is often a safer choice in these problematic clouds.

- *Oblique sun angles*: In some particular viewing geometries with high solar zenith angles, the CER tests may incorrectly identify liquid phase clouds.

2.5. Separate Cloud Effective Radius Retrievals at 1.6, 2.1, and 3.7 μm

Cloud effective radius, optical thickness, and water path retrievals are now performed and reported separately for channel pairs that include the 1.6 and 3.7 μm channels, to complement the retrievals using the 2.1 μm channel. These spectral retrievals were also performed in C5 (and C5.1), but only the size results were reported, and then only as CER differences between 1.6 and 2.1 μm (and 3.7 and 2.1 μm), with the ‘primary’ suite of retrievals being reported only for 2.1 μm . By reporting the retrievals as separate SDSs for band pairs using the 1.6, 2.1, and 3.7 μm channels, it is now possible to do analysis and L3 aggregations that enable improved spectral retrieval inter-comparisons. **Table 2.5-1** shows the new C6 SDSs and the difference from C5.

Table 2.5-1. Cloud property retrieval SDS listing.

Spectral Retrieval	C5 SDS Name	C6 SDS Name
Optical Thickness 1.6 μm	–	Cloud_Optical_Thickness_16
Effective Radius 1.6 μm	Effective_Radius_Difference (plane 1)	Cloud_Effective_Radius_16
Water Path 1.6 μm	–	Cloud_Water_Path_16
Optical Thickness 2.1 μm	Cloud_Optical_Thickness	Cloud_Optical_Thickness
Effective Radius 2.1 μm	Cloud_Effective_Radius	Cloud_Effective_Radius
Water Path 2.1 μm	Cloud_Water_Path	Cloud_Water_Path
Optical Thickness 3.7 μm	–	Cloud_Optical_Thickness_37
Effective Radius 3.7 μm	Effective_Radius_Difference (plane 2)	Cloud_Effective_Radius_37
Water Path 3.7 μm	–	Cloud_Water_Path_37

In addition to the desired result of enabling easy inter-comparisons of three different retrieval outcomes, it is important to appreciate that the three different spectral cloud retrievals have sometimes dramatically different failure patterns. For example, retrievals sometimes fail using the VNIR and 2.1 μm channel pair but may yield a successful retrieval using the VNIR and 3.7 μm channels (see Sect. 2.6 for retrieval failure details). Therefore, the pixel population comprising one retrieval pair may be significantly different than another; this can be particularly true for broken liquid water cloud scenes where cloud heterogeneity scales are on the order of, or less than, the 1 km nadir pixel scale and/or for cases where a significant drizzle mode is found in the column [Lebsock *et al.*, 2011; Zhang *et al.*, 2012].

Figure 2.5-1 illustrates the COT and CER retrievals available in C5. **Figure 2.5-2** illustrates data sets available for C6. Notice that the $3.7\ \mu\text{m}$ retrieval in C6 has significantly more successful retrievals than $2.1\ \mu\text{m}$. When the $3.7\ \mu\text{m}$ retrieval is stored as a difference from $2.1\ \mu\text{m}$ in this particular case, as was done in C5, almost 140,000 additional successful retrievals are lost, a situation that is common. The C5 removal of successful $3.7\ \mu\text{m}$ retrievals due to filtering by successful $2.1\ \mu\text{m}$ retrievals also leads to a systematic shift in the $3.7\ \mu\text{m}$ retrieval histogram as illustrated in **Figure 2.5-3**. The effect on liquid water retrievals is greater because liquid water $2.1\ \mu\text{m}$ CER retrievals tend to fail (i.e., reach values larger than $30\ \mu\text{m}$) more often than $3.7\ \mu\text{m}$, effectively removing the latter retrievals from the C5 dataset.

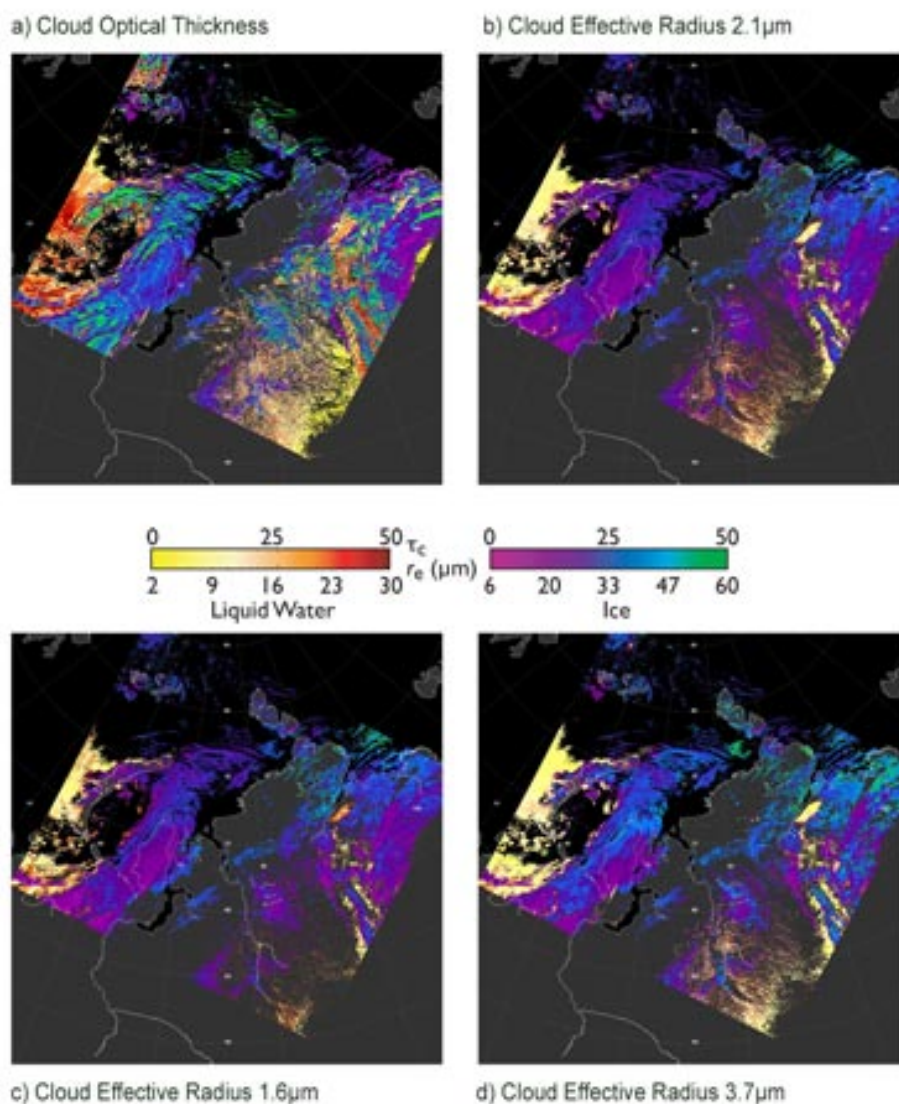


Figure 2.5-1. Terra MODIS (2005, day 091, 0635 UTC) C5 spectral CER retrievals from three channel pairs. Size retrievals from channel pairs using a VIS/NIR plus the 1.6 or $3.7\ \mu\text{m}$ channels were only available in C5 as differences relative to the VIS/NIR and $2.1\ \mu\text{m}$ channel pair, and thus were only available for successful $2.1\ \mu\text{m}$ channel retrievals.

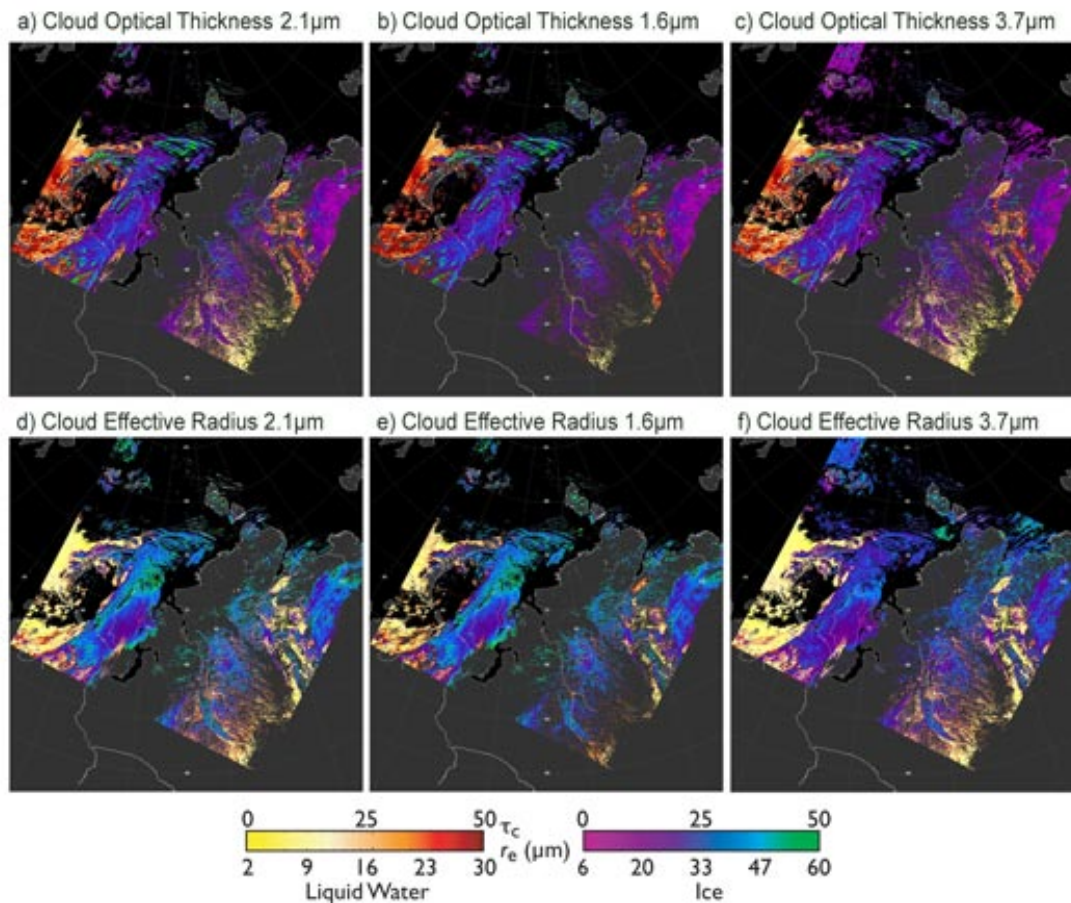


Figure 2.5-2. Same as Fig. 2.5-1 but using the new spectral CER SDSs from the C6 product. Successful retrieval fractions for retrieval pairs using the 1.6, 2.1, and 3.7 μm channels are summarized in Table 2.5-1.

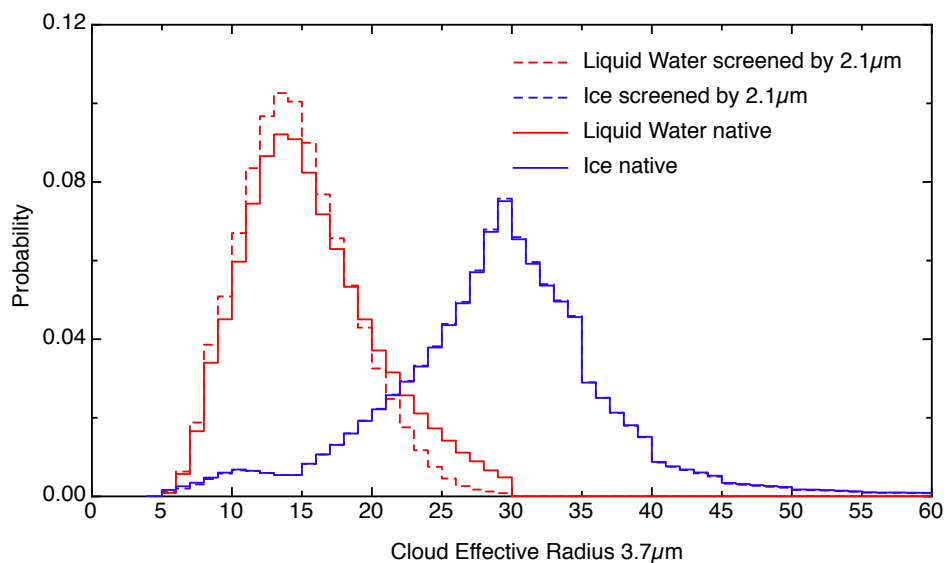


Figure 2.5-3. Set of 3.7 μm derived CER histograms based on the C6 retrievals from Fig. 2.5-2, showing sensitivity of liquid water cloud statistics to filtering by 2.1 μm successful retrievals.

Spectral retrieval successful fraction statistics are shown in **Table 2.5-2** for both C5 and C6 algorithms. Note, however, the pixel population (denominator) is different for the two columns. C5 includes only pixels identified as “overcast” (CSR=0) while C6 also includes pixels identified as “partly cloudy” (CSR=1 and 3); see Sect. 2.8 for further details on these classifications.

Table 2.5-2. Successful spectral cloud retrieval statistics for the data granule of Figs. 2.5-1 and -2.

Retrieval Channel Pair	C5 successful retrievals (%)	C6 successful retrievals (%)
VNIR + 1.6 μ m	74.2	57.3
VNIR + 2.1 μ m	81.7	67.5
VNIR + 3.7 μ m	79.3	84.0
Cloud Fraction	51.6	60.8

Figure 2.5-4 shows monthly mean gridded CER maps (Aqua MODIS, April 2005, 1° grid) for the main three spectral channel combinations (i.e., the first three rows of Table 2.5-1). For this month, the successful VNIR + 2.1 μ m effective radius retrievals (**CER_2.1**) generally exceed those of the other channel combinations in most grid boxes, regardless of whether the pixels were identified by the CSR algorithm as overcast or partly cloudy (i.e., CER_2.1 > CER_1.6 > CER_3.7), a result consistent with the findings of *Nakajima et al.* [2010]. Further, partly cloudy pixels have significantly smaller CER than the overcast pixels; this is surprising given the expectation of a general overestimate of CER in marine boundary layer broken cloud scenes due to the use of plane-parallel forward models (e.g., *Zhang and Platnick* [2011]; *Zhang et al.* [2012]). However, analysis of Terra means (not shown) are more consistent with those studies in that CER_1.6 increases such that CER_1.6 ~ CER_2.1 > CER_3.7. We note that the Aqua 1.6 μ m channel, with native 500 m resolution, has 13 inoperable detectors. While the quality of the remaining detectors and their aggregation to the 1 km L1B file used by MOD06 is not suspect, further study of individual detector results is warranted. For users interested in looking at individual L2 CER_1.6 retrievals, **Table 2.5-3** indicates which aggregated 1.6 μ m 1 km pixel rows correspond to missing measurements in the MOD021KM L1B file. The pattern repeats with each 10 km along-track MODIS scan.

CER differences for April 2005, calculated as the monthly mean value of the overcast population minus the total population (overcast plus partly cloudy pixel population), is shown in **Fig. 2.5-5**. The overcast population’s gridded CER can be larger or smaller than the total population, depending on the location. A positive (red) difference indicates that the partly cloudy pixels have reduced the grid mean CER while negative (blue) differences indicate an increase in the partly cloudy mean CER. An interesting region is the tropical Atlantic, where overcast

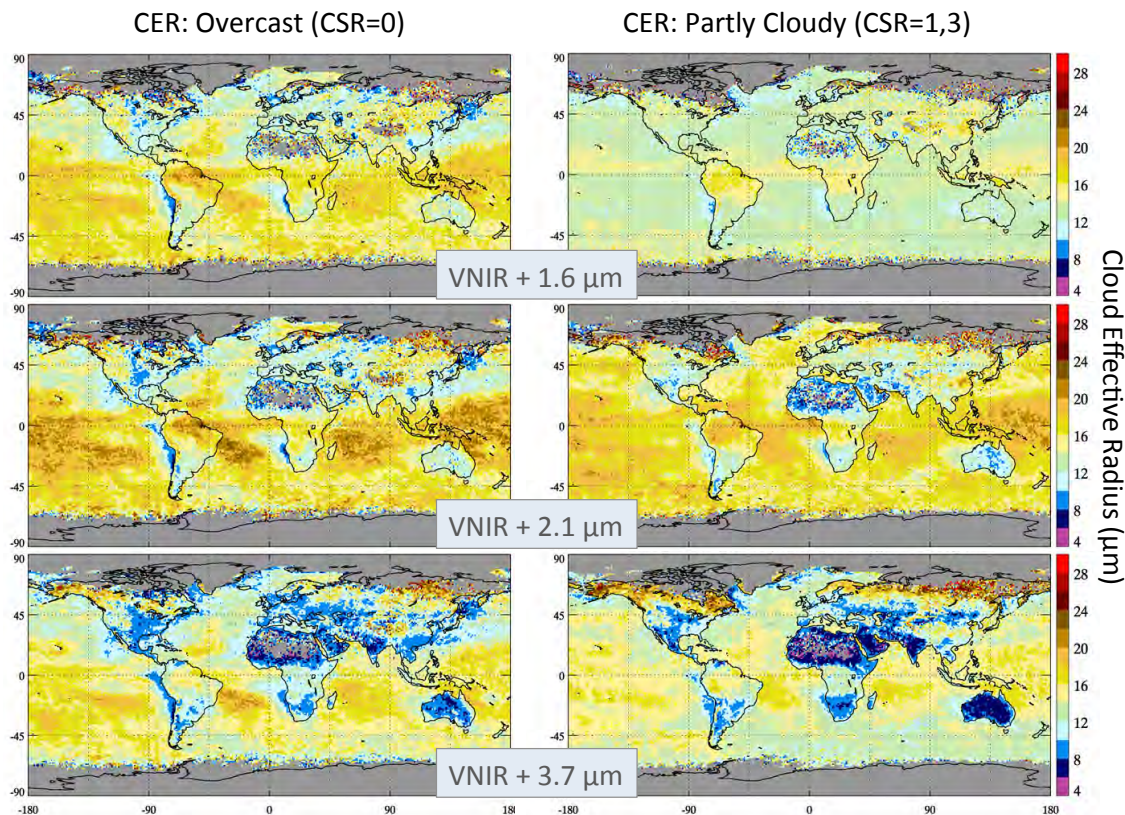


Figure 2.5-4. Aqua MODIS monthly (April 2005) mean 1° gridded effective radius for three separate SWIR/MWIR spectral channel combinations, filtered for liquid water pixels with cloud-top temperatures greater than 270K. Panels on the left are aggregated from pixels that the clear sky rostral (CSR) algorithm identifies as “overcast”; panels to the right are identified as “partly cloudy”.

pixel retrievals are larger than the total population in the west (near Brazil) but smaller in the central/eastern portion; this is especially pronounced for the CER_2.1 and CER_3.7 retrievals. While the reason for this gradient in sign is not obvious, the cloud retrieval fraction (not shown) has a gradient across that region with lower fraction (<0.1) corresponding to the positive difference and higher fraction (~ 0.4 and larger) corresponding to negative differences. This suggests that the differences in the tropical Atlantic may be related to cloud morphology. Significant gradients in sign are also seen over continents (e.g., North America).

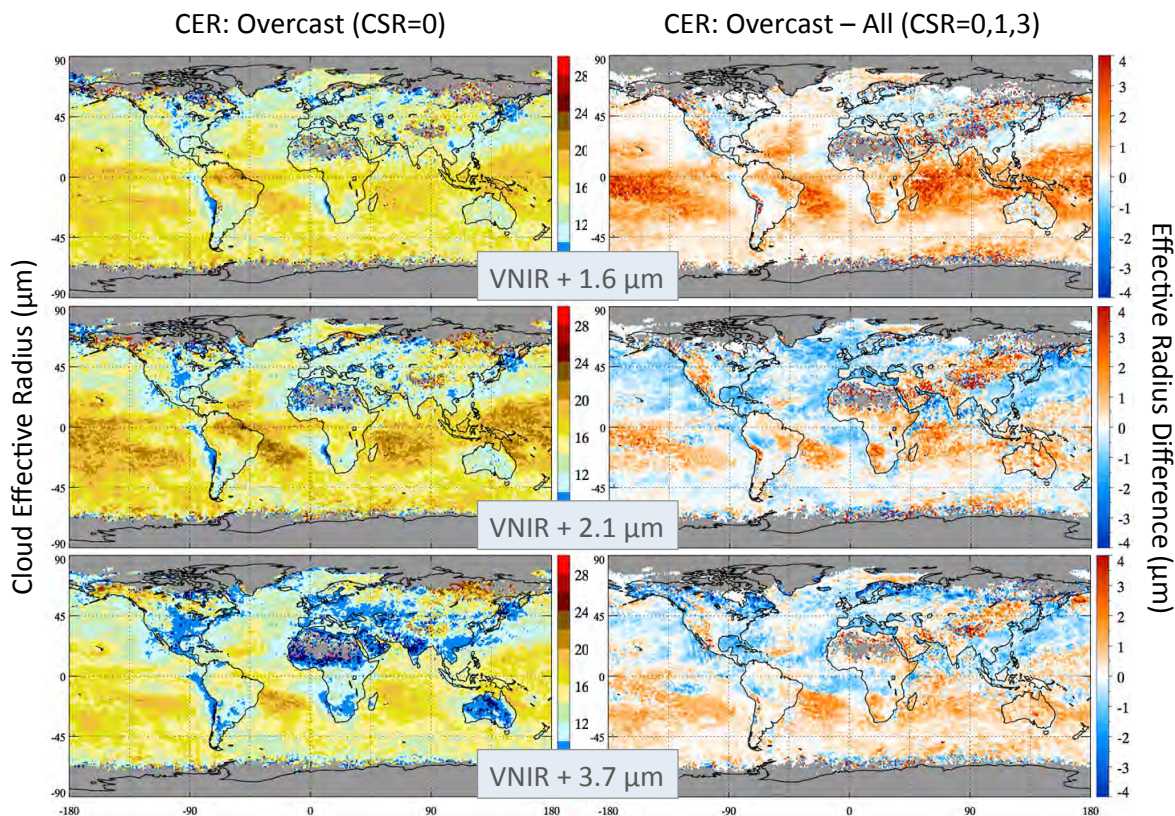


Figure 2.5-5. Same as Fig. 2.5-4 but for the right panels showing the difference CER calculated as the mean for overcast pixel population minus the mean for the total (overcast + partly cloudy) population.

Table 2.5-3. Missing band 6 ($1.6\mu\text{m}$) 1 km aggregated measurement data by pixel row (with beginning of data granule as row number 1).

Pixel Row	Status
1	Available
2	Available
3	Missing
4	Available
5	Available
6	Available
7	Missing
8	Missing
9	Available
10	Missing

2.6. Retrieval Failure Metrics (RFM)

In many cases, observed reflectances for the relatively non-absorbing VIS and NIR (VNIR) channels most sensitive to COT and the significantly absorbing SWIR or MWIR channels sensitive to CER will lie outside the pre-computed look-up table (LUT) solution space. Less frequently, observed reflectances may lie inside the solution space but yield multiple CER retrieval solutions, though these cases are typically only associated with optically thinner liquid water phase clouds. In these situations, the previously described standard solution logic (SSL) (Sect. 1.2) that is used to infer retrievals from the LUTs will fail to produce a successful COT/CER retrieval pair. In C5, pixels outside the solution space resulted in either partial COT retrievals (i.e., COT retrieved assuming a CER of 10 or 30 μm for liquid or ice phase clouds, respectively), with CER assigned fill values, or completely failed retrievals, with both COT and CER assigned fill values; pixels inside the solution space with multiple possible CER solutions were assigned the largest valid CER solution. In C6, an **alternate solution logic (ASL)** algorithm is now implemented that gives the COT and/or CER of the LUT grid point closest to the observation, as well as a *cost metric* indicating the relative distance of the observation from the LUT solution space. **Table 2.6-1** gives the new C6 **Retrieval_Failure_Metric (RFM)** SDS for pixels retrieved using the new alternate solution logic routine.

Table 2.6-1. The 3-element vector SDS used to provide information for pixels retrieved using the alternate solution logic.

Dataset	SDS
COT	Retrieval_Failure_Metric<_Wavelength*> (1)
CER	Retrieval_Failure_Metric<_Wavelength*> (2)
Cost Metric	Retrieval_Failure_Metric<_Wavelength*> (3)

* **Wavelength** is **16** or **37** for VNSWIR-1.6,-3.7 retrievals, **1621** for 1.6-2.1 retrievals, or omitted for VNSWIR-2.1 retrievals

2.6.1. Algorithm Overview

For C6, all pixels that lie outside the LUT solution space, or those that lie within yet have multiple possible retrieval solutions for CER, will be passed to the ASL code, which then selects the LUT grid point closest to the observation point as the final COT/CER solution. This is shown schematically by the 0.86 and 2.1 μm channel liquid water phase LUT in **Figure 2.6-1**, where the observation, denoted by the green diamond, is located well below the edge of the solution space. The vector **B** points from the observation to the closest LUT point which, for this pixel, would yield a retrieved COT of 26 and a 30 μm CER. The selection of the closest LUT point is made through the use of a cost metric, defined here as

$$\text{cost metric (CM)} = 100 \frac{|\mathbf{B}|}{|\mathbf{A}|} = 100 \frac{|\mathbf{C} - \mathbf{A}|}{|\mathbf{A}|} \quad (2.6-1)$$

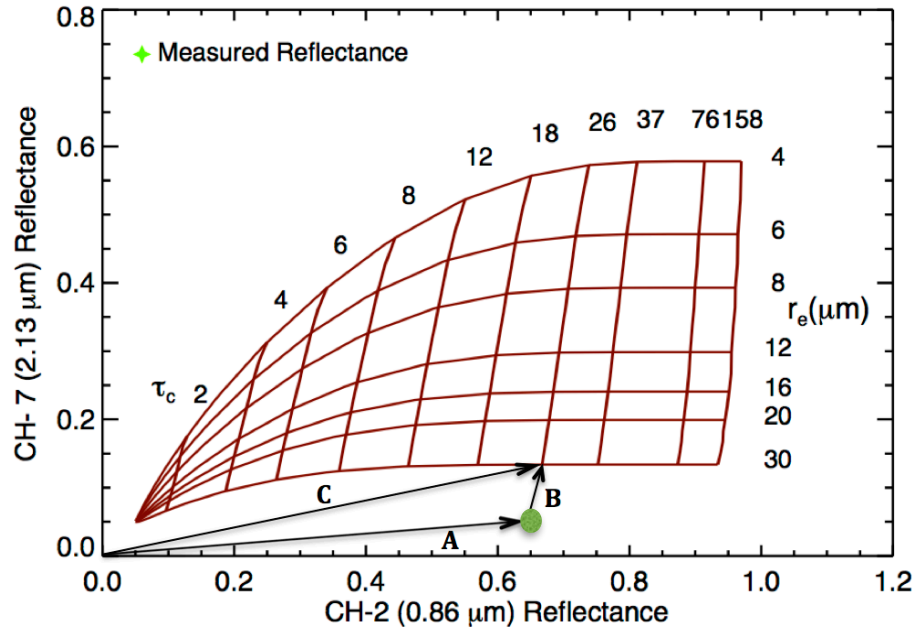


Figure 2.6-1. Bi-spectral solar reflectance look-up table (LUT) for a liquid water phase cloud over a land surface, with observed reflectance (green marker) outside the pre-computed solution space. Here, $\theta_0=26.75^\circ$, $\theta=61.8^\circ$, and $\Delta\Phi=176.78^\circ$, with a 5% surface albedo. Also shown are the vectors **A**, **B**, and **C**, used for computing the cost metric (Eq. 2.6.1).

where the vectors **A** and **C** are distances from origin of the observation point and LUT grid point, respectively, as shown in Fig. 2.6-1. The cost metric is essentially a measure of the percent relative distance between the observation and the closest LUT COT and CER grid point.

The ASL is applied to standard solution logic failure pixels in all cloud optical property retrieval channel combinations (i.e., combination of channel pairs with 1.6, 2.1, or 3.7 μm channel, and the 1.6 and 2.1 μm combination), with the resulting COT, CER, and cost metric assigned to the new RFM SDS. In order to make RFM assignments, the exterior of the LUT solution space is divided into four regions as shown by the shaded areas surrounding the liquid water phase LUT in **Figure 2.6-2**. Also shown are example pixel locations illustrating a successful full retrieval in the LUT interior (i.e., SSL solution, red diamond), a multiple CER solution retrieval within the LUT interior (ASL solution, blue diamond), and an alternate solution logic retrieval in the LUT exterior (ASL, green diamond).

Table 2.6-2 provides an overview of the RFM SDS assignments for each region of the solution space in Fig. 2.6-2. These SDSs will be assigned fill values for pixels having successful COT/CER retrieval pairs present in either the standard overcast SDSs or the partly cloud (PCL) SDSs (see Sect. 2.8). For all retrieval channel pairs except 1.6/2.1 μm , pixels with an x-axis reflectance larger than the maximum LUT reflectance (i.e, the green region to the right of the LUT in Fig. 2.6-2) are considered successful retrievals, with COT set to the maximum allowed value (note that the LUT COT maximum is 158 but the maximum reported value is limited to 150); thus, the RFM SDS for these pixels will contain fill values even though the

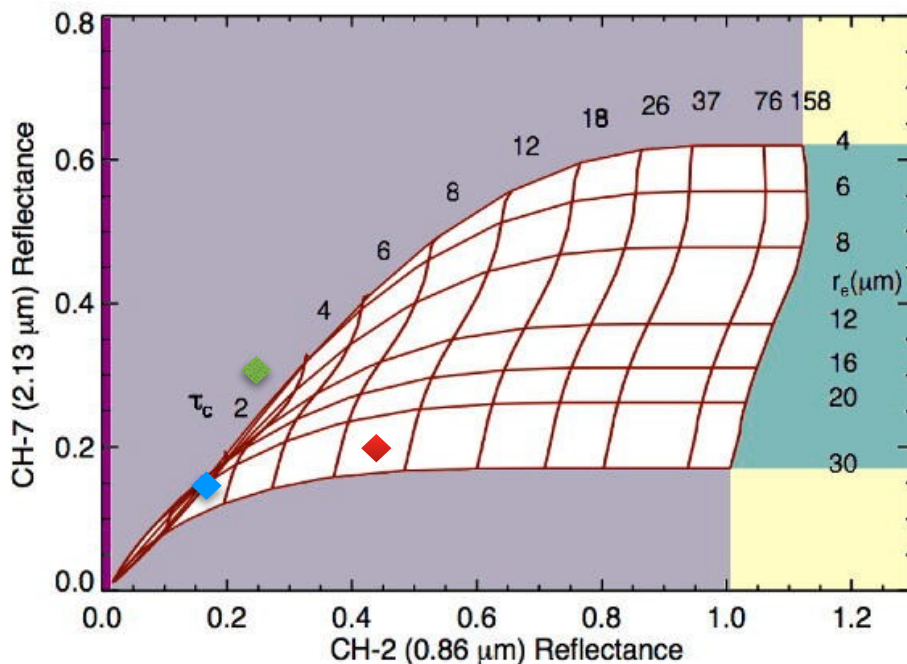


Figure 2.6-2. Retrieval space for a liquid phase cloud over an ocean surface, highlighting successful retrievals (solutions within the LUT space) and Retrieval Failure Metric (RFM) categories and cost metric assignments. Also shown are example pixels illustrating a successful retrieval (red marker), a retrieval outside the solution space (green), and a multiple CER solution retrieval (blue). The space is computed for $\theta_0=19.89^\circ$, $\theta=22.39^\circ$, $\Phi=174.4^\circ$ and a $7\text{ m}\cdot\text{sec}^{-1}$ wind speed.

Table 2.6-2. Mapping of retrieved solutions and cost metric from the solution space regions

Region	Band Pairs	Retrieval Failure Metric SDS		
		COT	CER	Cost Metric (CM)
Solution Space Interior				
Successful Solution	All	Fill	Fill	Fill
Multiple CER Solutions	All	Valid	Valid	≥ 0
Solution Space Exterior				
	All	Fill	Fill	Max
	All	Fill	Fill	Fill
	All	Nearest LUT COT	Nearest LUT CER	≥ 0
	1.6-2.1 μm	Fill	Valid	≥ 0
	All Others	Fill	Fill	Fill

solutions came from the ASL routine. For the 1.6/2.1 μm channel pair, because of substantial cloud particle absorption for the x-axis reflectance (1.6 μm channel), only the ASL CER retrieval is useful when the reflectance pair is in the green region of the solution space (see solution space plot in Sect. 1.2 as an example). Because there is no accompanying COT for this case, the CER solution is not considered a successful retrieval and therefore is not placed into the standard retrieval SDS; users interested in using the CER from this channel pair will find the value in the second element of the RFM vector as indicated in the above table.

Note also that, due to differences in the absorbing CER wavelengths (e.g., penetration depths, sensitivities to cloud inhomogeneity or 3D radiative effects, atmospheric transmittance corrections, etc.), the various spectral RFM SDSs should not be expected to contain identical populations of pixels. For instance, a pixel lying outside the VNSWIR-2.1 μm retrieval space, and thus requiring the alternate solution logic, may in fact lie inside the VNSWIR-1.6 μm or VNSWIR-3.7 μm retrieval spaces and yield successful COT/CER retrieval pairs. Spectral CER retrieval differences were discussed in Sect. 2.5 and in the recent literature [Nakajima *et al.*, 2010; Zhang and Platnick, 2011; Zhang *et al.*, 2012].

Figure 2.6-3 shows gridded liquid water retrieval failure statistics for Aqua MODIS May 2007 over the open ocean for the C6 VNSWIR-2.1 and -3.7 μm retrievals. Pixels identified by the CSR algorithm as not overcast (CSR integer values of 1 or 3, see Sect. 2.8) have the highest failure rates, with rates of about 50% in many remote ocean regions, whereas pixels that are likely overcast (CSR=0) have significantly smaller failure rates. It is also seen that the

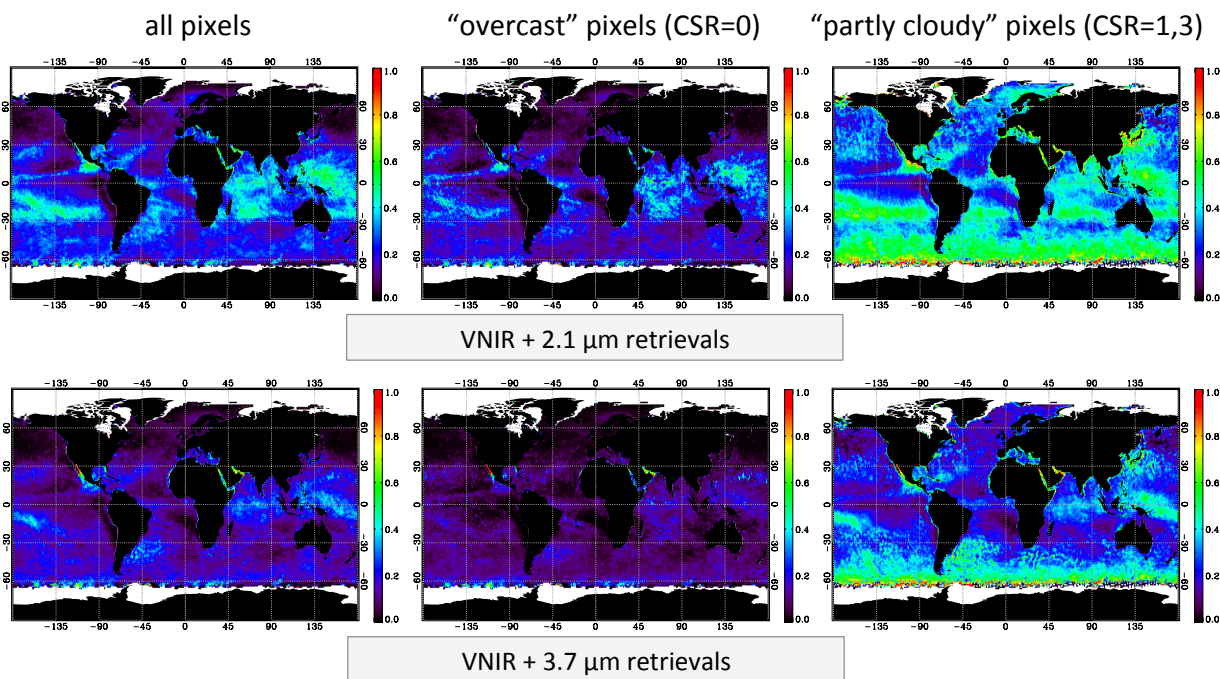


Figure 2.6-3. Gridded Aqua MODIS C6 cloud optical retrieval failure fractions for two band-pair retrievals for May 2007. The pixel population is for liquid water clouds over open ocean (no sea ice). [courtesy H.-M. Cho *et al.*, UMBC]

VNSWIR-2.1 μm retrievals have larger failure rates than the 3.7 μm retrievals, especially in the broken cloud marine BL regions. Thus, even if the C5 algorithm had attempted retrievals on this “partly cloudy” pixel population, a large fraction of these pixels would not have been retrievable (i.e., non-physical). Further, the large failure rates—likely indicative of a failure in the homogeneous cloud radiative model—strongly suggests caution in using the successful retrievals that do manage to occur in this pixel population. The RFM SDS is available to provide diagnosis of the retrieval failure mechanism (e.g., SWIR observations result in CERs that are smaller/larger than the LUT min/max values).

2.7. Improved Pixel-level Uncertainties

Estimates of the pixel-level uncertainty (RMS relative uncertainty normalized to percent) in cloud optical thickness, effective radius, and water path were added in C5 as first described by *Platnick et al.* [2004]. The uncertainty estimates are derived by propagating uncertainties applied to component error sources that are inherent to the retrieval. This is done by calculating partial derivative sensitivities (Jacobians)—for example, of cloud-top reflectance with respect to optical thickness at the two channels used in the retrieval, while holding the other parameters (effective radius, surface spectral reflectance, etc.) constant - coupled with estimates of cloud-top reflectance uncertainties associated with each error source. In this way, each error source uncertainty is mapped into cloud-top reflectance uncertainty which is then mapped into retrieval uncertainty. The partial derivatives can be calculated from the radiative transfer LUTs. For C6, error sources include the following four categories: instrument calibration, atmospheric corrections, surface spectral reflectance, and other forward model error sources. While not part of the reported uncertainty budget, work on flagging, understanding, and perhaps improving 3-D error sources is ongoing.

The mapping of measured and model uncertainty components into retrieval uncertainty is represented by the covariance matrix

$$\left(\mathbf{K}^T \mathbf{S}_y^{-1} \mathbf{K}\right)^{-1} + \sum_i \left(\mathbf{K}^{-1} \mathbf{K}_{b_i}\right) \mathbf{S}_{b_i} \left(\mathbf{K}^{-1} \mathbf{K}_{b_i}\right)^T, \quad (2.7-1)$$

where \mathbf{S}_y and \mathbf{S}_b are the measurement and model covariance matrices, respectively. Partial derivatives in \mathbf{K} map cloud-top reflectance error into retrieval error (e.g., matrix elements $\partial R_\lambda / \partial \tau$ and $\partial R_\lambda / \partial r_e$). For our two channel–two retrieval problem the matrices are of size 2x2. The elements of \mathbf{K}_b contain partial derivatives of reflectance with respect to some channel-dependent model parameter (spectral surface albedo, spectral above-cloud atmospheric transmittance, etc.); the i -index summation is over each independent model error source. The \mathbf{K}_b matrices are diagonal with the exception of atmospheric transmittance errors due to water vapor uncertainties that affect each channel in a correlated manner.

The matrix formulation of Eq. 2.7-1 can be derived from standard variance algebra and only keeping first order (linear) terms. It is equivalent to the retrieval error covariance matrix formulation used in optimal estimation retrievals [*Rodgers, 2000*] when the *a priori* information is removed (i.e., given large error covariance values). The difference in our retrieval solution and an optimal estimation solution is that we search through the entire solution space instead of iterating through the solution space starting with the *a priori* vector and constrained by its covariances. If the *a priori* error covariance is large enough to effectively remove its constraint, the two solutions are equivalent as long as the cloud optical retrieval space is unique, i.e., the optimal estimation iteration does not get trapped in a cost function local minimum; similarly, the resulting retrieval uncertainties would be equivalent as well.

Table 2.7-1. Mapping of retrieved solutions and cost metric from the solution space regions in Figure 2.6-2 to the Retrieval Failure Metric (RFM) SDS.

Category	Error Source	Specification
Ancillary Data Related to Surface Reflectance	MODIS-derived A MCD43B3 for land/snow surfaces, sfc. wind speed in Cox-Munk calculation	$\pm 15\%$ of A MCD43, $\pm 20\%$ of sfc. wind speed for water surfaces
Above-Cloud Atmospheric Corrections (water vapor, all bands)	Above-cloud ancillary Precipitable Water (PW) vapor	$\pm 20\%$
	Above-Cloud Atmos. Transmittance LUT	Provided in spectral transmittance LUT, derived from profile variances
Above-Cloud Atmospheric Corrections (O MODIS Band 1)	Analytic transmittance formula	$\pm 20\%$
Observations	Measurement Relative Error	Max. of value associated with L1B Uncertainty Index or 2% (bands 1-4) and 3% (bands 5-7)
Model	Cloud model error from size distribution effective variance (Standard deviation from = 0.05 to 0.2 (0.1 nominal) for liquid water and ice clouds, provided in cloud LUTs, derived from analytic gamma distributions
	Water surface reflectance model error from using Cox-Munk reflectances averaged over wind direction	Standard deviation of 4 vector wind directions provided in cloud LUTs
3.7 μm -specific cloud reflectance and cloud/surface emission	ΔT_c	
	ΔP_c	± 50 mb
	ΔPW	$\pm 20\%$
	ΔT_{sfc}	$\pm 1\text{K}$
	$\Delta F_0 / F_0, \Delta F_0$ lation	- $\sim 4\%, 0.42 \text{ W-m}$

C5 processing assumed the instrument radiometric calibration relative uncertainty was fixed at 5% in all VNIR/SWIR spectral channels, the relative uncertainty in water vapor (from NCEP GDAS) used in above-cloud atmospheric corrections was set to 20%, and the spectral

surface albedo uncertainty associated with the MOD43B product was 15% in all spectral channels and in all land locations.

In C6 processing, error sources were modified/expanded to include: (a) scene-dependent calibration uncertainty that depends on the band and detector-specific uncertainty index provided in the L1B file, (b) new model error sources derived from the look-up tables, which includes sensitivities associated with wind direction and speed over the ocean and uncertainties in liquid and ice size distribution effective variance, (c) thermal emission uncertainties in the 3.7 μm band associated with cloud and surface temperatures that are needed to extract reflected solar radiation from the total radiance signal, (d) uncertainty in the solar spectral irradiance at 3.7 μm , and (e) addition of stratospheric ozone uncertainty in the visible (MODIS Band 1) atmospheric correction. These source uncertainty assignments used in C6 pixel-level retrieval uncertainty calculations are summarized in **Table 2.7-1**. Retrieval uncertainties of course depend on the solar and view zenith geometry in addition to the table items.

With respect to item (a) above, in C6 we now use the L1B pixel-level uncertainty index (**UI**) that ranges from 0-15 as an indication of relative measurement uncertainty. A constant uncertainty of 5% was used for all channels in C5; the fixed value was intended also to include nominal model error. To cover a broad range of relative uncertainty for all MODIS channels, the uncertainty is calculated from the UI as follows:

$$\text{uncertainty (\%)} = \text{specified_uncertainty} \times \exp\left(\frac{\text{UI}}{\text{scale_factor}}\right) \quad (2.7-2)$$

where the values of *specified_uncertainty* and *scale_factor* depend on the spectral band (see **Table 2.7-2**). With this definition, relative uncertainties range between 1.5% (UI=0) and 12.8% (UI=15) for bands 1 and 2, between 1.5% (UI=0) and 30% (UI=15) for bands 5-7, and between 0.56% (UI=0) and 24% (UI=15) for band 20. These relative radiometric uncertainties, assumed to be uncorrelated spectrally, are used in the computation of optical property retrieval uncertainty. While useful for capturing scene-dependent calibration sensitivities, we set a minimum allowable relative radiometric uncertainty of 2% for bands 1 and 2 and 3% for bands 5, 6, 7 and 20.

Table 2.7-2. Attributes for converting uncertainty index (UI) to relative uncertainty (%).

Band	CWL (μm)	<i>specified_uncertainty</i>	<i>scale_factor</i>
1	0.67	1.5	7
2	0.86	1.5	7
5	1.24	1.5	5
6	1.64	1.5	5
7	2.13	1.5	5

As was the case in C5, the uncertainty in cloud optical thickness over the ocean is typically smallest when the COT lies between 3 and 20, increasing with optical thickness (due to saturation in VNIR reflectance and thereby increased sensitivity to error source uncertainties affecting the knowledge of cloud-top reflectance), and for small optical thickness due to uncertainty in surface reflectance and atmospheric corrections. In all cases, the radiometric uncertainty component to the overall pixel-level uncertainty is much smaller in C6 than what was assumed (5%) in C5. In contrast, the uncertainty in cloud effective radius (ΔCER) over the ocean is the largest for small effective radius (due to atmospheric correction and calibration uncertainty) and at large effective radius (due to Cox-Munk surface reflectance uncertainty), with the most accurate effective radius retrievals lying in the sweet spot between about 14 and 24 μm .

Figures 2.7-1 and 2.7-2 show C5 and C6 retrievals of COT and CER, and their uncertainties, for a data granule over Greenland and nearby ocean where clouds overly sea ice. This example highlights the pixel-level uncertainties over land, ocean, and ice surfaces, and for a wide variety of optical properties and phase.

2-D and 1-D uncertainty distributions are shown in **Figs. 2.7-3 and 2.7-4**, respectively, for COT, CER_21 and CER_37 liquid water retrievals for a data granule off Baja California (2 July 2008). All successful retrievals from the ‘overcast’ pixel population are included in the distribution, and therefore a variety of view angles are included. As expected, based on the solution space figures previously discussed (e.g., Fig. 2.6-1), the largest COT uncertainties in Fig. 2.7-3 occur at small and large COT where the solution space contours are most closely spaced, while the largest uncertainties for CER occur at the smaller COTs before the SWIR/MWIR reflectances asymptote; however, CER_37 uncertainties also peak at the larger COT due to emission components (dashed green line in the right hand panel of Fig. 2.7-4).

The overall take-away message from Figs. 2.7-1–2.7-4 is that asking for a single metric for the optical retrieval uncertainty is an ill-posed question. The answer depends on surface type, solar/view geometry, atmospheric state, surface and cloud temperature (3.7 μm), and most importantly where the solution lies in the COT, CER space.

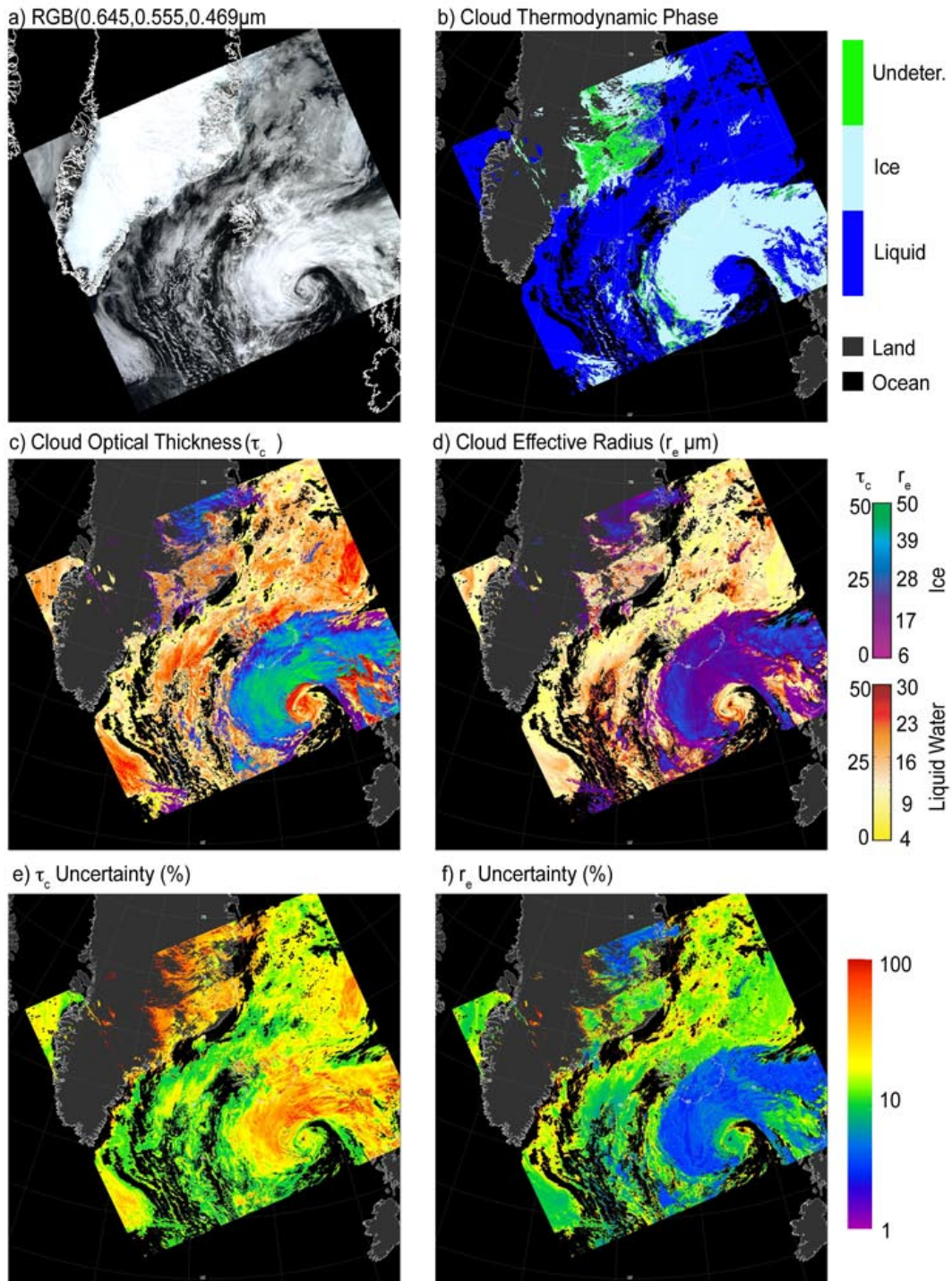


Figure 2.7-1. C5 COT and CER retrievals using the 2.1 μ m channel and their uncertainties. From an Aqua MODIS data granule over Greenland (2008, day 183, 1400 UTC).

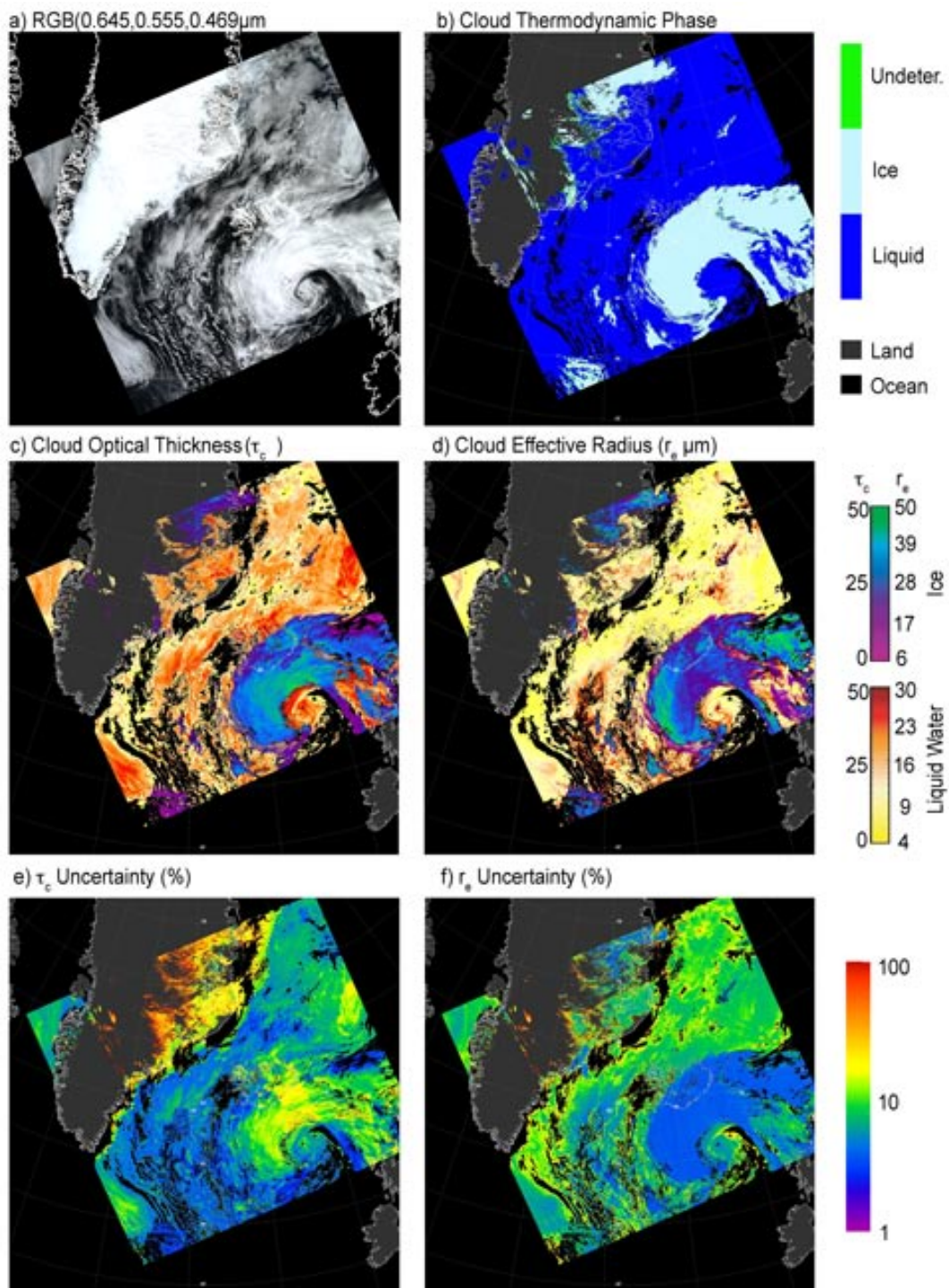
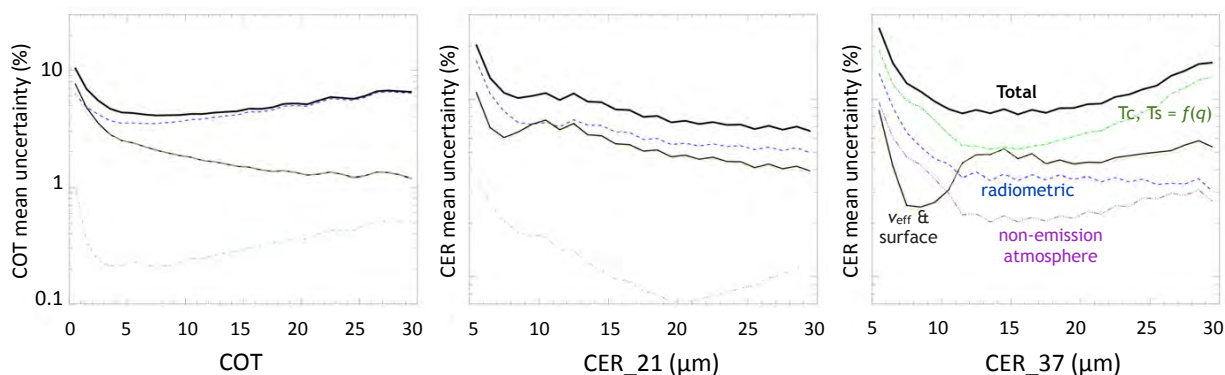
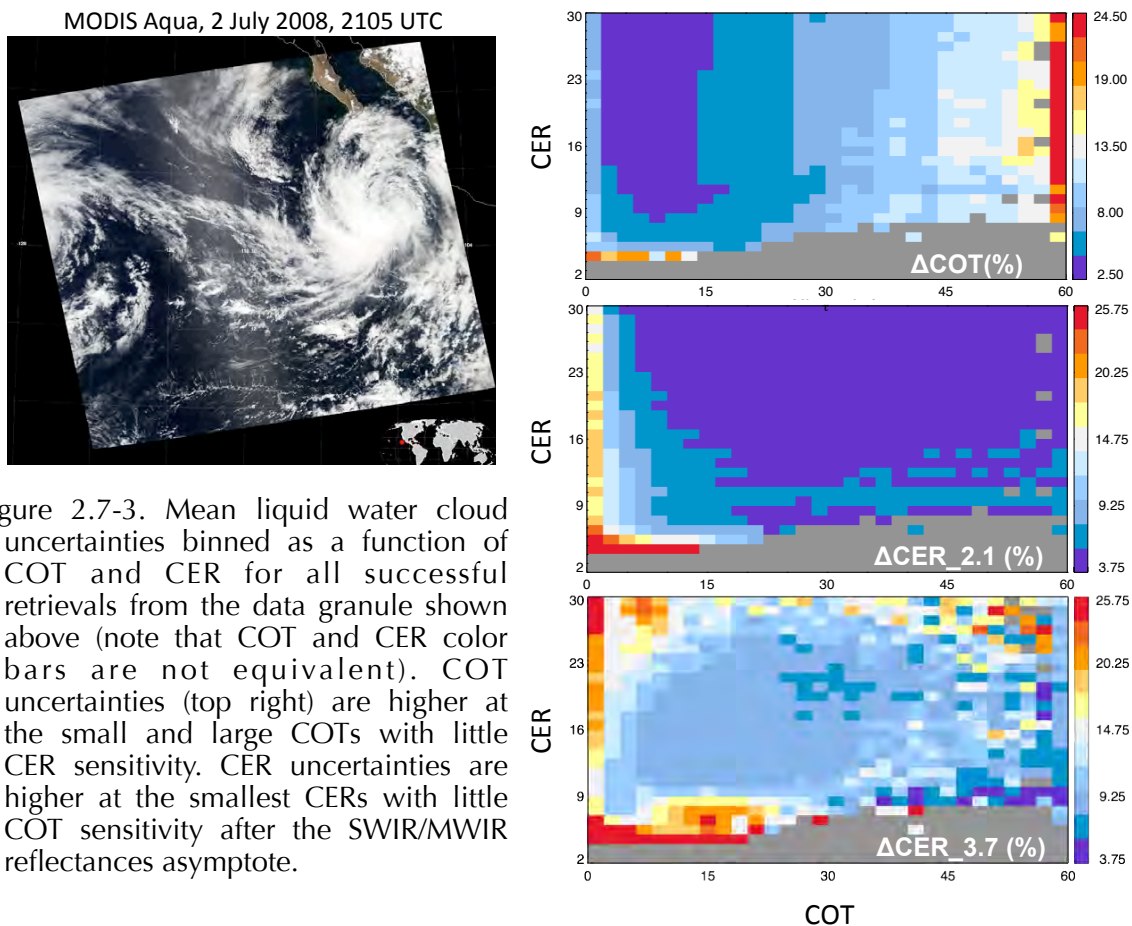


Figure 2.7-2. Same as Fig. 2.7-1 but for C6 retrievals. Uncertainties are generally reduced in C6 calculations due to the smaller instrument calibration uncertainty assignment, especially for high optically thick clouds where other error sources are more minor.



2.8 Clear Sky Restoral and Processing of Pixels Flagged as Partly Cloudy

Correctly identifying cloudy pixels appropriate for the MOD06 cloud optical and micro-physical property retrievals is accomplished in large part using results from the MOD35 1 km cloud mask tests (note there are also two 250 m sub-pixel cloud mask tests that can independently report the 1 km cloudy designations as clear sky with a separate set of bits). However, because MOD35 is by design clear sky conservative (i.e., it seeks to identify “not clear” pixels), certain situations exist in which pixels identified by MOD35 as “cloudy” are nevertheless likely to be poor retrieval candidates. For instance, near the edge of clouds or within broken cloud fields, a given 1 km MODIS field of view (FOV) may in fact only be partially cloudy. This can be problematic for the MOD06 retrievals because in these cases the assumptions of a completely overcast homogenous cloudy FOV and 1-dimensional plane-parallel radiative transfer no longer hold, and subsequent retrievals will be of low confidence. Furthermore, some pixels may be identified by MOD35 as “cloudy” for reasons other than the presence of clouds, such as scenes with thick smoke or lofted dust, and should therefore not be retrieved as clouds. With such situations in mind, a Clear Sky Restoral (CSR) algorithm was introduced in C5 that attempts to identify pixels expected to be poor retrieval candidates. **Table 2.8-1** provides SDS locations for CSR and partly cloudy pixels.

Table 2.8-1. SDS locations for the CSR flag and partly cloudy pixels.

Dataset	SDS Location
CSR Flag	Quality_Assurance_1km
Partly Cloudy Pixels	<Parameter_Name>_PCL

2.8.1. Algorithm Overview

All MOD35 “cloudy” pixels pass through the CSR logic shown in **Fig. 2.8-1** with the resulting CSR designations stored as bit values within the **Quality_Assurance_1km** SDS (see the Quality Assurance [QA] Table in **Appendix B** for specific bit locations). There are four possible outcomes of the CSR algorithm:

- *Overcast Cloudy (CSR = 0)*: Pixels that are not identified as clear or partly cloudy by the CSR tests. Note: cloud mask clear pixels will also have CSR=0.
- *Not Cloudy (CSR = 2)*: Pixels identified by spatial reflectance variability and spectral curvature tests as likely dust, smoke, or sunglint pixels, and are restored to clear sky.
- *Partly Cloudy (CSR = 3)*: Pixels over water surfaces that are identified by sub-pixel 250 m MOD35 cloud mask variability as partly cloudy.
- *Cloud Edge (CSR = 1)*: Overcast cloudy pixels (CSR=0) with “clear” adjacent neighbors (i.e, adjacent pixels with MOD35 “not cloudy” or CSR=2)

Figure 2.8-1a

Clear-Sky Restoral (CSR) Logic

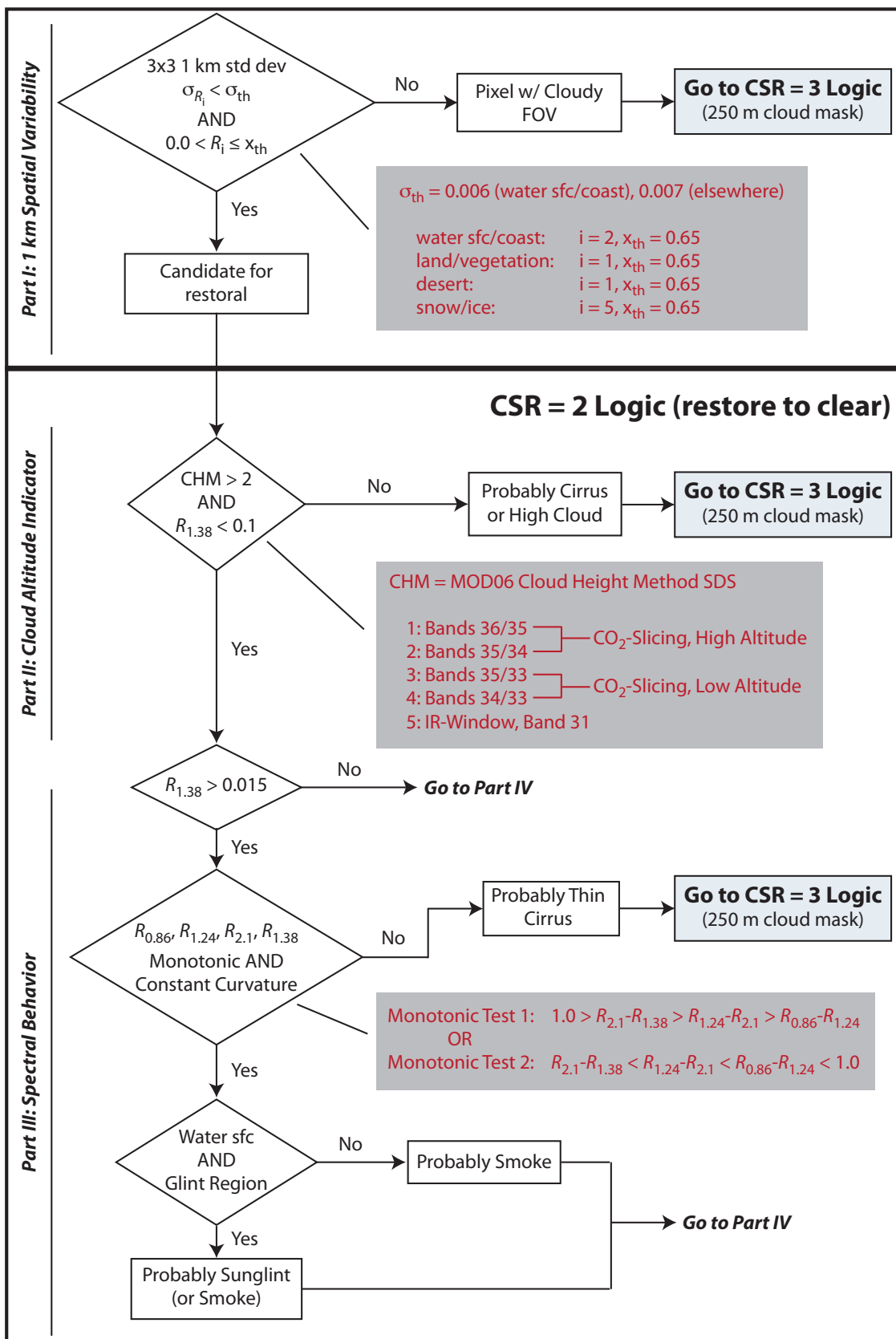
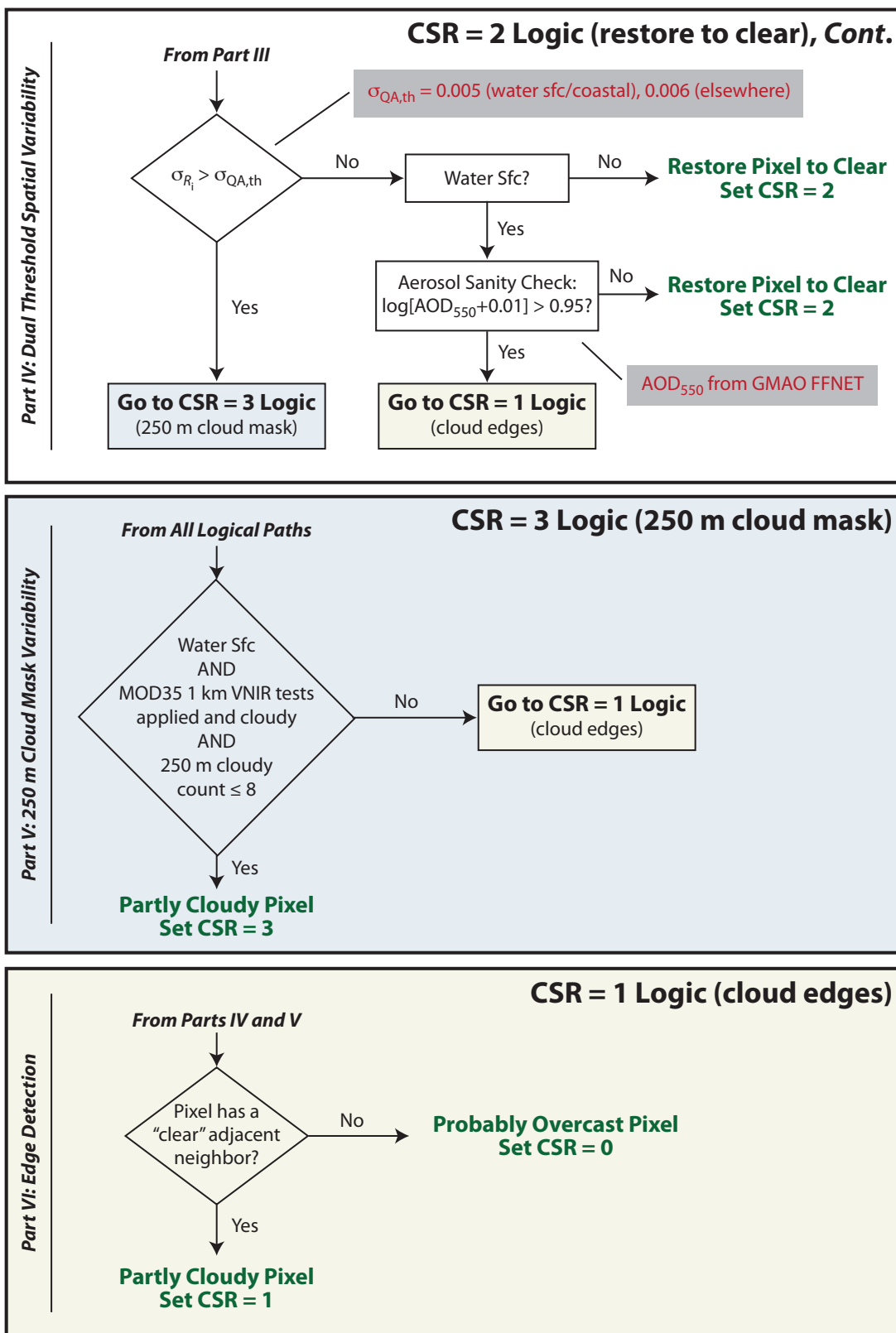


Figure 2.8-1b **Clear-Sky Restoral (CSR) Logic (Cont.)**

Note that for C6, optical and microphysical property retrievals are attempted on pixels designated as CSR=1,3 as well as CSR = 0 (overcast), as described below. Further, by default, all cross track pixels of along-track columns 2 and 1353 are set to PCL (CSR=1) because there is no available cloud mask for pixels 1 and 1354.

2.8.2. Changes for Collection 6

The C6 CSR algorithm is nearly identical to its C5 counterpart, with only minor modifications and enhancements. C6 updates related to CSR include:

- *New SDSs for partly cloudy retrievals.* Previously in C5, all pixels identified by CSR as partly cloudy (CSR=1,3) or not clear (CSR=2) were restored to clear sky, and the corresponding cloud retrieval SDSs were assigned fill values. For C6, only pixels having CSR=2 are restored to clear sky and assigned fill values. Pixels identified by the CSR=1 or 3 tests that also have successful cloud optical and microphysical property retrievals now populate the partly cloudy *PCL* SDSs. All pixels with unsuccessful or partially successful retrievals populate the Retrieval Failure Metric *RFM* SDSs (**Section 2.6**). Mapping of pixel retrieval outcome status to SDS assignments and *RFM* assignment details may be found in **Appendix B**.
- *Enhanced thin cirrus handling.* The CSR logic has been modified in an attempt to minimize cases of thin cirrus clouds being restored to clear sky via CSR=2 tests. Previously, the altitude indicator test (see *Part II*, Figure 2.8-1) relied on the inferred cloud thermodynamic phase, which may erroneously identify the optically thin edges of cirrus clouds as liquid water phase. For C6, cloud thermodynamic phase is replaced by the cloud height method (CHM) used for cloud top (CT) altitude determination. CT altitude is determined using one of five “methods,” namely the infrared (IR) window technique or one of four CO₂ slicing band combinations. For high altitude clouds such as thin cirrus, the two longer-wavelength CO₂ slicing bands, which are more sensitive to the upper troposphere, are typically the bands that converge to a CT solution; their use by the cloud top algorithm for a given pixel is thus considered a high-confidence indicator of high altitude clouds.
- *New sanity check for low altitude stratocumulus clouds.* For C6, the CSR logic now includes a sanity check to minimize cases of low altitude, homogeneous stratocumulus clouds over water surfaces being restored to clear sky via the CSR=2 dual threshold spatial variability test (*Part IV*). The spatial reflectance variability of such clouds can be relatively small, and may result in positive CSR=2 outcomes. This sanity check applies a threshold to 550 nm aerosol optical depth (AOD) inferred from a multi-spectral feed-forward neural network algorithm developed by NASA’s Global Modeling and Assimilation Office (GMAO) (Arlindo da Silva, personal communication). CSR=2 pixels in which the GMAO retrieval yields large AOD are assumed to be unphysical for typical

aerosols, and are instead likely indicative of clouds; such pixels are thus reassigned to overcast, i.e., CSR=0.

2.8.3. Examples

Figure 2.8-2 shows an example granule from Aqua MODIS, observed on 9 April 2005 (1050 UTC) over the Black Sea, Turkey, and eastern Mediterranean Sea. What appears to be lofted dust is apparent over the Mediterranean at the bottom of the true color RGB (0.66-0.55-0.47 μm) in (a), and is identified as “cloudy”, or not clear, by the MOD35 cloud mask (b). This feature, however, is correctly identified by the CSR algorithm (c), and is restored to clear sky by the CSR=2 tests. Note also the CSR=1 cloud edge pixels, visible as the regions of dark blue outlining the cloud features in the CSR image.

Also of interest is the fraction of restored pixels, that is, the number of 1 km pixels identified as CSR=2, divided by the number of MYD35 “not clear” pixels. A global map of the mean restored pixel fraction in a 1° grid is shown in **Fig. 2.8-3 a** for MODIS Aqua, April 2005. For context, the MYD35 cloud fraction is shown in **Fig. 2.8-3 b**. April is an active time of year for Atlantic Saharan dust outbreaks (e.g., *Kaufman et al.* [2005]), a region of high restoral fraction in the figure. Likewise, a high fraction region to the southeast of Argentina may be associated with Patagonia dust transport [*Gasso et al.*, 2010; *Johnson et al.*, 2011] though such events typically occurs farther south. Also of note is the high restoral fractions in the Arabian Sea, Persian Gulf, and Red Sea. This could result from the CSR algorithm detecting a combination of both dust and sunglint signals. It is very likely that the elevated fraction off Baja California is due almost extensively to sunglint detection by the CSR algorithm. Fi-

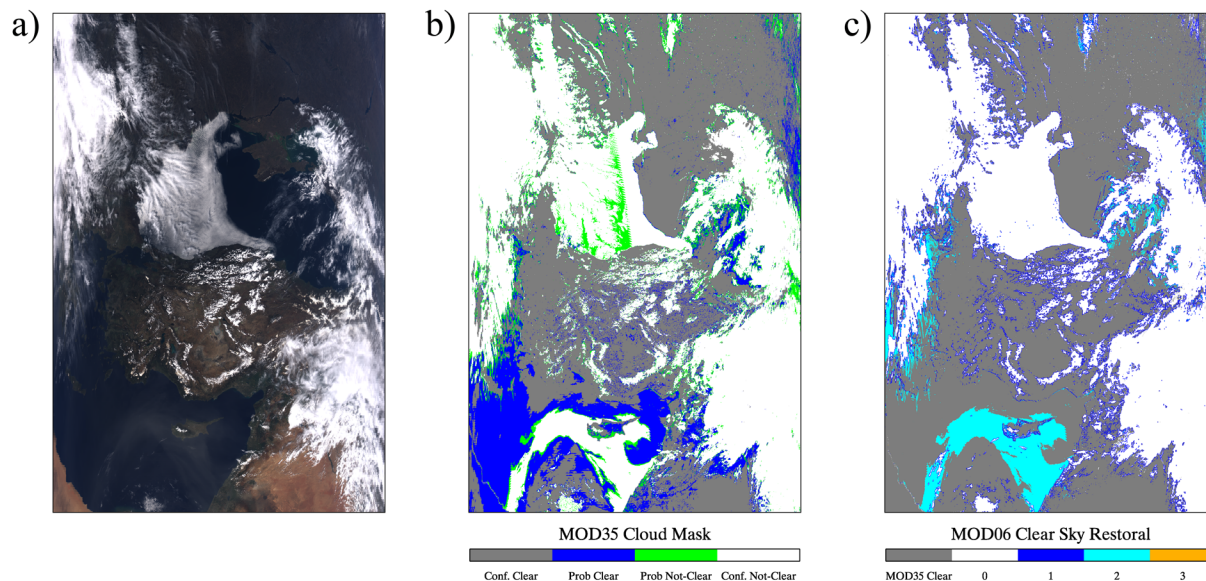


Figure 2.8-2. Left: True color RGB (0.66-0.55-0.47 μm) from an Aqua MODIS granule on 9 April 2005 (1050 UTC). Center: MOD35 cloud mask results. Right: MOD06 C6 CSR algorithm results (0: overcast; 1: cloud edge; 2: restored to clear sky; 3: partly cloudy).

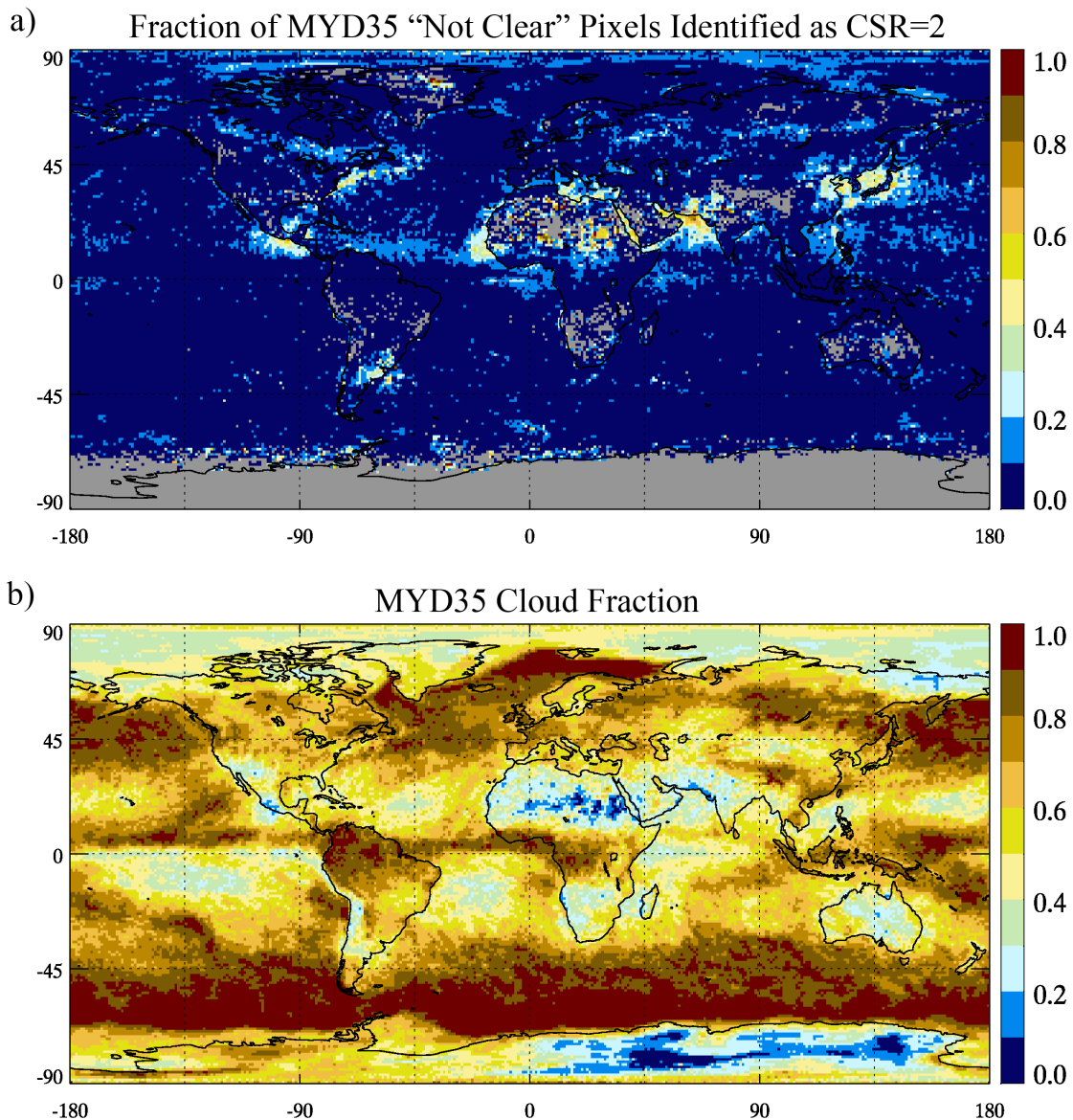


Figure 2.8-3. Monthly fraction of MYD35 “not clear” pixels identified as CSR=2 (a) and MYD35 cloud fraction (b) for April 2005 Aqua MODIS.

nally, the high fraction off the East China Sea and Sea of Japan may be dust and/or aerosol associated with pollution. While we have not quantified the incidence of clear sky false positives by the CSR algorithm, high restoral fractions appear to be occurring in sensible locations.

2.8.4. Known Issues

Thin Cirrus

Despite modifying the altitude test (Part II, see Fig. 2.8-2a) to minimize cases of thin cirrus clouds being restored to clear sky, thin cirrus continues to be problematic for the CSR algorithm. In **Fig. 2.8-4** for example, on 6 April 2005 (1830 UTC) Aqua MODIS observed a layer of very thin cirrus clouds off the coast of the southeastern United States, as shown within the red outlined region of the true color RGB (0.66-0.55-0.47 μm). The 1.38 μm reflectance image in **Fig. 2.8-5 a** indicates the extent of this cirrus, as well as the optical thinness of the layer (note the reflectance is logarithmically scaled from 0.001 to 0.1). Much of this region is identified as “cloudy” by the C6 cloud mask in **Fig. 2.8-5 b**, even though MOD35 has some difficulty identifying the entire cirrus layer. Moreover, portions of what is identified as cloudy by MOD35 are subsequently restored to clear sky by the CSR=2 tests, as indicated by the light blue regions.

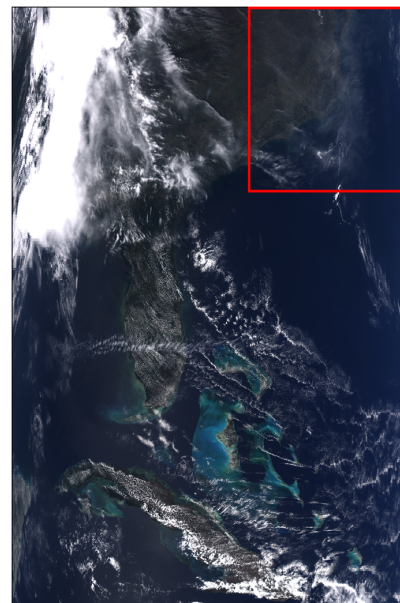


Figure 2.8-4. *Thin cirrus clouds.* On April 6, 2005 (1830 UTC), thin cirrus clouds were observed by Aqua MODIS off the SE coast of the Florida, as shown within the red outlined region in the true color RGB image.

Comparing to C5, shown in **Figs. 2.8-5 c**, the C6 CSR algorithm offers little improvement for this scene. The cirrus is sufficiently optically thin that the CO₂-slicing cloud height methods evidently do not converge on a solution, thus the cloud

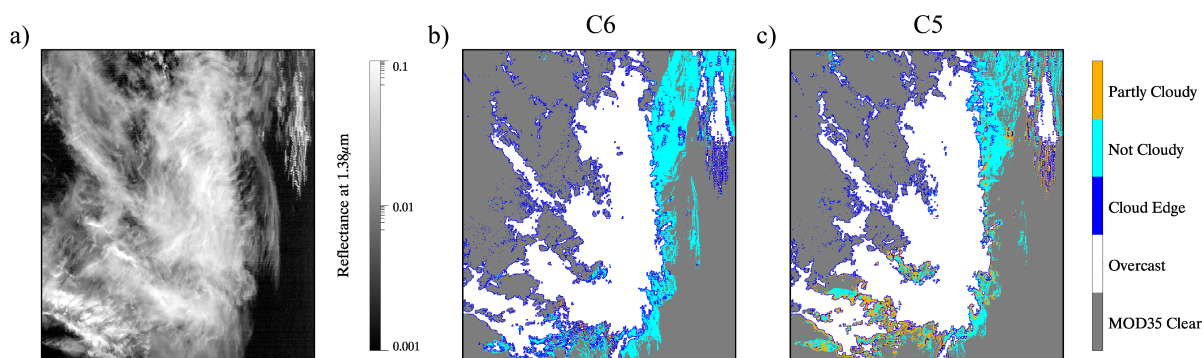


Figure 2.8-5. Reflectance at 1.38 μm (a), corresponding to the red outlined region in Figure 2.8-4, showing both the full spatial extent of the cirrus as well as the optically thin nature of the layer. The MOD35 cloud mask with MOD06 CSR results are shown for both C6 and C5 in (b) and (c), respectively. Colors other than gray denote MOD35 “not clear” pixels.

altitude test (Part II) does not indicate the presence of high-altitude clouds, and the cirrus is restored to clear sky via the spectral behavior (Part III) or dual-threshold spatial variability (Part IV) tests. It is worth noting, however, that many of these thin cirrus pixels are likely to

yield unsuccessful cloud optical and microphysical property retrievals, as the small reflectances associated with such clouds often lie outside the standard MOD06 retrieval space. Thus very thin cirrus clouds often will not be aggregated to level-3 global statistics regardless of the CSR results.

Heavy Dust

Dust, particularly when transported over water surfaces, is often identified as “not clear” by the MOD35 cloud mask, and may also remain identified as overcast after passing through the CSR tests. A remarkable example of this occurred on 1 July 2008, over the Persian Gulf. Here, a particularly strong dust event was observed by Terra MODIS (0720 UTC), as shown within the red outlined region in the true color RGB (0.66-0.55-0.47 μm) in **Fig. 2.8-6**. The C6 MOD35 cloud mask in **Fig. 2.8-7 a** clearly identifies much of this dust over the Gulf as “cloudy.” The C6 CSR algorithm does correctly restore much of this dust to clear sky (i.e., CSR=2), as indicated by the light blue regions. However, large portions remain overcast (i.e., CSR=0), in part via the dual-threshold spatial variability test (Part IV), and MOD06 cloud optical and microphysical property retrievals are subsequently attempted on these pixels.

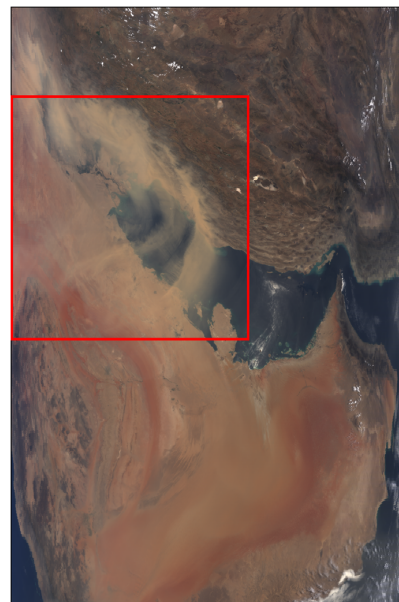


Figure 2.8-6. *Heavy dust*. On 1 July 2008 (0720 UTC), a strong dust storm was observed by Terra MODIS over the Persian Gulf, shown above by the true color RGB image.

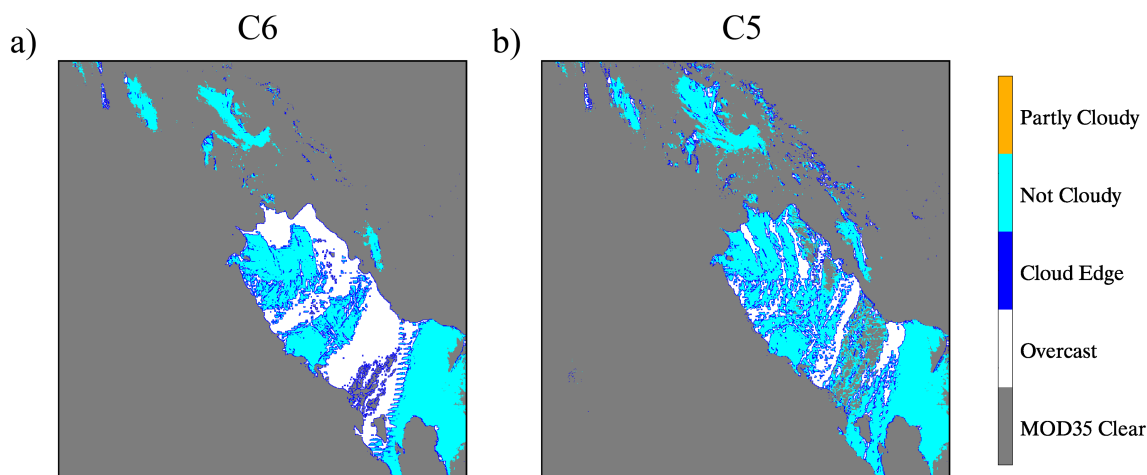


Figure 2.8-7. *Heavy dust identified as “overcast” cloud*. The C6 MOD35 cloud mask with MOD06 CSR results, corresponding to the red outlined region in Figure 2.8-6, are shown in (a). For comparison, the respective C5 results are shown in (b). Colors other than gray denote MOD35 “not clear” pixels.

Furthermore, disregarding cloud mask differences, the C6 CSR algorithm in fact restores less dust to clear sky than does C5, the MOD35 and CSR results of which are shown in **Fig. 2.8-7b**. The apparently worsened performance of C6 is primarily a result of the new GMAO AOD sanity check, which is applied to all pixels over water surfaces having CSR=2. Dust pixels previously restored to clear sky in C5 are now returned to “overcast” in C6 because the inferred AOD exceeds the sanity check threshold. This dust event was also observed three hours later by Aqua MODIS, albeit obliquely, with similar cloud mask and CSR results (not shown). It persisted over this region for several consecutive days, and is clearly evident in the Terra and Aqua MODIS visible imagery throughout that time.

Sunglint

While the MOD35 cloud mask attempts to account for sunglint using elevated thresholds for the visible/near-infrared (VIS/NIR) reflectance and reflectance ratio tests in regions where sunglint is expected, and the CSR algorithm is designed to identify glint using spatial variability and altitude indicator tests, occasionally glint regions are bright enough to not only be identified as “not clear” by the mask but also to emerge from the CSR algorithm as overcast. In **Fig. 2.8-8**, for example, Aqua MODIS observed an exceptionally strong sunglint case on 10 April 2005 (0630 UTC), over the Gulf of Thailand, outlined by the red box in the true color RGB (0.66-0.55-0.47 μm) image. This “mega-glint” region, with 0.66 μm reflectances around or greater than 1.0 (0.86 μm is largely saturated), is bright enough to be identified as “cloudy” by the VIS/NIR reflectance test, despite taking the sunglint processing path in MOD35 (which uses the elevated reflectance thresholds); interestingly, the VIS/NIR reflectance ratio test also identifies much of this glint region as cloudy, notwithstanding saturation at 0.86 μm .



Figure 2.8-8. *Sunglint*. On 10 April 2005 (0630 UTC), an exceptional sunglint scene was observed by Aqua MODIS over the Gulf of Thailand, shown above by the true color RGB.

The reflectances in this sunglint region are so large, in fact, that these pixels do not even meet the criteria to be candidates for restoral to clear sky, as they clearly exceed the reflectance threshold applied in *Part I* and are thus not processed through the CSR=2 logic. Similarly, the MOD35 250 m VIS/NIR tests also indicate clouds, negating the CSR=3 logic, and the pixels either remain “overcast” or are identified as “cloud edge” (i.e., CSR=1), as shown in **Fig. 2.8-9 a**. Comparing to its C5 counterpart, shown in **Fig. 2.8-9 b**, any differences in C6 are largely a result of improved performance by the cloud mask.

It is worth noting, however, that many of the pixels associated with this “mega-glint” region ultimately yield unsuccessful cloud optical and microphysical property retrievals and are

therefore not aggregated in the L3 dataset regardless of the CSR results. Moreover, sunglint of this magnitude is fortunately not a common occurrence. Nevertheless, caution should be taken when using MOD06 retrievals in locations where sunglint is expected.

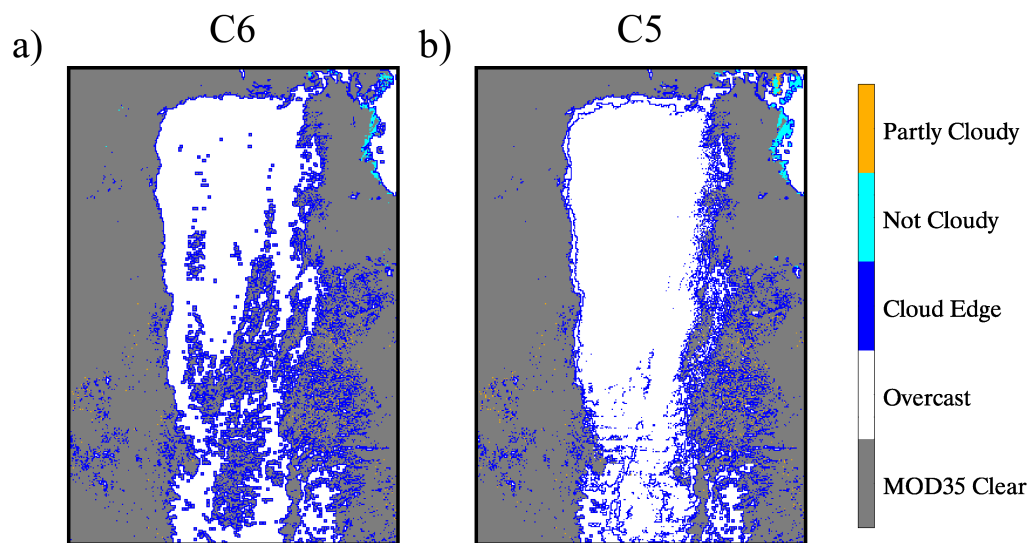


Figure 2.8-9. *Sunglint identified as overcast clouds.* The C6 MOD35 cloud mask with MOD06 CSR results, corresponding to the red outlined region in Fig. 2.8-8, are shown in (a). For comparison, the respective C5 results are shown in (b). Colors other than gray denote MOD35 “not clear” pixels.

2.9. New Cloud Radiative Transfer Look-up Tables (LUTs)

The use of asymptotic theory for optically thick atmospheres in C5 and earlier version has been replaced with a straightforward use of cloud reflectance and emissivity look-up tables containing a complete range of optical thickness values. For optically thick atmospheres, the resulting reflectance computations are the same to those obtained from asymptotic theory, but this change simplifies the maintenance of the Fortran 90 code such that multiple paths (optically thin and optically thick atmospheres, followed by interpolation between them) are no longer required. In addition, more optically thin COTs are included in the LUTs.

In order to minimize angular interpolation errors during the retrieval process, only the multiple scattering (**MS**) component to the cloud-top bidirectional reflectance function (**R**) is stored in the LUTs. During the retrieval process, the single scattering (**SS**) component is constructed on the fly from the phase function which is also stored in the LUT, and added to the MS component. The SS calculation uses the exact pixel-level angular information. This is done for six MODIS channels centered at 0.65, 0.86, 1.24, 1.62, 2.13, and 3.70 μm , as a function of optical thickness, effective radius, solar zenith angle (θ_0), satellite viewing angle (θ), relative azimuth angle between the sun and the satellite ($\Delta\phi$) for ocean/water surfaces with several wind speeds (u) and for land surfaces with a zero surface albedo. **Table 2.9.1** below shows the number of grid points and the range of parameter values that went into making these LUTs.

Table 2.9-1. Range of Values of Look up table (LUT) parameters.

Variable	# of grid points and Range
τ_c	34 (0, 159)
r_e	18 [2, 30] liquid water phase 12 [5, 60] ice phase
θ_0	33 [0, 82]
θ (deg)	28 [0, 67]
$\Delta\phi$ (deg)	37 [0, 180]
u	3 [3, 7, 15]

In addition, reflected flux, transmitted flux and spherical albedo for the above six channels and the one centered at 11 μm (band 31) were also computed and included in the land LUT for use with a Lambertian surface whose albedo is added separately (see next section). Ocean LUTs also contain effective surface and cloud emissivities for channels centered at 3.7 and 11 μm ; for the land LUTs, these effective emissivities are calculated from the flux and spherical albedo data.

Addition of ocean/water LUTs and separation of R into the MS part is a significant difference between C6 LUTs and those from previous collections. The single scattering part (SS) of the total reflectance is added dynamically to the interpolated MS part, for a particular sun-satellite geometry, during the retrieval. To facilitate this process a separate LUT with single scattering properties of both ice and liquid water clouds were also generated. **Figure 2.9.1** illustrates the MS part and the total bidirectional reflectance as a function of viewing zenith angle in the forward and backscattered directions for MODIS band 1 ($0.65 \mu\text{m}$). It is evident that the MS part of the reflectance is a smoother function compared to the full (MS + SS) reflectance, and thus certainly minimizes the interpolation errors. The details of the radiative transfer calculations, discretization of the LUT variables, and the individual SDSs included in

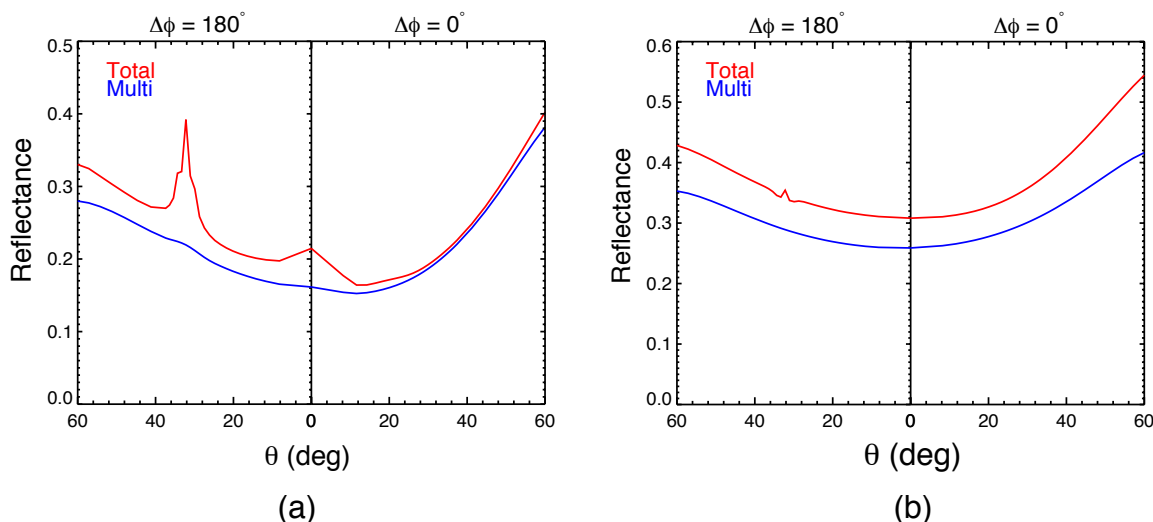


Figure 2.9-1. Total reflectance (red line) and MS part (blue line) of the TOA reflectance for MODIS band 1 ($\lambda=0.65 \mu\text{m}$) with $\text{COT}=4.14$, $\theta_0=35.7^\circ$ and (a) liquid water clouds with $\text{CER}=10 \mu\text{m}$, and (b) ice clouds with severely roughened aggregated columns and $\text{CER}=60 \mu\text{m}$. The MS part of the reflectance is a much smoother than the total reflectance that includes single plus multiple scattering.

the LUTs are summarized in the sections below. More details about the wind speed interpolated ocean reflectances can be found in Sect. 2.2.

2.9.1 Radiative Transfer Calculations

Radiative transfer calculations, in the absence of an atmosphere were based on the discrete ordinates radiative transfer (DISORT) model developed by *Stamnes et al.* [1988, 2000], and the calculations were performed with 64 streams (32 up and 32 down). We have incorporated the Cox-Munk ocean bidirectional reflectance model implemented in libRadTran 1.4 [*Mayer et al.*, 2005] into DISORT in order to model the ocean bidirectional surface reflectance. Subsequently, we have conducted a thorough investigation of the accuracy and the efficiency of DISORT with Cox-Munk ocean BRDF, and have modified DISORT routines to achieve a great deal of improvement of our simulations over an ocean surface (see Sect. 2.2).

The modeled atmosphere-surface system we have used in the simulations over ocean consists of three adjacent plane parallel homogeneous layers having a cloud layer at the top, at a height of 8 km above the surface. All the Rayleigh layers except the lowest layer below the cloud layer are combined to form the second layer, and a boundary-layer, coarse-mode, aerosol layer with an optical depth of 0.1 is combined with the lowest Rayleigh layer to form the third layer. Single scattering albedo and asymmetry parameter for the aerosol layer were taken from the MOD04/MYD04 aerosol retrieval ATBD and a Henyey-Greenstein model was assumed for the aerosol phase function calculations. A zero surface albedo is used for LUTs that are incorporated into land surface retrievals; these LUTs provide fluxes and spherical albedos that allow the incorporation of ancillary surface spectral albedo datasets (see Sect. 2.3); the LUT are modeled using a single cloud layer and no Rayleigh or aerosol layers.

Mie calculations were performed to compute the single scattering properties of liquid water clouds assuming a Modified Gamma drop size distribution,

$$n(r) = N_0 r^{(1-3v_{eff})/v_{eff}} \exp\left(\frac{-r}{r_{eff} v_{eff}}\right) \quad (2.9.1)$$

with effective variance $v_{eff} = 0.10$ and a known index of refraction database. In computing the optical constants for liquid water, we used the complex refractive indices tabulated by *Hale and Querry* [1973] for wavelengths in the range $0.25 \leq \lambda \leq 0.69 \mu\text{m}$, *Palmer and Williams* (1974) for $0.69 < \lambda \leq 2.0 \mu\text{m}$, and *Downing and Williams* [1975] for $\lambda > 2.0 \mu\text{m}$. As explained in Sect. 2.1, for ice clouds, the ice crystal habit (severely roughened aggregated columns) developed by Ping Yang et al. at Texas A&M was used and input to **Eq. 2.9.1** with $v_{eff} = 0.10$ (same as liquid water distribution). Computed single scattering properties (single scattering albedo, asymmetry parameter, extinction efficiency, phase function) for both ice and liquid water clouds are stored in a separate LUT. The δ -fit method by *Hu et.al.* [2000] is implemented to truncate the phase functions and a 64-term Legendre polynomial expansion of the phase function is then used. Input parameters, optical thickness and the single scattering albedo, are then adjusted with the truncation factor, f (fraction of photons in the forward peak due to diffraction) and expressed as

$$\omega' = \frac{(1-f)\omega}{1-f\omega} \quad \tau' = (1-f\omega)\tau, \quad (2.9.2)$$

where,

$$\tau = \frac{Q_e(r_e, \lambda)}{Q_e(r_e, \lambda_{0.65})} \tau_c, \quad (2.9.3)$$

The MS part of the reflectance was extracted from DISORT calculations after the SS part is subtracted from the total reflectance. For a particular sun-satellite geometry, the SS part of

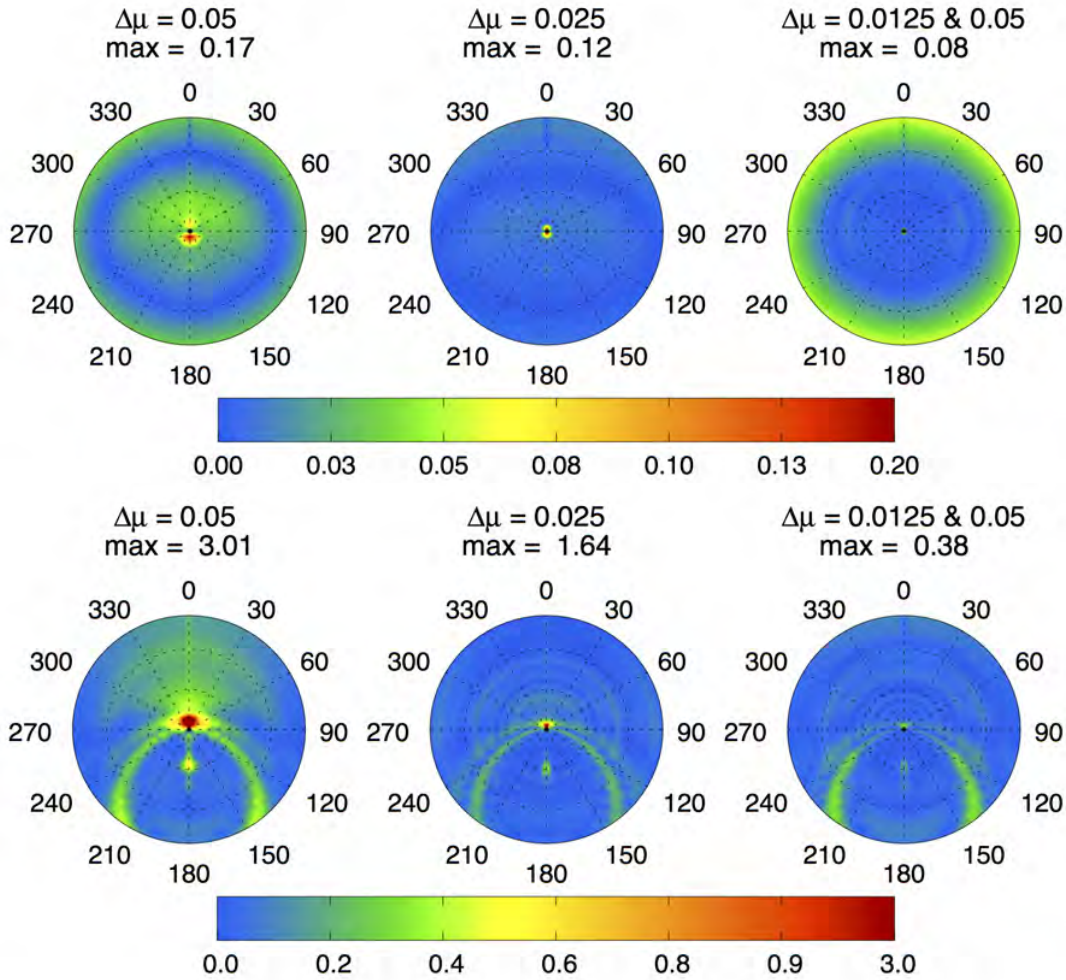


Figure 2.9-4. Maximum interpolation error for $COT=4.14$, $\theta_0=35^\circ$ for the MS part of the reflectance. The top row is for ice clouds with $CER=60\mu m$ (severely roughened aggregated columns), and the bottom row is for liquid water clouds with $CER=10\mu m$. The hybrid discretization scheme (right column) has the least error near nadir.

the bidirectional reflectance (R_{ss}) is then added back dynamically to the interpolated MS part by interpolating the phase function in scattering angle space (Θ) and using the formula,

$$R_{SS}(\tau, r_e, \mu, \mu_0, \Delta\phi) = \frac{1}{4(\mu + \mu_0)} * \frac{\omega}{(1.0 - f\omega)} * PF(\Theta, r_e) (1 - \exp[-\tau'(1/\mu + 1/\mu_0)]), \quad (2.9.4)$$

where PF is the phase function. Over land surfaces, the effect of surface albedo is incorporated to compute the reflectance according to the formula described by King (1987) and given by

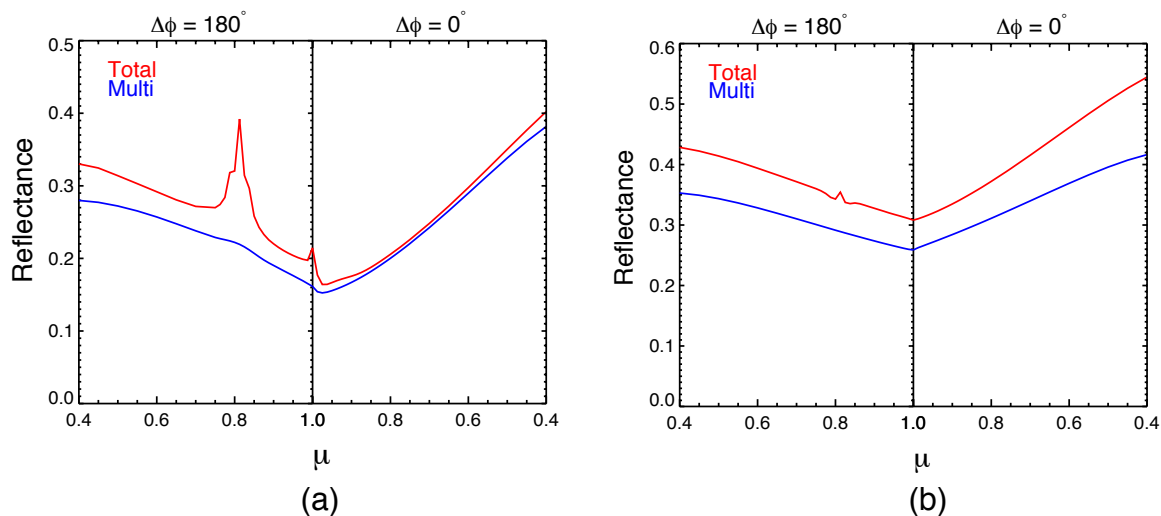


Figure 2.9-2. Same as Fig. 2.9-1 but as a function of $\mu = \cos\theta$. The MS part of the reflectance function exhibits more linearity in μ space.

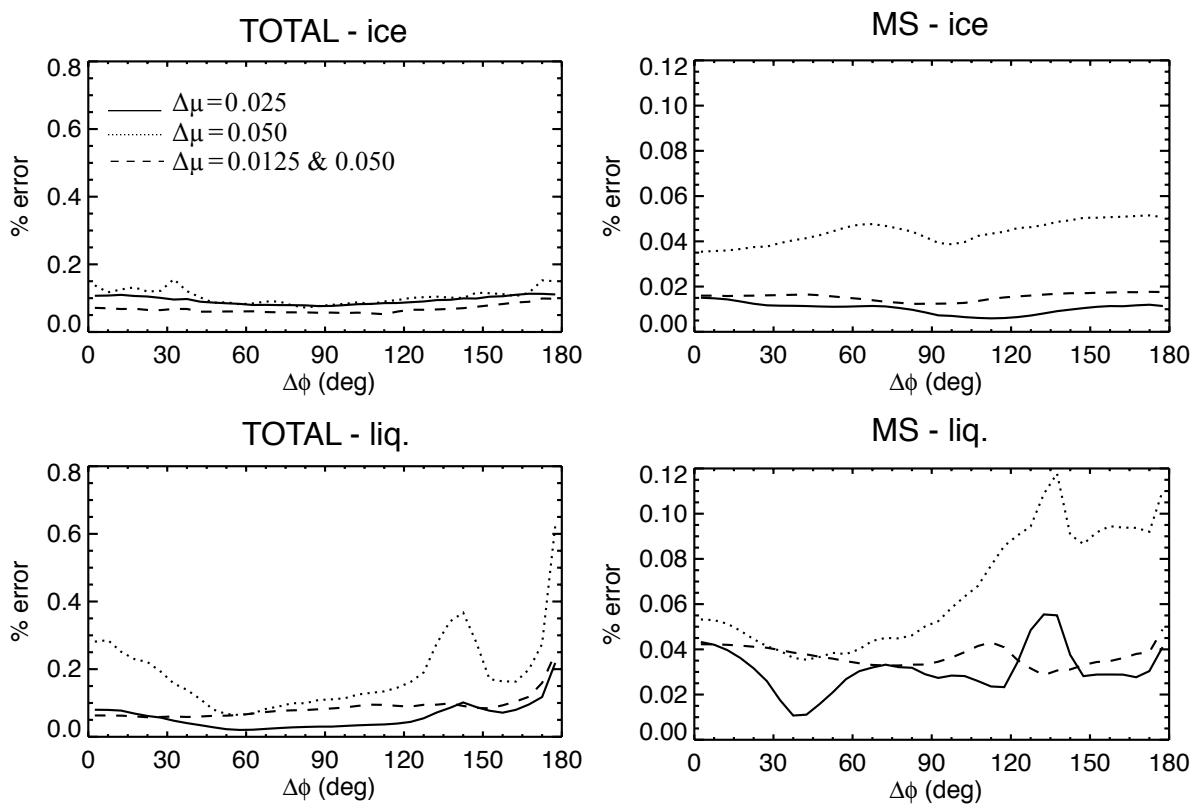


Figure 2.9-3. Median band 1 LUT interpolation error (over all COT, CER, μ , and μ_0 entries) vs. $\Delta\phi$ for total reflectance (left panels) and the MS part of the reflectance (right panels) for an ice cloud with severely roughened aggregated columns and CER = 60 μm (top row), and a water cloud with CER = 10 μm (bottom row). Note the order of magnitude error reduction in the MS plots. The legend indicates the discretization scheme (see text).

Table 2.9-2. Grid point values of the lookup table (LUT) parameters.

Quantity	# of points	Grid point values
COT	34	0.05, 0.10, 0.25, 0.5, 0.75, 1.0, 1.25, 1.5, 1.75, 2.0, 2.39, 2.87, 3.45, 4.14, 4.97, 6.0, 7.15, 8.58, 10.30, 12.36, 14.83, 17.80, 21.36, 25.63, 30.76, 36.91, 44.30, 53.16, 63.80, 76.56, 91.88, 110.26, 132.31, 158.78
CER (μm)	18 12	2, 4, 5, 6, 7, 8, 9, 10, 12, 14, 16, 18, 20, 22, 24, 26, 28, 30 (liquid water cloud) 5, 10, 15, 20, 25, 30, 35, 40, 45, 50, 55, 60 (ice cloud)
μ	28	0.40, 0.45, 0.50, 0.55, 0.60, 0.65, 0.70, 0.75, 0.7625, 0.7750, 0.7875, 0.8000, 0.8125, 0.8250, 0.8375, 0.8500, 0.8625, 0.8750, 0.8875, 0.900, 0.9125, 0.9250, 0.9375, 0.9500, 0.9625, 0.9750, 0.9875, 1.0
μ	33	0.15, 0.20, 0.25, 0.30, 0.35, 0.40, 0.45, 0.50, 0.55, 0.60, 0.65, 0.70, 0.75, 0.7625, 0.7750, 0.7875, 0.8000, 0.8125, 0.8250, 0.8375, 0.8500, 0.8625, 0.8750, 0.8875, 0.900, 0.9125, 0.9250, 0.9375, 0.9500, 0.9625, 0.9750, 0.9875, 1.0
$\Delta\phi$ (deg)	37	[0, 180] equally spaced with increments of 5°
u	3	3, 7, 15

$$R_{A_g}(\tau, r_e, \mu, \mu_0, \Delta\phi) = R_0(\tau, r_e, \mu, \mu_0, \Delta\phi) + \frac{A_g t(\tau, r_e, \mu) t(\tau, r_e, \mu_0)}{1 - A_g \bar{r}(\tau, r_e)}, \quad (2.9.5)$$

where t is the transmitted flux, \bar{r} is the spherical albedo, and A_g is the surface albedo. R_0 is the Lambertian reflectance with zero surface albedo. Over ocean/water surfaces, for each wind speed, the average multiple scattering part of the bidirectional reflectance and average effective cloud and surface emissivities over four wind directions 0° , 90° , 180° and 270° were computed to generate three separate ocean LUTs for the three wind speeds.

2.9.2 Discretization of LUT parameters and interpolation error

As previously indicated, the MS part of the reflection function is much smoother than the total reflection function. Furthermore, as shown in **Fig. 2.9-2**, the MS reflection function is more nearly linear as a function of $\mu = \cos\theta$, than it is as a function of θ (cf. Fig. 2.9.1). Taking this into account, we conducted a lengthy interpolation error investigation to determine the best angular discretization scheme. For cloud optical thickness, we followed the same scheme suggested by *A. K. Heidinger* [2013, personal communication] where optical thickness values greater than 2 are discretized in equally intervals in log space. The MS reflection and flux/albedo calculations are discretized in solar and satellite zenith angles as a function of μ . **Fig. 2.9.3** shows the median interpolation error for full reflectance LUTs and MS reflectance LUTs with three different discretization schemes for μ and μ_0 : (1) equally spaced with $\Delta = 0.025$, (2) equally spaced with $\Delta = 0.05$ and (3) a hybrid scheme with intervals of 0.0125 and 0.05 at larger and smaller μ , respectively (see **Table 2.9-2**). A decrease in interpo-

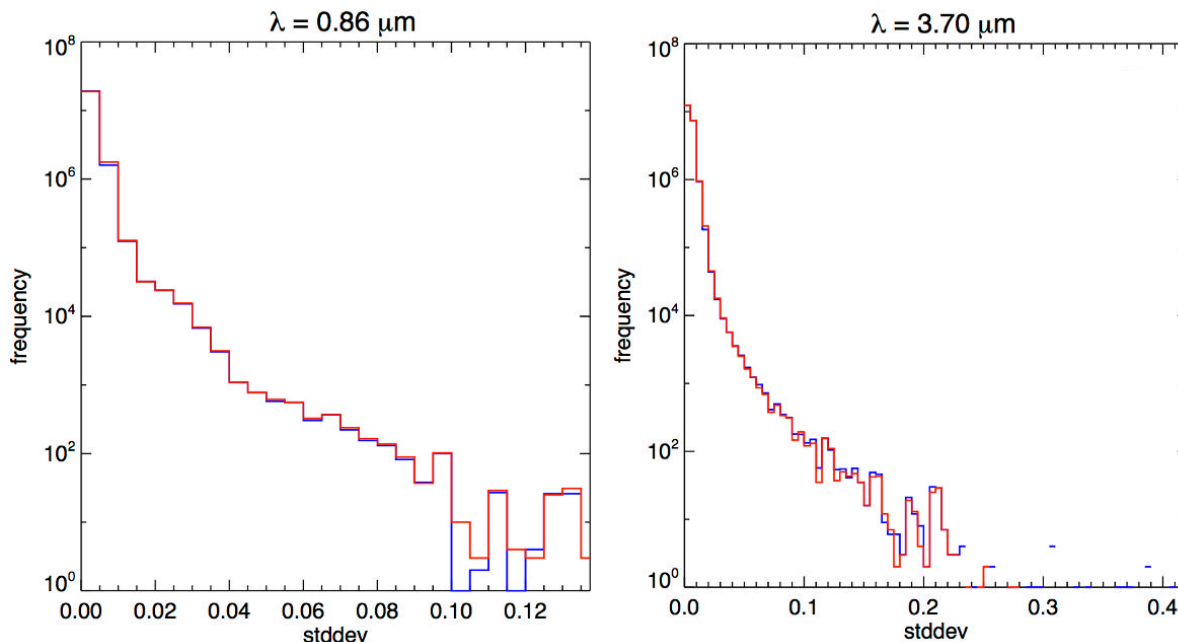


Figure 2.9-5. Histograms of standard deviation calculated for the ocean LUT with $u = 3 \text{ ms}^{-1}$ (blue line) and from the land LUT (red line) for MODIS bands 2 and 20. No significant difference can be seen over about 3 orders of magnitude.

lation error by an order of magnitude can be noted with the MS reflectance LUTs. The hybrid discretization scheme (broken lines in Fig. 2.9-3) produced the lowest maximum error for the MS LUTs and minimize the interpolation error near $\mu = 1.0$, as shown by the polar plots in **Fig. 2.9-4**. As such, we implemented the hybrid discretization scheme in μ space for both solar and satellite zenith angles, while the relative azimuth angle was discretized in degree space. **Table 2.9-2** summarizes the grid points for COT, CER, μ , μ_0 and $\Delta\Phi$ used in constructing the C6 LUTs.

2.9.3 Effective variance and wind direction uncertainties

To incorporate an effective variance model error in the retrieval uncertainty calculations, the total reflectances for clouds having droplet size distributions with effective variances of 0.05 and 0.20 were also computed for both ice and liquid water. Then the standard deviation of the full reflectance values for the three effective variances (including the default 0.10 value) was added as an SDS in the MS reflectance land LUTs. To also incorporate wind vector model uncertainty for ocean/water surfaces, standard deviations of the total reflectances were computed corresponding to the 0° , 90° , 180° and 270° wind direction relative to the principle plane for each of three LUT wind speeds. This wind direction standard deviation and the one corresponding to the effective variance as described above were added assuming the two error sources are independent (i.e., a root-sum-square (RSS) calculation). **Figure 2.9-5** shows the histograms of this standard deviation for the ocean LUT for $u = 3 \text{ ms}^{-1}$ for MODIS bands 2 and 20; the land (black surface) LUT histograms are also shown. There is no significant difference between the two histograms and therefore, to save computational time, we decided to

use the effective variance standard deviations from the land LUTs for the ocean LUTs instead of calculating them separately. The net ocean LUT model uncertainty value (RSS of effective variance and wind direction) was not included as an SDS to the ocean LUT but provided as a separate LUT due to file size constraints.

There are a total of 15 LUTs in an HDF4 format. One LUT provides phase function data (needed for the single scattering calculation) and other scattering properties for both phases. Two LUTs—one for each phase—provide the MS reflectances and effective variance standard deviations, as well as fluxes/albedos, for land (black surface) retrievals. There are 12 ocean LUTs—6 for each phase corresponding to 3 MS reflectance and flux/albedo/effective emissivity LUTs and 3 reflectance standard deviation LUTs representing the effective variance and wind direction error sources for the three wind speeds (3.0, 7.0, and 15.0 ms^{-1}). Note that the ocean standard deviation LUTs also includes effective surface and cloud emissivity standard deviations associated with wind direction; these are not used in the C6 retrieval uncertainty calculations but were added in anticipation of a future capability. We plan to make these C6 LUTs publicly available in the future.

2.10. Miscellaneous Changes

2.10.1. Multilayer cloud detection updates

The multilayer cloud detection algorithm [Wind *et al.*, 2010] has been updated for C6.

An additional multilayer cloud detection method is now applied as outlined in Pavolonis and Heidinger [2004]. The Pavolonis and Heidinger (**PH**) algorithm was designed for general-purpose cloud overlap detection, whereas MOD06 is focused on flagging pixels where cloud microphysical retrievals would adversely be affected by cloud overlap. The PH results appeared to be overly aggressive in flagging multilayer scenes (i.e., producing more detection than necessary). DISORT-based simulations of multilayer clouds run through the PH algorithm also suggest somewhat aggressive multilayer detection by the algorithm. A latitude-based channel 34 brightness temperature (BT13.6) threshold was implemented to help reduce false positives with some success. The PH algorithm is run when BT13.6 is greater than thresholds of **210 K** (latitude within $\pm 30^\circ$) or **227 K** (poleward of $\pm 30^\circ$ latitude). Regardless, it was decided in later C6 science testing that, while the result of the PH algorithm would be reported in the Byte 6 QA results (discussed later), the test would not be used to determine whether a retrieval is included in the L3 multilayer aggregation SDSs.

Figure 2.10.1-1 illustrates the issue. Locations where the PH algorithm is the sole contributor to multilayer result are have Cloud_Multi_Layer_Flag SDS values of 3 (light blue color). Whereas it is of course possible that those clouds are indeed multilayered, MOD06 seeks a specific kind of multilayer situation where cloud layering would have an adverse impact on an assumed single phase cloud effective radius retrieval. The example granule regions where the PH algorithm has made a positive detection do not indicate such a CER sensitivity and thus is not entirely optimal for the specified purpose.

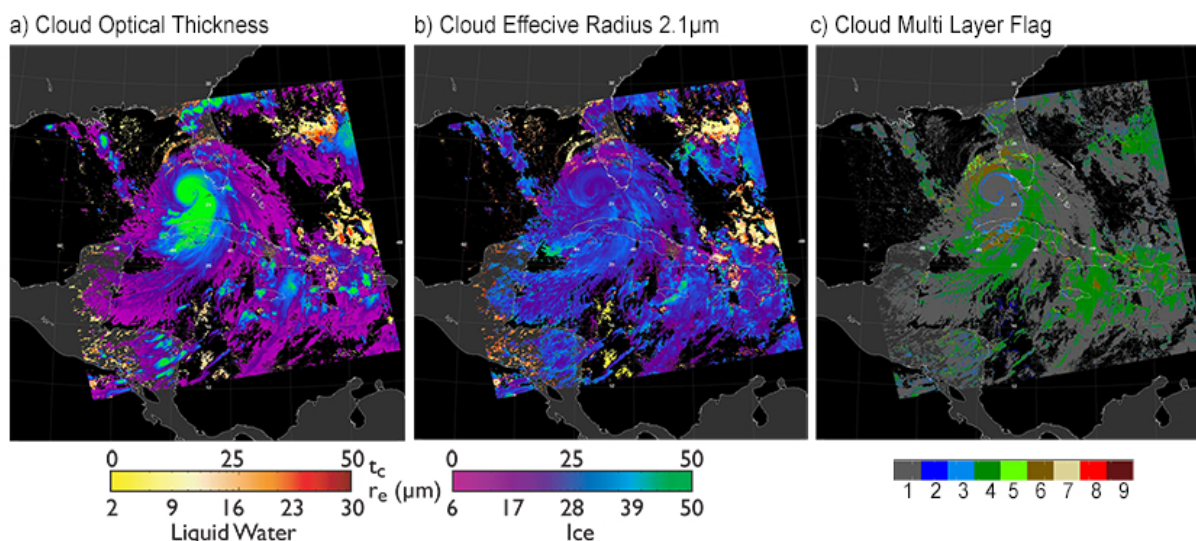


Figure 2.10.1-1. Example VNSWIR-2.1 μm retrievals and multilayer cloud SDS results (Aqua MODIS, day 238, 1840 UTC).

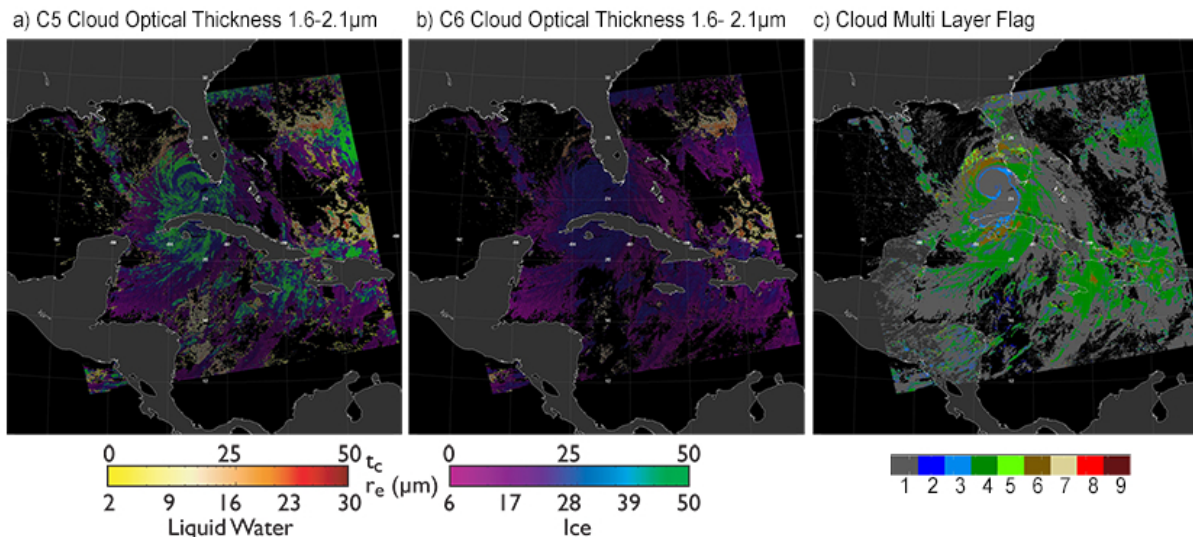


Figure 2.10.1-2. Example 1.6–2.1 μm retrievals and multilayer cloud SDS results (Aqua MODIS, day 238, 1840 UTC).

Additionally, the C6 algorithm includes a new test using the difference between standard optical thickness retrieval (VNSWIR–2.1 μm) and the one derived from the 1.6–2.1 μm pair retrieval channel combination. It was found in C5 and early C6 testing that a significantly larger 1.6–2.1 μm COT often indicates the presence of multilayer clouds in the scene. In particular this test has some skill in flagging thin cirrus over liquid water clouds, something also confirmed via DISORT multilayer cloud simulations. However due to a change in 1.6–2.1 μm retrieval logic, the test is rarely positive anymore. This is because the original C5 solution logic allowed 1.6–2.1 μm retrievals inadvertently to be outside the library space under multilayer cloud conditions while the C6 logic minimizes such a spurious outcome. The solution logic update was late in the C6 development cycle and so the test remains in C6. **Figure 2.10.1-2** illustrates the change between C5 and C6 COT from the 1.6–2.1 μm retrievals. The C5 retrieval is maximum in areas that are likely multilayered. We will further investigate the source of the multilayer information content that was evident in the C5 retrieval solution space.

The 0.94 μm -based precipitable water retrieval has been refined somewhat by interpolating between the table values of precipitable water instead of using the closest available point.

Finally, output information from the multilayer algorithm has been revised. In C5, integer values in the Cloud_Multi_Layer_Flag SDS indicated which tests were positive for any pixel and it was up to the user to decide the overall confidence level. In C6 each multilayer cloud test is now assigned a set detection confidence value and the sum of those values is recorded in the SDS as a pseudo confidence level (see third column of **Table 2.10.1-1**). As indicated in the third column of the table, the maximum SDS value that can be encountered by the user is 10 when all tests are positive (the default SDS value is 1). The PH test was assigned a high value based on early C6 development and is expected to be reduced in subsequent collections (see previous discussion). Individual results from the five multilayer cloud tests (1 and 0 inte-

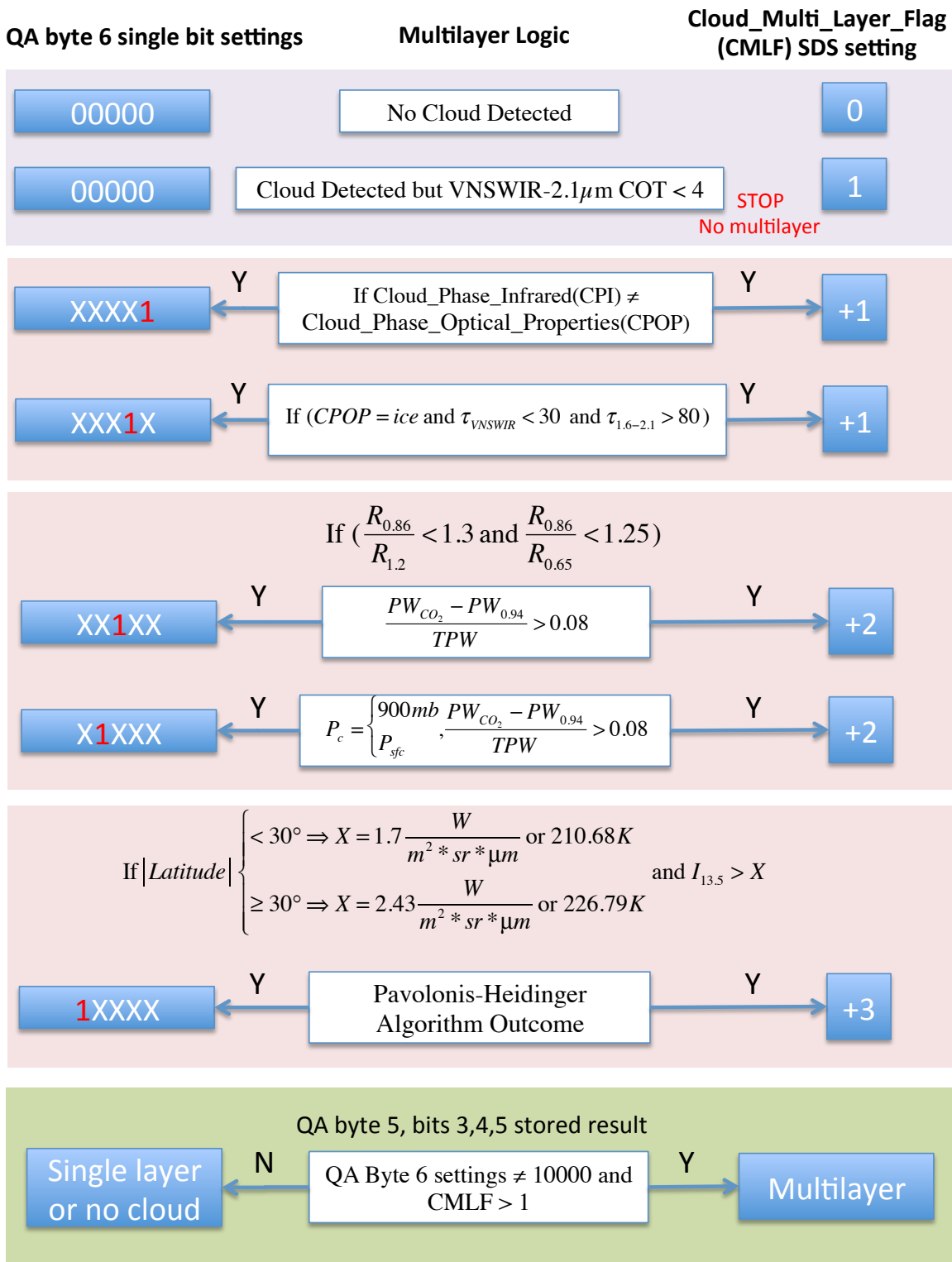


Figure 2.10.1-3. Schematic of multilayer cloud detection logic and QA and SDS assignments.

ger values for positive and negative detection, respectively) are now available in a new Byte 6 of the Quality_Assurance_1km SDS as described in **Table 2.10.1-1** (also see Appendix B).

The L3 product aggregates retrievals into multilayer datasets only if one of the tests associated with bits 0 through 3 show positive detection. The assignment of multilayer cloud status by phase (QA bits 5, 6, 7 of Byte 5) are the same as in C5. If any multilayer test from Table 2.10.1-1 is positive, including the PH test, then the Byte 5 bits are set to indicate a multilayer cloud. A schematic depiction of the multilayer algorithm logic is shown in **Fig. 2.10.1-3**.

Recommendation: Users should look carefully at the Byte 6 results and either (1) use the results as they see fit, or (2) use the same filtering methodology used by the MOD06 team for L3 multilayer statistical aggregations as described above. Because of the high weighting given to the PH test in early C6 development, users should not use the Cloud_Multi_Layer_Flag SDS to infer overall confidence in the multilayer detection result.

Table 2.10.1-1. Multilayer cloud detection QA bit assignment in Byte 6.

Bit position (Big-endian)	Multilayer Test	Detection Confidence Value (added to SDS)
0	IR and SWIR cloud phase difference	+1
1	Delta precipitable water	+2
2	Delta precipitable water with cloud at 900mb	+2
3	VNSWIR-2.1 and 1.6-2.1 μm COT divergence	+1
4	Pavolonis-Heidinger	+3

2.10.2. Cloud model single scattering properties vs. CER

The C6 file includes arrays of asymmetry parameter (g_λ), single scattering albedo ($\omega_{0,\lambda}$), and extinction efficiency factor ($Q_{e,\lambda}$) so that users can compare or scale retrievals to their own radiative transfer models should they so desire. These scattering properties are provided for both the ice and liquid water cloud models. This is particularly useful for ice models where variability in assumed ice habit/surface roughness can significantly impact the asymmetry parameter in all solar reflectance bands as well as the single scattering albedo in the SWIR. SDS scattering property names are given in **Table 2.10.2-1**; array formats and values are given in **Appendix D**.

2.10.3. Ancillary data sources

MOD06 uses several external ancillary data sources, the primary source being NCEP GDAS output. The NCEP GDAS files are generated by the spectral Medium Range Forecast

Table 2.10.2-1. Listing of single scattering properties and their respective SDS names. See Appendix D for further details.

Scattering Property	SDS Name
Ice g	Asymmetry_Parameter_Ice
Ice	Single_Scatter_Albedo_Ice
Ice	Extinction_Efficiency_Ice
Liquid water g	Asymmetry_Parameter_Liquid
Liquid water	Single_Scatter_Albedo_Liquid
Liquid water	Extinction_Efficiency_Liquid

model (MRF), which is a version of the NCEP GFS model. The dataset is a 6-hour archive product (also known as Final Run at NCEP) and includes late arriving conventional and satellite data. It is produced every 6 hours, starting at 00:00 UTC each day, and is distributed in GRIB (GRIdded Binary) format at a 1x1 degree grid. Table 2.10.6-1 lists the 2D and 3D model data fields utilized by MOD06.

Table 2.10.3-1. Listing of GDAS model fields used by the MOD06 code.

Field name	Description
TMP:* mb	Level temperature profile at 26 pressure levels between 10 and 1000 mb
RH:* mb	Level relative humidity profile at 21 pressure levels between 100 and 1000 mb
UGRD/VGRD: 10 m above gnd	U and V components of wind vector at 10m altitude above ground (not sea level)
PRES:sfc	Surface pressure
TMP:sfc	Surface Temperature
RH: 2m above gnd	Relative humidity at 2m above ground (not sea level)
PRMSL	Pressure at mean sea level (MSL)
TOZNE: atmos col	Integrated total column ozone amount

2.10.4. Increased vertical resolution of NCEP temperature and moisture profiles

The algorithm now reads in all 26 levels of temperature and moisture from the NCEP GDAS files rather than the lowest 16 levels as in C5. This ancillary information is used in the atmospheric correction (water vapor attenuation) calculations, as well as for estimating thermal emission in the 3.7 μm channel. In addition, C6 uses the NCEP GDAS analysis of sea surface temperature, which is created by the same algorithm as the weekly Reynolds SST used previously in C5 but updated every six hours. This SST is necessary for determining the thermal emission from the ocean surface in the 3.7 μm and 11 μm channels.

2.10.5. Improved spatial interpolation of surface temperature

Because the TOA radiance at 3.7 μm includes both reflected solar and emitted thermal radiation, and the 3.7 μm cloud optical properties retrieval uses the reflected solar radiation component only, the TOA surface, cloud, and atmospheric emission components must be removed before the retrieval is performed. To characterize the surface component, the NCEP GDAS “TMP:2 m above gnd” field (T2M) is now used instead of “TMP:sfc” field (TSFC) for surface temperature, since the 2 m above ground temperature is smoother than the gridded land surface temperature; over the ocean we use the GDAS sea surface temperature as discussed in the previous section. Further smoothing of the land surface temperatures is accomplished via spatial interpolation, a process that has been improved for C6. Effective surface and cloud emissivities are contained in the LUTs.

2.10.6. Spatially and temporally interpolated column ozone from GDAS

Spatially and temporally interpolated column ozone data from GDAS are now used as opposed to the TOAST daily column ozone product values (nearest-neighbor lookup) used in C5. This change affects retrievals over land only and primarily impacts the retrieval of cloud optical thickness.

2.10.7. Adjust low cloud top temperature retrievals for non-unity emissivity

The MOD06 cloud-top properties algorithm assumes unity cloud emissivity whenever the 11 μm window channel (MODIS channel 31) is used to infer the temperature of lower tropospheric clouds (see Sect. 1.1.1). To better calculate the the 3.7 μm channel effective emission for low clouds, we use the retrieved cloud optical thickness to iteratively adjust the 11 μm cloud emissivity for use in the window cloud-top temperature retrieval. This involves LUTs of 11 μm effective surface and cloud emissivity similar to what is done for the 3.7 μm channel [Platnick and Valero, 1994]. A final adjusted cloud-top temperature is achieved using a stand-alone version of the U. Wisconsin 11 μm cloud-top temperature algorithm coupled with the 3.7 μm COT retrievals, and iterating until convergence is achieved (typically only a couple of

iterations are required). This has a modest but predictable effect on the 3.7 μm -derived effective radius; the non-unity 11 μm cloud emissivity gives rise to warmer cloud-top temperatures (for typical surface/cloud temperature contrasts), reducing the 3.7 μm thermal emission which increases the 3.7 μm reflectance component, and ultimately results in a *smaller* 3.7 μm -derived effective radius.

The iterative procedure is as follows:

When the cloud-top QA indicates that the CO₂ slicing algorithm was run, the 5 km cloud-top temperature (CTT) dataset is used. However, if the QA indicates that the IR window (**IRW**) algorithm is used, then for the 3.7 μm retrievals the CTT is recalculated using a stand-alone 1 km IRW algorithm within the cloud optical properties code. The cloud and surface effective emissivities are a function of cloud optical thickness and effective radius, and the new CTT is is

$$T_c = B^{-1} \left[\frac{B(T_{c,IRW}) - \epsilon_s(COT, CER)T_s}{\epsilon_c(COT, CER)} \right] . \quad (2.10.1)$$

This new CTT is used in the next 3.7 μm retrieval iteration. The CTT retrieval converges when the difference between the original and new CTT is less than 0.01 K. In practice, the convergence is very rapid and normally occurs within 2-3 iterations. This modified CTT is stored in a new SDS named *IRW_Low_Cloud_Temperature_From_COP*. While this may provide a more realistic CTT for thin low clouds for general users, in the current algorithm it is used solely to improve the 3.7 μm retrievals.

The impact of this change is that CER₃₇ decreases slightly for optically thin clouds for the typical situation where the surface is warmer than CTT. This is due to the fact that the surface radiance escaping at cloud-top is removed while the net cloud emission is reduced. Since the measured radiance doesn't change, the reflected radiance component is increased and thus the retrieved effective radius decreases.

2.10.8. Improved surface albedo at 3.7 μm

In C6, a land surface emissivity database at 3.7 μm [Seemann *et al.*, 2003] is used to determine the corresponding surface albedo ($A_g = 1 - \epsilon$). In C5, it was assumed that the surface albedo was one-half of that at 2.1 μm . The emissivity-derived surface albedo is generally *lower* than the previously-used albedo that was extrapolated from the MOD43 dataset (Sect. 2.3). This leads to somewhat *smaller* 3.7 μm effective radii retrievals.

2.10.9. Other 3.7 μm updates: above-cloud emission and solar irradiance

For C6 we use atmospheric transmittance tables derived from FASCODE instead of MODTRAN, and include the above-cloud atmospheric emission in accounting for the total

measured 3.7 μm signal. In addition, the 3.7 μm band-averaged solar irradiance was changed to $10.93 \text{ Wm}^{-2}\mu\text{m}^{-1}$ (vs. $11.74 \text{ Wm}^{-2}\mu\text{m}^{-1}$ in C5) based on *Platnick and Fontenla* [2008].

2.10.10. Maximum retrievable cloud optical thickness extended to 150

The maximum COT value reported in C6 is now 150, rather than the maximum of 100 used in C5. The choice of 150 was based on pixel-level uncertainty calculations that often showed the COT uncertainty at COT=150 to be similar to that for small COTs (~ 1 or less). **Figure 2.10.10-1** illustrates the relationship between pixel-level uncertainty and retrieved COT for an example granule (Aqua MODIS 2005 day 096 at 18:30 UTC). The COT mean uncertainty at COT=150 for water clouds is less than that for COT<0.5, though this relationship is reversed for ice clouds in this example granule.

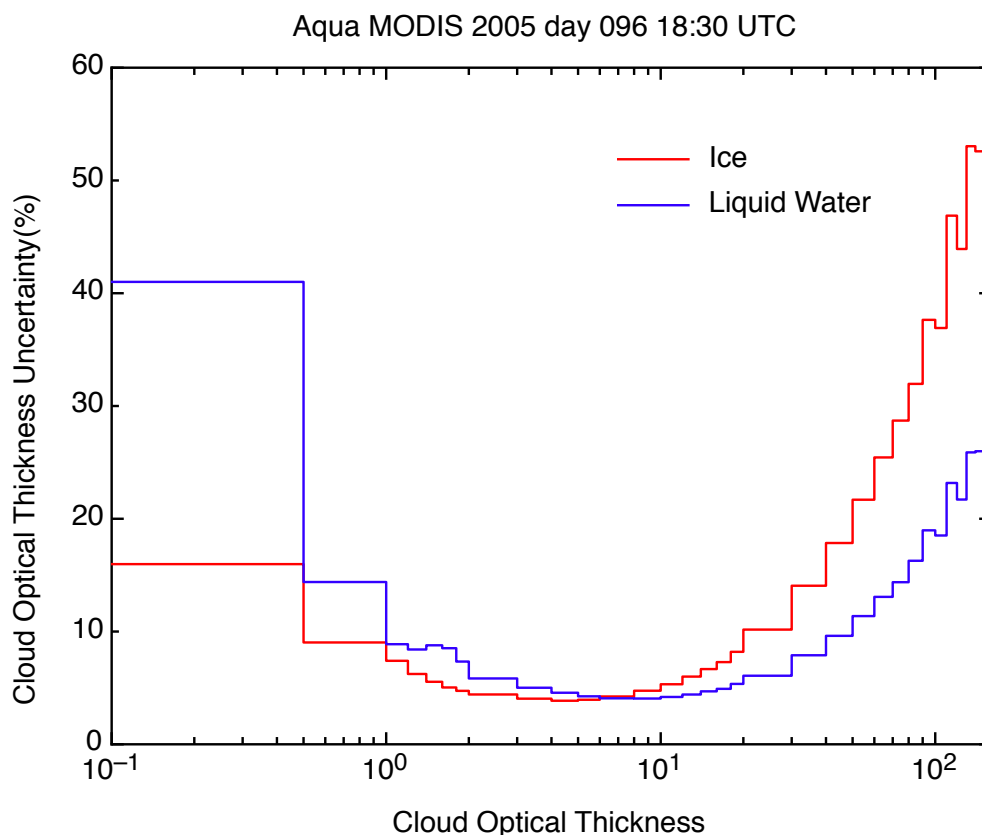


Figure 2.10.10-1: Histogram of cloud optical thickness uncertainty as a function of cloud optical thickness for an example granule.

2.10.11. Use of new 1 km cloud-top property retrievals

New 1 km resolution cloud top pressure datasets are used in atmospheric correction in lieu of 5 km cloud top pressures in Collection 5. This leads to more successful retrievals and fewer failed retrievals associated with broken and variable cloud situations.

2.10.12. *Statistics_1km and Statistics_1km_sds*

The C5 MODIS cloud product file template provided for a vector (VData) of various statistics about retrievals within the granule file. However by omission that vector had never been actually filled in (i.e., zeros). Part of the reason for that was that the file specification defined any 1-D SDS as a VData, making it quite difficult to access because a different set of HDF tools must be invoked in order to see the content. Additionally, the attributes of a VData object are invisible unless a special tool from the HDF library is read. Thus, even if the values were visible, users would not know what those values meant. In C6 we have correctly populated the VData vector *Statistics_1km* and additionally provided equivalent information in an easy to read 1-D SDS named *Statistics_1km_sds*. The SDS provides information for users interested in the set of granule-level statistics shown in Table 2.10.12-1.

Table 2.10.12-1. Information continued in *Statistics_1km* and *Statistics_1km_sds*.

Position	Information and units where applicable
1	Successful retrieval rate (%)
2	Land cover fraction (%)
3	Water cover fraction (%)
4	Snow cover fraction (%)
5	Cloud cover fraction (%)
6	Liquid water cloud fraction (%)
7	Ice cloud fraction (%)
8	Mean liquid water cloud optical thickness
9	Mean ice cloud optical thickness
10	Mean liquid water cloud effective radius (μm)
11	Mean ice cloud effective radius (μm)
12	Mean liquid water cloud top pressure (mb)
13	Mean ice cloud top pressure (mb)
14	Mean undetermined cloud top pressure (mb)
15	Mean liquid water cloud top temperature (K)
16	Mean ice cloud top temperature (K)
17	Mean undetermined cloud top temperature (K)

3. Level-3 Cloud Optical/Microphysical Dataset Overview

There is a single set of L3 files produced by the MODIS Atmosphere Team. All spatial aggregations are at a 1° equal-angle grid. An important property to note when considering L3 gridding occurs due to distortion in the latitude-longitude map projection as one moves poleward; for example, at the equator each 1° grid cell is roughly 12,000 km² in size, at the pole each 1° grid cell is less than 100 km² (over two orders of magnitude difference). Temporal aggregations are provided for daily (**MOD08_D3**), eight-day (**MOD08_E3**), and monthly (**MOD08_M3**) periods. A variety of statistical datasets are provided (scalars, 1D and 2D histograms). The eight-day (reset at the beginning of each calendar year) and monthly aggregations are derived directly from the daily files. As with previous collections, daily files aggregate all pixels that map into a grid cell for all overpasses during the day, resulting in an aggregation over multiple satellite overpasses for grid cells poleward of about 30° latitude. It should also be noted that there is a variation of pixel size in L2 (input) products due to viewing (scan angle) distortion. For example, for a 1 km (nadir) resolution L2 retrieval product, the L2 pixels expand to about 4 km due to view angle distortion when moving from nadir towards the swath edge. These same distortion factors apply to 5 and 10 km native resolution L2 retrievals.

The assignment of L2 pixels to a L3 grid cell that fall exactly on a L3 grid boundary is performed using the following convention: L2 pixels that fall exactly on the first whole degree boundary 90°N (+90.0) latitude and 180°W (-180.0) longitude are binned in the L3 grid column and row #1. L2 pixels that fall exactly on the second whole degree boundary 89°N (+89.0) and 179°W (-179.0) are binned in L3 grid column and row #2. The exception to this logic occurs in the last L3 grid row (89°S to 90°S), which contains both whole degree latitude boundary pixels (-89.0 as well as -90.0). There is no exception for the last L3 grid column (179°E to 180°E) since +180.0 and -180.0 represent the same physical location (these L2 pixels are binned in the first L3 grid column).

C6 L3 Changes:

The “definition of the day” for earlier collections coincided with UTC. However, this caused spatial gaps around 0° and 180° longitude that made comparison with other EOS daily L3 products difficult in those regions. For C6, the “definition of the day” has been modified to move the spatial gap (which is impossible to avoid) to the nighttime poles. Specifically, we first subtract/remove early (0000 to 0300 UTC) measurements just to the east of the dateline (daytime observations) and just to the east of the Greenwich meridian (nighttime). Then we add early measurements from the following day to the same longitude zones. This gives orbit-to-orbit continuity except for seams at the Dateline (day) and Greenwich meridian (night). For Terra C6, the exercise is similar with some end-of-day measurements excluded and prior day end-of-day measurements included. All excluded measurements will contribute to the next day. An example is given in **Fig. 3-1**.

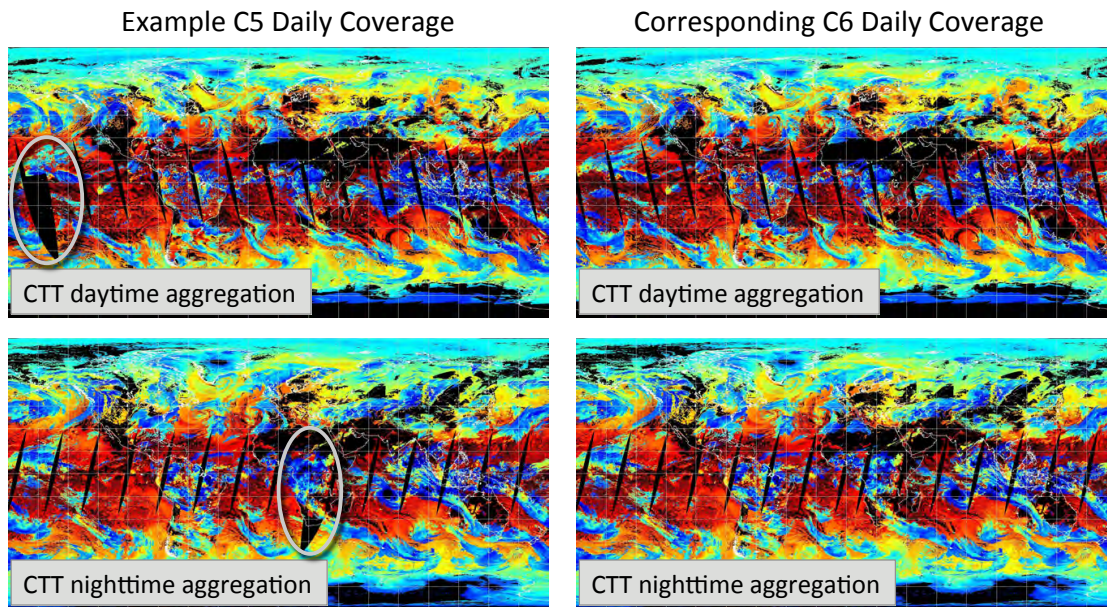


Figure 3-1. Example of daily spatial coverage using “definition of the day” from C5 vs. C6. Cloud-top temperature is used for the example since the product has both day and night retrievals. The location of the spatial data gaps caused by using a strict UTC definition for C5 and earlier collections are indicated.

Statistics for a number of additional SDSs have been added for C6. For cloud optical properties, the most notable addition are statistics for separate “partly cloudy” retrievals (*_PCL SDS names associated with CSR = 1,3 designations, c.f., Sect. 2.8) along with separate aggregations for retrievals from band pairs using the 1.6 μm and 3.7 μm channels (Sect. 2.5). This includes joint COT-CER histograms for the additional spectral retrievals in addition to the usual complement of scalar statistics.

Throughout the C6 L3 file, there have been a number of SDS name changes. For cloud optical properties, one change of note is from the SDS name *Cloud_Fraction_** to *Cloud_Retrieval_Fraction_** (where the asterisk represents Liquid, Ice, Undetermined phase and other spectral retrievals beyond the standard retrieval pair that includes the 2.1 μm channel). This is done to eliminate confusion with the cloud mask fraction (*Cloud_Fraction*, *Cloud_Fraction_day*, *Cloud_Fraction_night*, etc.). This name change also better conveys that the fraction represents successful retrievals in a grid cell from the optical retrieval algorithm normalized by the total number of pixels that fall into the grid cell. As with the L2 products, users should always look at the corresponding HDF “long names” that provide details beyond what can be inferred from the SDS “short” names.

A summary of the C6 L3 cloud optical/microphysical statistical parameters is given in **Appendix F**. A complete list of C6 Atmosphere Team L3 statistics is available on the team web site (modis-atmos.gsfc.nasa.gov/products_C006update.html).

Previous L3 versions included QA-weighted cloud optical property statistics. The pixel-level *Retrieval Confidence* QA-weightings were two bit integer values (with 3 being the best quality) used to reduce the impact of retrievals expected to be in a part of the solution space where the uncertainties would be greatest. For C5, reduced confidence QA values were assigned for liquid water clouds only (see modis-atmos.gsfc.nasa.gov/C005_Changes/C005_-_CloudOpticalProperties_ver311.pdf). With improved pixel-level COT, CER, and CWP uncertainty estimates in C6, it was decided to drop QA-weightings in the L3 C6 optical property datasets. Instead, users are referred to the uncertainty of the mean SDSs that have been provided in the L3 dataset since C5. For example, for each grid box, the L3 daily SDS *Cloud_Optical_Thickness_Liquid_Mean_Uncertainty* provides an estimate of the uncertainty in the L3 daily mean COT (*Cloud_Optical_Thickness_Liquid_Mean*) based on the L2 uncertainty SDS *Cloud_Optical_Thickness_Uncertainty* for the relevant liquid water pixels (details in modis-atmos.gsfc.nasa.gov/reference_atbd.html). Note that the L3 uncertainty SDSs are in absolute units (e.g, μm for CER) whereas the L2 uncertainty SDSs are in percent.

Due to an HDF4 uncompressed file size limitation of 2 GB, several 2D histograms are only available in the daily MOD08_D3 file (see ‘*d*’ designation in the tables of Appendix F). However, eight-day and monthly aggregations can be computed by calculating pixel-weighted (count-weighted) aggregations directly from the daily files (consult the C5 L3 ATBD for further details: modis-atmos.gsfc.nasa.gov/reference_atbd.html).

4. MODIS-Atmosphere Team Web Site and Browse Imagery

The MODIS Atmosphere Team web site provides L2 and L3 browse imagery for many of the key scalar statistics from the various team data products. L2 imagery is currently displayed on the main browse imagery page (**Fig. 4-1**, modis-atmos.gsfc.nasa.gov/IMAGES) with zoom and rotation functionality; links to L3 browse pages are provided within the left side bar.

For L3 products, users can select specific daily, 8-day, and monthly statistics with separate pages for each major discipline group (see **Figs. 4-2, 4-3**). Daily and 8-day product browse imagery is only available in the native latitude-longitude rectangular grid. Monthly browse images are also available in an equal-area projection (Hammer-Aitoff), though users should be aware that some mild distortion, and occasionally even loss of data, can be seen while converting from one map projection to another in regions (especially high latitudes) where there are sparse data. The native latitude-longitude projection is the preferred choice for quantitative understanding. A discretized modified-rainbow color bar is applied to each image and the data scale is optimized to maximize image detail. Fill (missing) data are always colored black. Multiple statistics (SDSs) for a single parameter can be viewed by using a built-in “mouse-over” functionality on the web page by rolling the mouse cursor over the statistic “bars” to the right of each image (**Fig. 4-3**).

In addition to browse imagery, there is an assortment of product and reference information that is provided on the team web site including complete file specifications, details on the format and content, modification history, and known problems. Also available are programs and tools that can read and image L3 HDF file SDSs. C6 team documents (including this user guide) are maintained on the following page: modis-atmos.gsfc.nasa.gov/products_C006update.html.

The screenshot shows the front page of the MODIS Atmosphere Team browse page. The page title is "Global Browse of MODIS Atmosphere". It features a navigation menu at the top with links like HOME, PRODUCTS, HANDS, DATABASE, NEWS, FAQ, FORM, REFERENCE, TOOLS, and HELP. Below the navigation, there are search and filter options for satellite/collection (Aqua, Terra) and date ranges. The main content area displays a grid of global thumbnail images for various SDSs. The grid is organized by satellite/collection (Aqua, Terra) and then by SDS type (e.g., Cloud Fraction, Cloud Top Temperature, Cloud Top Pressure, Cloud Optical Thickness, Cloud Effective Radius, Cloud Phase Infrared, Cirrus Reflectance, Aerosol Optical Depth, Deep Optical). The first row shows "Not Available" for Aqua, Collection 6, and Terra, Collection 5. The second row shows global maps for Aqua, Collection 5, and Terra, Collection 5, with columns for Julian day, RGB True Color Image, RGB False Color Image, Cloud Fraction from Cloud Mask, Cloud Top Temperature, Cloud Top Pressure, Cloud Optical Thickness, Cloud Effective Radius, Cloud Phase Infrared, Cirrus Reflectance, Aerosol Optical Depth, and Deep Optical.

Julian day	RGB True Color Image MYD09	RGB False Color Image MYD09	Cloud Fraction from Cloud Mask MYD06_L2	Cloud Top Temperature MYD06_L2	Cloud Top Pressure MYD06_L2	Cloud Optical Thickness MYD06_L2	Cloud Effective Radius MYD06_L2	Cloud Phase Infrared MYD06_L2	Cirrus Reflectance MYD06_L2	Aerosol Optical Depth Land and Ocean MYD04_L2	Deep Optical MYD04_L2
2014 132	Not Available	Not Available									
05/12											
2014 131											
05/11											
2014 130											
05/10											

Figure 4-1. Front page of the MODIS Atmosphere Team browse page showing global L2 thumbnail images for a variety of key team SDSs.

The screenshot shows the MODIS Atmosphere web interface. At the top, there is a navigation bar with links for HOME, PRODUCTS, IMAGES, DATA ISSUES, NEWS, STAFF, FORUM, REFERENCE, TOOLS, and HELP. Below this, there are tabs for AEROSOL, H₂O VAPOR, CLOUD, PROFILE, CLD_MASK, JOINT, and (Level 2 Products). Underneath, there are sub-tabs for DAILY, EIGHT DAY, MONTHLY, (Level 3 Products), ALBEDO, NDVI, ECOSYSTEM, and (Level 3 Analysis). The main content area is titled 'IMAGES' and contains a message: 'First: Update Selections from Available Days for Aqua or Terra'. Below this, there are selection options for Version (Collection 51, Collection 5), Mission (Aqua, Terra), Year (2002-2014), Month (01-04), and Day (01-05). A second message says: 'Next: Select a Parameter Group to Load Images for Aqua 2014 04 05 (Day 095)'. Below this, there are buttons for Parameter Group: Aerosol Global, Aerosol Land, Aerosol Ocean, Water Vapor, Cirrus, Cloud Top, Cloud Optical, and Profiles. On the left side, there is a sidebar with a tree view of data products, including L1 & L2 H-RES GLOBAL, TERRA IMAGES, L1B, L1B GRANULES, L3 - Collection 051, L3 LOW-RES DAILY, L3 LOW-RES EIGHTDAY, L3 LOW-RES MONTHLY, L3 - Collection 005, L3 LOW-RES DAILY, L3 LOW-RES EIGHTDAY, L3 LOW-RES MONTHLY, AQUA IMAGES, L1B, L1B GRANULES, L3 - Collection 051, L3 LOW-RES DAILY, L3 LOW-RES EIGHTDAY, L3 LOW-RES MONTHLY, L3 - Collection 005, L3 LOW-RES DAILY, L3 LOW-RES EIGHTDAY, and L3 LOW-RES MONTHLY.

Figure 4-2. The interface that allows viewing of key scalar statistical images in the Atmosphere Team L3 HDF files. A user selects a “derived-from” product group, the time period, and map projection.

The screenshot shows the Aqua Browse Imagery web interface. At the top, there is a section titled 'Aqua Browse Imagery' with a note: 'NOTE: On the color bar Lavender denotes data values equal to (or less than) the bottom scale number. Maroon denotes data values equal to (or greater than) the top scale number.' Below this, there are 'Quick Navigation Links (same day, same projection)' for MYD04_L2 Aerosol Global, MYD04_L2 Aerosol Ocean, MYD06_L2 Cirrus Detection, MYD06_L2 Cloud Optical Properties, MYD04_L2 Aerosol Land, MYD05_L2 Water Vapor, MYD06_L2 Cloud Top Properties, and MYD07_L2 Atmospheric Profile. There are also links for 'Return To Browse Menu' and 'Load Print Friendly Version'. The main content area is titled 'Cloud Optical Properties' and contains a paragraph: 'Standard 2.1μm-derived retrievals. With the exception of pixels identified as partly cloudy (PCL) by the Clear Sky Restoral (CSR) algorithm, all datasets were available in Collection 5.' Below this, there are two image displays. The first is titled 'Cloud_Optical_Thickness_Liquid_Mean' for 28Jan2008, showing a global map with a color scale from -1.0 to 70. The second is titled 'Cloud_Effective_Radius_Liquid_Mean_Uncertainty' for 28Jan2008, showing a global map with a color scale from 15 to 20. To the right of each image is a table of statistical data for various datasets. The first table has columns for 'Liquid', 'Ice', 'Undetermined', 'Combined', 'PCL_Liquid', 'PCL_Ice', 'PCL_Undetermined', and 'PCL_Combined', with rows for 'Uncertainty_Mean' and 'Standard_Deviation'. The second table has columns for 'Liquid', 'Ice', 'Undetermined', 'PCL_Liquid', 'PCL_Ice', and 'PCL_Undetermined', with rows for 'Uncertainty_Mean' and 'Standard_Deviation'. A note at the bottom right of each table says 'roll mouse over statistic bars'.

Figure 4-3. Example L3 daily browse images for cloud optical products (URL here). A variety of dataset can be viewed by using a mouse-over function implemented on the mean, uncertainty, and standard deviation bars to the right of each image.

5. MOD06 Optical Properties Data: Frequently Asked Questions

Coming soon!

6. References

- Ackerman, S. A., R. E. Holz, R. Frey, E. W. Eloranta, B. Maddux, and M. McGill, 2008: Cloud detection with MODIS. Part II: Validation. *J. Atmos. Oceanic Technol.*, **25**, 1073-1086.
- Baum, B. A., P. Yang, A. J. Heymsfield, S. Platnick, M. D. King, Y. X. Hu, and S. T. Bedka, 2005: Bulk scattering properties for the remote sensing of ice clouds. 2: Narrowband models. *J. Appl. Meteor.*, **44**, 1896-1911.
- Baum, B. A., W. P. Menzel, R. A. Frey, D. Tobin, R. E. Holz, Ackerman, S. A., A. K. Heidinger, and P. Yang, 2012: MODIS cloud top property refinements for Collection 6. *J. Appl. Meteor. Climatol.*, **51**, 1145-1163.
- Chahine, M. T., 1974: Remote sounding of cloudy atmospheres. I. The single cloud layer. *J. Atmos. Sci.*, **31**, 232-243.
- Cox, C., and W. Munk, 1954: The measurements of the roughness of the sea surface from photographs of the sun's glitter. *J. Opt. Soc. Amer.*, **44**, 838-850.
- Curran, R. J. and M. C. Wu, 1982: Skylab near-infrared observations of clouds indicating supercooled liquid water droplets. *J. Atmos. Sci.*, **39**, 635-647.
- Downing, H. D., and D. Williams 1975: Optical-constants of water in the infrared. *J. Geophys. Res.*, **80**, 1656-1661.
- Gao, B.-C., A. F. H. Goetz, and W. J. Wiscombe, 1993: Cirrus cloud detection from airborne imaging spectrometer data using the 1.38 μ m water vapor band. *Geophys. Res. Lett.*, **20**, 301-304.
- Gasso, S., A. Stein, F. Marino, E. Castellano, R. Udisti, and J. Ceratto, 2010: A combined observational and modeling approach to study modern dust transport from the Patagonia desert to East Antarctica. *Atmos. Chem. Phys.*, **10**, doi:10.5194/acp-10-8287-2010.
- Hale, G. M., and M. R. Querry, 1973 : Optical constants of water in the 200-nm to 200- μ m wavelength region, *Appl. Opt.*, **12**, 555-563.
- Han, Q., W. B. Rossow, and A. A. Lacis, "Near-global survey of effective droplet radii in liquid water clouds using ISCCP data," *J. Climate*, vol. 7, pp. 465-497, 1994.
- Holz, R. E. S. A. Ackerman, F. W. Nagle, R. Frey, R. E. Kuehn, S. Dutcher, M. A. Vaughan, and B. Baum., 2008: Global MODIS cloud detection and height evaluation using CALIOP. *J. Geophys. Res.*, **113**, D00A19, doi:10.1029/2008JD009837.
- Holz, R. E., S. Platnick, A. Heidinger, M. Vaughan, A. Garnier, R. Kuehn, and G. Wind, 2014: Resolving cirrus optical depth biases between CALIOP and MODIS using IR retrievals. *J. Atmos. Oceanic Technol.*, in preparation.
- Hu, Y. X., B. Wielicki, B. Lin, G. Gibson, S. C. Tsay, K. Stamnes, and T. Wong, 2000: Delta-Fit: A fast and accurate treatment of particle scattering phase functions with weighted singular-value decomposition least-squares fitting. *J. Quant. Spectrosc. Radiat. Trans.*,

65, 681-690.

- Hubanks, P. A., M. D. King, S. A. Platnick, and R. A. Pincus, 2008: MODIS Atmosphere Team Level-3 Algorithm Theoretical Basis Document (ATBD), 100 pp., modis-atmos.gsfc.nasa.gov/MOD08_D3/atbd.html.
- Johnson, N. Meskhidze, V. P. Kiliyanpilakkil, and S. Gasso, 2011: Understanding the transport of Patagonia dust and its influence on marine biological activity in the South Atlantic Ocean. *Atmos. Chem. Phys.*, 11, doi:10.5194/acp-11-2487-2011.
- Joiner, J. A. P. Vasilkov, P. K. Bhartia, G. Wind, S. Platnick, and W. P. Menzel, 2010: Detection of multi-layer and vertically-extended clouds using A-Train sensors. *Atmos. Meas. Tech.*, **3**, 233-247.
- Kaufman, Y. J., I. Koren, L. A. Remer, D. Tanra, P. Ginoux, and S. Fan, 2005: Dust transport and deposition observed from the Terra-MODIS spacecraft over the Atlantic Ocean. *J. Geophys. Res.*, 110, DOI: 10.1029/2003/JC004436.
- Koepke, P., 1984: Effective reflectance of oceanic whitecaps," *Appl. Opt.*, 23, 1816-1824.
- King, M. D., 1987: Determination of the scaled optical thickness of clouds from reflected solar radiation measurements. *J. Atmos. Sci.*, **44**, 1734-1751.
- King, M. D., Y. J. Kaufman, W. P. Menzel, and D. Tanré, 1992: Remote sensing of cloud, aerosol, and water vapor properties from the Moderate Resolution Imaging Spectrometer (MODIS). *IEEE Trans. Geosci. Remote Sens.*, **30**, 2-27.
- King, M. D., S. C. Tsay, S. E. Platnick, M. Wang and K. N. Liou, 1997: *Cloud Retrieval: Algorithms for MODIS: Optical Thickness, Effective Particle Radius, and Thermodynamic Phase*. Algorithm Theoretical Basis Document ATBD-MOD-05, 79 pp., modis-atmos.gsfc.nasa.gov/reference_atbd.html.
- King, M. D., W. P. Menzel, Y. J. Kaufman, D. Tanre, B.-C. Gao, S. Platnick, S. A. Ackerman, L. A. Remer, R. Pincus, and P. A. Hubanks, 2003: "Cloud and aerosol properties, precipitable, water, and profiles of temperature and water vapor," *IEEE Trans. Geosci. Remote Sens.*, vol. 41, no. 2, pp. 442-458.
- King, M. D., S. Platnick, P., G. T. Arnold, M. A. Gray, J. C. Riedi, S. A. Ackerman, and K. N. Liou, 2004: Remote sensing of liquid water and ice cloud optical thickness and effective radius in the arctic: Application of airborne multispectral MAS data. *J. Atmos. Oceanic Technol.*, **21**, 857-875.
- King, M. D., S. Platnick, G. Wind, G. T. Arnold, and R. T. Dominguez, 2010: Remote sensing of radiative and microphysical properties of clouds during TC⁴: Results from MAS, MASTER, MODIS, and MISR. *J. Geophys. Res.*, **115**, D00J07, doi: 10.1029/2009JD013277.
- King, M. D., S. Platnick, W. P. Menzel, S. A. Ackerman, and P. A. Hubanks, 2013: Spatial and temporal distribution of clouds observed by MODIS onboard the Terra and Aqua satellites *IEEE Trans. Geosci. Remote Sens.*, **51**, 3826-3852.
- Lebsock, M. D., T. S. L'Ecuyer and G. L. Stephens, 2011. Detecting the ratio of rain and

- cloud water in low-latitude shallow marine clouds. *J. Appl. Meteorol. Clim.*, **50**, 419–432.
- Liang, L., L. Di Girolamo, and S. Platnick, 2009: View-angle consistency in reflectance, optical depth, and spherical albedo of marine water clouds off the coast of California through MISR-MODIS fusion, *Geophys. Res. Lett.*, **36**, L09811, doi: 10.1029/2008GL037124.
- Maddux, B. C., S. A. Ackerman, and S. Platnick, 2010: Viewing geometry dependencies in MODIS cloud products. *J. Atmos. Oceanic Tech.*, **27**, 1519–1528.
- Mayer, B., and A. Kylling, 2005: Technical note: The libRadtran software package for radiative transfer calculations - description and examples of use. *Atmos. Chem. Phys.*, **5**, 1855–1877.
- Minnis, P., P. W. Heck, S. Mayor, and D. F. Young, “A near-global analysis of cloud microphysical properties,” in *Proc. IRS: Current Probl. Atmos. Radiat.*, W. L. Smith and K. Stamnes, Eds., Hampton, VA, 1997, pp. 445–448, Deepak Publ.
- Moody, E. G., M. D. King, S., Platnick, C. B. Schaaf, and F. Gao, 2005: Spatially complete global spectral surface albedos: Value-added datasets derived from Terra MODIS land products. *IEEE Trans. Geosci. Remote Sens.*, **43**, 144–158.
- Moody, E. G., M. D. King, C. B. Schaaf, D. K. Hall, and S. Platnick, 2007: Northern Hemisphere five-year average (2000–2004) spectral albedos of surfaces in the presence of snow: Statistics computed from Terra MODIS land products. *Remote Sens. Environ.*, **111**, 337–345.
- Moody, E. G., M. D. King, C. B. Schaaf, and S. Platnick, 2008: MODIS-derived spatially complete surface albedo products: Spatial and temporal pixel distribution and zonal averages. *J. Appl. Meteor. Climatol.*, **47**, 2879–2894.
- Nakajima, T., and M. D. King, 1990: Determination of the optical thickness and effective particle radius of clouds from reflected solar radiation measurements, Part I: Theory. *J. Atmos. Sci.*, **47**, 1878–1893.
- Palmer, K. F., and D. Williams, 1974: Optical properties of water in the near infrared. *J. Opt. Soc. Amer.*, **64**, 1107–1110.
- Pavolonis, M. J., and A. K. Heidinger, 2004: Daytime cloud overlap detection from AVHRR and VIIRS. *J. Appl. Meteor.*, **43**, 762–778.
- Pincus, R., S. Platnick, S. A. Ackerman, R. S. Hemler, R. J. P. Hofmann, 2012: Reconciling simulated and observed views of clouds: MODIS, ISCCP, and the limits of instrument simulators. *J. Climate*, **25**, 4699–4720.
- Platnick, S., and S. Twomey, 1994: Determining the susceptibility of cloud albedo to changes in droplet concentration with the advanced very high resolution radiometer. *J. Appl. Meteor.*, **33**, 334–347.
- Platnick, S., and F. P. J. Valero, 1995: A validation study of a satellite cloud retrieval during ASTEX. *J. Atmo. Sci.*, **52**, pp 2985–3001.

- Platnick, S., M. D. King, H. Gerber, P. V. Hobbs. 2001: A solar reflectance technique for cloud retrievals over snow and ice surfaces. *J. Geophys. Res.*, **106**, 15,185-15,199.
- Platnick, S., M. D. King, S. A. Ackerman, W. P. Menzel, B. A. Baum, J. C. Riedl, and R. A. Frey, 2003: "The MODIS cloud products: Algorithms and examples from Terra," *IEEE Trans. Geosci. Remote Sens.*, vol. 41, no. 2, pp. 459–473.
- Platnick, S., R. Pincus, B. Wind, M. D. King, M. Gray, and P. Hubanks, 2004: An initial analysis of the pixel-level uncertainties in global MODIS cloud optical thickness and effective particle size retrievals. *Passive Optical Remote Sensing of the Atmosphere and Clouds IV*, S.-C. Tsay, T. Yokota, and M.-H. Ahn, Eds., *Proc. of SPIE*, **5652**, 30-40.
- Platnick, S., and J. M. Fontenla, 2008: Model calculations of solar spectral irradiance in the 3.7- μm band for Earth remote sensing applications. *J. Appl. Meteor. Climatol.*, **47**, 124–134.
- Platnick, S., S. A. Ackerman, B. A. Baum, A. K. Heidinger, R. E. Holz, M. D. King, W. P. Menzel, S. Nasiri, El Weisz, and P. Yang, 2013: *Assessment of IDPS VIIRS Cloud Products and Recommendations for EOS-era Cloud Climate Data Record Continuity*, Suomi NPP Science Team report, 19 March.
- Yang, P., L. Bi, B. A. Baum, K. N. Liou, G. W. Kattawar, M. I. Mishchenko, and B. Cole, 2013: Spectrally consistent scattering, absorption, and polarization properties of atmospheric ice crystals at wavelengths from 0.2 to 100 μm . *J. Atmos. Sci.*, **70**, 330–347.
- Rawlins, F. and J. S. Foot, "Remotely sensed measurements of stratocumulus properties during FIRE using the C130 aircraft multichannel radiometer," *J. Atmos. Sci.*, vol. 47, pp. 2488–2503, 1990.
- Riedi, J., B. Marchant, S. Platnick, B. Baum, F. Thieuleux, C. Oudard, F. Parol, J.-M. Nicolas, and P. Dubuisson, 2010: Cloud thermodynamic phase inferred from merged POLDER and MODIS data. *Atmos. Chem. Phys.*, **10**, 11851-11865.
- Rodgers, C.D. *Inverse Methods for Atmospheric Sounding: Theory and Practice*; World Scientific Publishing Co., Inc.: Hackensack, NJ, USA, 2000.
- Seemann, S. W., E. E. Borbas, R. O. Knuteson, G. R. Stephenson, and H. L. Huang, 2003: Development of a global infrared land surface emissivity database for application to clear sky sounding retrievals from multispectral satellite radiance measurements. *J. Appl. Meteor. Climatol.*, **47**, 108–123.
- Stamnes, K., S. C. Tsay, W. Wiscombe, and K. Jayaweera, 1988: A numerically stable algorithm for discrete-ordinate-method radiative transfer in multiple scattering and emitting layered media. *Appl. Opt.*, **27**, 2502-2509.
- Stamnes, K., S. C. Tsay, W. Wiscombe, and I. Laszlo, 2000: DISORT, a General-Purpose Fortran Program for Discrete-Ordinate-Method Radiative Transfer in Scattering and Emitting Layered Media : Documentation of Methodology.
- Schaaf, C. L. B., J. Liu, F. Gao and A. H. Strahler, MODIS Albedo and Reflectance Anisotropy Products from Aqua and Terra, In *Land Remote Sensing and Global Environ-*

- mental Change: NASA's Earth Observing System and the Science of ASTER and MODIS *Remote Sensing and Digital Image Processing Series*, Vol. 11, B. Ramachandran, C. Justice, M. Abrams, Eds., Springer-Verlag, 873 pp., 2011.
- Strow L., S. Hannon, S. Machado, H. Motteler, D. Tobin, 2003: An overview of the AIRS radiative transfer model. *IEEE Trans. Geosci. Remote. Sens.* **41**, 303-313.
- Stubenrauch, C. J., W. B. Rossow, S. Kinne, S. Ackerman, G. Cesana, H. Chepfer, B. Getzewich, L. Di Girolamo, A. Guignard, A. Heidinger, B. Maddux, P. Menzel, P. Minnis, C. Pearl, S. Platnick, C. Poulsen, J. Riedi, S. Sun-Mack, A. Walther, D. Winker, S. Zeng, and G. Zhao, 2013: Assessment of global cloud datasets from satellites: Project and database initiated by the GEWEX Radiation Panel. *Bull. Am. Meteor. Soc.*, **94**, 1031–1049.
- Yang, P., L. Zhang, G. Hong, S. L. Nasiri, B. A. Baum, H.-L. Huang, M. D. King, and S. Platnick, 2007: Differences between collection 004 and 005 MODIS ice cloud optical/microphysical products and their impact on radiative forcing simulations. *IEEE Trans. Geosci. Remote Sens.*, **45**, 2886-2899.
- Yang, P., L. Bi, B. A. Baum, K. N. Liou, G. W. Kattawar, M. Mishchenko, and B. Cole, 2013: Spectrally consistent scattering, absorption, and polarization properties of atmospheric ice crystals at wavelengths from 0.2 to 100 μm . *J. Atmos. Sci.*, **70**, 330–347.
- Wind, G., S. Platnick, M. D. King, P. A. Hubanks, M. J. Pavolonis, A. K. Heidinger, P. Yang, and B. A. Baum, 2010: Multilayer cloud detection with the MODIS near-infrared water vapor absorption band. *J. Appl. Meteor. Climatol.*, **49**, 2315–2333.
- Zhang, Z., and S. Platnick, 2011: An assessment of differences between cloud effective particle radius for marine water clouds from three MODIS spectral bands. *J. Geophys. Res.*, **116**, D20215, doi:10.1029/2011JD016216.
- Zhang, Z., S. Platnick, P. Yang, A. Heidinger, and J. M. Comstock, 2010: Effect of ice particle size vertical inhomogeneity on the passive remote sensing of ice clouds, *J. Geophys. Res.*, **15**, D17203, doi:10.1029/2010JD013835.
- Zhang, Z., A. S. Ackerman, G. Feingold, S. Platnick, R. Pincus, and H. Xue, 2012: Effects of cloud horizontal inhomogeneity and drizzle on remote sensing of cloud droplet effective radius: Case studies based on large-eddy simulations. *J. Geophys. Res.*, **117**, D19208, doi:10.1029/2012JD017655.

APPENDIX A. SCIENTIFIC DATA SETS (SDSs) IN THE L2 CLOUD PRODUCT FILE

For completeness, all SDSs in the MOD/MYD06 file are given in the table below. The highlighted rows indicate just those datasets that are related to the optical and microphysical retrievals discussed in this user guide.

SDS name	Long Name	Dataset resolution (if applicable)
Above_Cloud_Water_Vapor_094	Above-cloud water vapor amount from 0.94um channel, ocean only, tau > 5.	1 km
Asymmetry_Parameter_Ice	Ice Asymmetry Parameter from the phase functions used to generate the forward lookup tables	-
Asymmetry_Parameter_Liq	Liquid Water Asymmetry Parameter from the phase functions used to generate the forward lookup tables	-
Atm_Corr_Refl	Atmospherically corrected reflectance used during cloud optical and microphysical properties retrieval	1 km
Band_Number	Band_Number	-
Brightness_Temperature	Observed Brightness Temperature from Cloudy Averaged Radiances in a 5x5 1-km Pixel Region	5 km
Cirrus_Reflectance	Cirrus Reflectance	1 km
Cirrus_Reflectance_Flag	Cirrus Reflectance Flag	1 km
Cloud_Effective_Emissivity	Cloud Effective Emissivity from Cloud Top Pressure Retrieval	5 km
Cloud_Effective_Emissivity_Day	Cloud Effective Emissivity from Cloud Top Pressure Retrieval, Day Only	5 km
Cloud_Effective_Emissivity_Nadir	Cloud Effective Emissivity from Cloud Top Pressure Retrieval for Sensor Zenith (View) Angles <= 32 Degrees	5 km
Cloud_Effective_Emissivity_Nadir_Day	Cloud Effective Emissivity from Cloud Top Pressure Retrieval for Sensor Zenith (View) Angles <= 32 Degrees, Day Data Only	5 km
Cloud_Effective_Emissivity_Nadir_Night	Cloud Effective Emissivity from Cloud Top Pressure Retrieval for Sensor Zenith (View) Angles <= 32 Degrees, Night Data Only	5 km
Cloud_Effective_Emissivity_Night	Cloud Effective Emissivity from Cloud Top Pressure Retrieval, Night Only	5 km
Cloud_Effective_Radius	Cloud Particle Effective Radius two-channel retrieval using band 7(2.1um) and either band 1(0.65um), 2(0.86um), or 5(1.2um) (specified in Quality Assurance 1km)from best points: not failed in any way, not marked for clear sky restoral	1 km
Cloud_Effective_Radius_PCL	Cloud Particle Effective Radius two-channel retrieval using band 7(2.1um) and either band 1(0.65um), 2(0.86um), or 5(1.2um) (specified in Quality Assurance 1km)from points identified as either partly cloudy from 250m cloud mask test or 1km cloud edges	1 km
Cloud_Effective_Radius_16	Cloud Particle Effective Radius two-channel retrieval using band 6(1.6um) and either band 1(0.65um), 2(0.86um), or 5(1.2um) (specified in Quality Assurance 1km)from best points: not failed in any way, not marked for clear sky restoral	1 km
Cloud_Effective_Radius_16_PCL	Cloud Particle Effective Radius two-channel retrieval using band 6(1.6um) and either band 1(0.65um), 2(0.86um), or 5(1.2um) (specified in Quality Assurance 1km)from points identified as either partly cloudy from 250m cloud mask test or 1km cloud edges	1 km
Cloud_Effective_Radius_1621	Cloud Particle Effective Radius two-channel retrieval using band 7(2.1um) and band 6(1.6um)from best points: not failed in any way, not marked for clear sky restoral	1 km
Cloud_Effective_Radius_1621_PCL	Cloud Particle Effective Radius two-channel retrieval using band 7(2.1um) and band 6(1.6um)from points identified as either partly cloudy from 250m cloud mask test or 1km cloud edges	1 km
Cloud_Effective_Radius_37	Cloud Particle Effective Radius two-channel retrieval using band 20(3.7um) and either band 1(0.65um), 2(0.86um), or 5(1.2um) (specified in Quality Assurance 1km)from best points: not failed in any way, not marked for clear sky restoral	1 km
Cloud_Effective_Radius_37_PCL	Cloud Particle Effective Radius two-channel retrieval using band 20(3.7um) and either band 1(0.65um), 2(0.86um), or 5(1.2um) (specified in Quality Assurance 1km)from points identified as either partly cloudy from 250m cloud mask test or 1km cloud edges	1 km
Cloud_Effective_Radius_Uncertainty	Cloud Effective Particle Radius (from band 7(2.1um)) Relative Uncertainty (Percent)from both best points and points identified as cloud edge at 1km resolution or partly cloudy at 250m	1 km
Cloud_Effective_Radius_Uncertainty_16	Cloud Effective Particle Radius (from band 6(1.6um) Relative Uncertainty (Percent)from both best points and points identified as cloud edge at 1km resolution or partly cloudy at 250m	1 km
Cloud_Effective_Radius_Uncertainty_1621	Cloud Effective Particle Radius Relative Uncertainty (Percent) using band 7(2.1um) and band 6(1.6um)from both best points and points identified as cloud edge at 1km resolution or partly cloudy at 250m	1 km
Cloud_Effective_Radius_Uncertainty_37	Cloud Effective Particle Radius (from band 20(3.7um)) Relative Uncertainty (Percent)from both best points and points identified as cloud edge at 1km resolution or partly cloudy at 250m	1 km
cloud_emiss11_1km	11 micron Cloud Emissivity at 1-km resolution from LEOCAT for All Clouds	1 km
cloud_emiss12_1km	12 micron Cloud Emissivity at 1-km resolution from LEOCAT for All Clouds	1 km
cloud_emiss13_1km	13.3 micron Cloud Emissivity at 1-km resolution from LEOCAT for All Clouds	1 km
cloud_emiss85_1km	8.5 micron Cloud Emissivity at 1-km resolution from LEOCAT for All Clouds	1 km
cloud_emissivity_1km	Cloud Emissivity at 1-km resolution from LEOCAT Cloud Top Pressure Retrieval	1 km
Cloud_Fraction	Cloud Fraction in Retrieval Region (5x5 1-km Pixels) from 1-km Cloud Mask	5 km
Cloud_Fraction_Day	Cloud Fraction in Retrieval Region (5x5 1-km Pixels) from 1-km Cloud Mask, Day Only	5 km
Cloud_Fraction_Nadir	Cloud Fraction in Retrieval Region (5x5 1-km Pixels) from 1-km Cloud Mask for Sensor Zenith (View) Angles <= 32 Degrees	5 km
Cloud_Fraction_Nadir_Day	Cloud Fraction in Retrieval Region (5x5 1-km Pixels) from 1-km Cloud Mask for Sensor Zenith (View) Angles <= 32 Degrees, Day Data Only	5 km
Cloud_Fraction_Nadir_Night	Cloud Fraction in Retrieval Region (5x5 1-km Pixels) from 1-km Cloud Mask for Sensor Zenith (View) Angles <= 32 Degrees, Night Data Only	5 km
Cloud_Fraction_Night	Cloud Fraction in Retrieval Region (5x5 1-km Pixels) from 1-km Cloud Mask, Night Only	5 km
Cloud_Height_Method	Index Indicating MODIS Bands Used for Cloud Top Pressure Retrieval	5 km
Cloud_Mask_1km	MODIS Cloud Mask, L2 MOD06 QA Plan	1 km
Cloud_Mask_5km	First Byte of MODIS Cloud Mask Plus Additional Stats for L3 (2nd Byte)	5 km
Cloud_Mask_SPI	Dispersion in bands 1 (plane 1) and 2 (plane 2) from 250m reflectance statistics of cloud mask	1 km
Cloud_Multi_Layer_Flag	Cloud Multi Layer Identification From MODIS Shortwave Observations	1 km
Cloud_Optical_Thickness	Cloud Optical Thickness two-channel retrieval using band 7(2.1um) and either band 1(0.65um), 2(0.86um), or 5(1.2um) (specified in Quality Assurance 1km)from best points: not failed in any way, not marked for clear sky restoral	1 km
Cloud_Optical_Thickness_PCL	Cloud Optical Thickness two-channel retrieval using band 7(2.1um) and either band 1(0.65um), 2(0.86um), or 5(1.2um) (specified in Quality Assurance 1km)from points identified as either partly cloudy from 250m cloud mask test or 1km cloud edges	1 km
Cloud_Optical_Thickness_16	Cloud Optical Thickness two-channel retrieval using band 6(1.6um) and either band 1(0.65um), 2(0.86um), or 5(1.2um) (specified in Quality Assurance 1km)from best points: not failed in any way, not marked for clear sky restoral	1 km
Cloud_Optical_Thickness_16_PCL	Cloud Optical Thickness two-channel retrieval using band 6(1.6um) and either band 1(0.65um), 2(0.86um), or 5(1.2um) (specified in Quality Assurance 1km)from points identified as either partly cloudy from 250m cloud mask test or 1km cloud edges	1 km
Cloud_Optical_Thickness_1621	Cloud Optical Thickness two-channel retrieval using band 7(2.1um) and band 6(1.6um)from best points: not failed in any way, not marked for clear sky restoral	1 km
Cloud_Optical_Thickness_1621_PCL	Cloud Optical Thickness two-channel retrieval using band 7(2.1um) and band 6(1.6um)from points identified as either partly cloudy from 250m cloud mask test or 1km cloud edges	1 km
Cloud_Optical_Thickness_37	Cloud Optical Thickness two-channel retrieval using band 20(3.7um) and either band 1(0.65um), 2(0.86um), or 5(1.2um) (specified in Quality Assurance 1km)from best points: not failed in any way, not marked for clear sky restoral	1 km
Cloud_Optical_Thickness_37_PCL	Cloud Optical Thickness two-channel retrieval using band 20(3.7um) and either band 1(0.65um), 2(0.86um), or 5(1.2um) (specified in Quality Assurance 1km)from points identified as either partly cloudy from 250m cloud mask test or 1km cloud edges	1 km
Cloud_Optical_Thickness_Uncertainty	Cloud Optical Thickness Relative Uncertainty (Percent)from both best points and points identified as cloud edge at 1km resolution or partly cloudy at 250m based on the Cloud Optical Thickness and Cloud Effective Radius results	1 km
Cloud_Optical_Thickness_Uncertainty_16	Cloud Optical Thickness Relative Uncertainty (Percent)from both best points and points identified as cloud edge at 1km resolution or partly cloudy at 250m based on the Cloud Optical Thickness 16 and Cloud Effective Radius 16 results	1 km
Cloud_Optical_Thickness_Uncertainty_1621	Cloud Optical Thickness Relative Uncertainty (Percent) using band 7(2.1um) and band 6(1.6um)from both best points and points identified as cloud edge at 1km resolution or partly cloudy at 250m	1 km
Cloud_Optical_Thickness_Uncertainty_37	Cloud Optical Thickness Relative Uncertainty (Percent)from both best points and points identified as cloud edge at 1km resolution or partly cloudy at 250m based on the Cloud Optical Thickness 37 and Cloud Effective Radius 37 results	1 km

Cloud_Phase_Infrared	Cloud Phase from 8.5 and 11 um Bands	5 km
Cloud_Phase_Infrared_1km	Cloud Phase at 1-km resolution from 8.5- 11 um BTDs and cloud emissivity ratios (12/11, 8.5/11, and 7.2/11 um)	1 km
Cloud_Phase_Infrared_Day	Cloud Phase from 8.5 and 11 um Bands, Day Only	5 km
Cloud_Phase_Infrared_Night	Cloud Phase from 8.5 and 11 um Bands, Night Only	5 km
Cloud_Phase_Optical_Properties	Cloud Phase Determination Used in Optical Thickness/Effective Radius Retrieval	1 km
Cloud_Top_Height	Geopotential Height at Retrieved Cloud Top Pressure Level (rounded to nearest 50 m)	5 km
cloud_top_height_1km	Cloud Top Height at 1-km resolution from LEOCAT, Geopotential Height at Retrieved Cloud Top Pressure Level rounded to nearest 50 m	1 km
Cloud_Top_Height_Nadir	Geopotential Height at Retrieved Cloud Top Pressure Level for Sensor Zenith (View) Angles <=32 Degrees (rounded to nearest 50 m)	5 km
Cloud_Top_Height_Nadir_Day	Geopotential Height at Retrieved Cloud Top Pressure Level for Sensor Zenith (View) Angles <=32 Degrees, Day Data Only (rounded to nearest 50 m)	5 km
Cloud_Top_Height_Nadir_Night	Geopotential Height at Retrieved Cloud Top Pressure Level for Sensor Zenith (View) Angles <=32 Degrees, Night Data Only (rounded to nearest 50 m)	5 km
cloud_top_method_1km	Index indicating the MODIS Band(s) Used to Produce the Cloud Top Pressure Result	5 km
Cloud_Top_Pressure	Cloud Top Pressure Level (rounded to nearest 5 mb)	5 km
cloud_top_pressure_1km	Cloud Top Pressure at 1-km resolution from LEOCAT, Cloud Top Pressure Level rounded to nearest 5 mb	1 km
Cloud_Top_Pressure_Day	Cloud Top Pressure Level, Day Only (rounded to nearest 5 mb)	5 km
Cloud_Top_Pressure_From_Ratios	Cloud Top Pressure Levels from Ratios of Bands 36/35, 35/34, 35/33, 34/33 from the CO2-slicing Algorithm	5 km
Cloud_Top_Pressure_Infrared	Cloud Top Pressure from IR Window Retrieval	5 km
Cloud_Top_Pressure_Nadir	Cloud Top Pressure Level for Sensor Zenith (View) Angles <= 32 Degrees (rounded to nearest 5 mb)	5 km
Cloud_Top_Pressure_Nadir_Day	Cloud Top Pressure Level for Sensor Zenith (View) Angles <= 32 Degrees (rounded to nearest 5 mb), Day Data Only	5 km
Cloud_Top_Pressure_Nadir_Night	Cloud Top Pressure Level for Sensor Zenith (View) Angles <= 32 Degrees (rounded to nearest 5 mb), Night Data Only	5 km
Cloud_Top_Pressure_Night	Cloud Top Pressure Level, Night Data Only (rounded to nearest 5 mb)	5 km
Cloud_Top_Temperature	Temperature from Ancillary Data at Retrieved Cloud Top Pressure Level	5 km
cloud_top_temperature_1km	Cloud Top Temperature at 1-km resolution from LEOCAT, Temperature from Ancillary Data at Retrieved Cloud Top Pressure Level	1 km
Cloud_Top_Temperature_Day	Temperature from Ancillary Data at Retrieved Cloud Top Pressure Level, Day Only	5 km
Cloud_Top_Temperature_Nadir	Temperature from Ancillary Data at Retrieved Cloud Top Pressure Level for Sensor Zenith (View) Angles <= 32 Degrees	5 km
Cloud_Top_Temperature_Nadir_Day	Temperature from Ancillary Data at Retrieved Cloud Top Pressure Level for Sensor Zenith (View) Angles <= 32 Degrees, Day Data Only	5 km
Cloud_Top_Temperature_Nadir_Night	Temperature from Ancillary Data at Retrieved Cloud Top Pressure Level for Sensor Zenith (View) Angles <= 32 Degrees, Night Data Only	5 km
Cloud_Top_Temperature_Night	Temperature from Ancillary Data at Retrieved Cloud Top Pressure Level, Night Only	5 km
Cloud_Water_Path	Column Water Path two-channel retrieval using band 7(2.1um) and either band 1(0.65um), 2(0.86um), or 5(1.2um) (specified in Quality Assurance 1km)from best points: not failed in any way, not marked for clear sky restoral	1 km
Cloud_Water_Path_PCL	Column Water Path two-channel retrieval using band 7(2.1um) and either band 1(0.65um), 2(0.86um), or 5(1.2um) (specified in Quality Assurance 1km)from points identified as either partly cloudy from 250m cloud mask test or 1km cloud edges	1 km
Cloud_Water_Path_16	Column Water Path two-channel retrieval using band 6(1.6um) and either band 1(0.65um), 2(0.86um), or 5(1.2um) (specified in Quality Assurance 1km)from best points: not failed in any way, not marked for clear sky restoral	1 km
Cloud_Water_Path_16_PCL	Column Water Path two-channel retrieval using band 6(1.6um) and either band 1(0.65um), 2(0.86um), or 5(1.2um) (specified in Quality Assurance 1km)from points identified as either partly cloudy from 250m cloud mask test or 1km cloud edges	1 km
Cloud_Water_Path_1621	Column Water Path two-channel retrieval using band 7(2.1um) and band 6(1.6um)from best points: not failed in any way, not marked for clear sky restoral	1 km
Cloud_Water_Path_1621_PCL	Column Water Path two-channel retrieval using band 7(2.1um) and band 6(1.6um)from points identified as either partly cloudy from 250m cloud mask test or 1km cloud edges	1 km
Cloud_Water_Path_37	Column Water Path two-channel retrieval using band 20(3.7um) and either band 1(0.65um), 2(0.86um), or 5(1.2um) (specified in Quality Assurance 1km)from best points: not failed in any way, not marked for clear sky restoral	1 km
Cloud_Water_Path_37_PCL	Column Water Path two-channel retrieval using band 20(3.7um) and either band 1(0.65um), 2(0.86um), or 5(1.2um) (specified in Quality Assurance 1km)from points identified as either partly cloudy from 250m cloud mask test or 1km cloud edges	1 km
Cloud_Water_Path_Uncertainty	Cloud Water Path Relative Uncertainty (Percent)from both best points and points identified as cloud edge at 1km resolution or partly cloudy at 250m based on the Cloud Water Path result	1 km
Cloud_Water_Path_Uncertainty_16	Cloud Water Path Relative Uncertainty (Percent)from both best points and points identified as cloud edge at 1km resolution or partly cloudy at 250m using the VNSWIR-1.6um retrieval	1 km
Cloud_Water_Path_Uncertainty_1621	Cloud Water Path Relative Uncertainty (Percent) using band 7(2.1um) and band 6(1.6um)from both best points and points identified as cloud edge at 1km resolution or partly cloudy at 250m	1 km
Cloud_Water_Path_Uncertainty_37	Cloud Water Path Relative Uncertainty (Percent)from both best points and points identified as cloud edge at 1km resolution or partly cloudy at 250m using the VNSWIR-3.7um retrieval	1 km
Extinction_Efficiency_Ice	Ice Extinction Efficiency from the phase functions used to generate the forward lookup tables	1 km
Extinction_Efficiency_Liq	Liquid Water CE from the phase functions used to generate the forward lookup tables	1 km
IRP_CTH_Consistency_Flag_1km	Indicates Cloud Phase Infrared 1km results changed to ice from water when cloud top method 1km reports valid band 36/35 CO2-slicing result (1=change)	1 km
IRW_Low_Cloud_Temperature_From_COP	Low Cloud Temperature from IR Window retrieval using cloud emissivity based on cloud optical thickness	1 km
os_top_flag_1km	Upper Tropospheric/Lower Stratospheric (UTLS) Cloud Flag at 1-km resolution - valid from -50 to +50 Degrees Latitude	1 km
Quality_Assurance_1km	Quality Assurance at 1x1 Resolution	1 km
Quality_Assurance_5km	Quality Assurance at 5x5 Resolution	5 km
Radiance_Variance	Band 31 Radiance Standard Deviation	5 km
Retrieval_Failure_Metric	Retrievals and other information for points that failed to retrieve via standard solution logic for retrieval using band 7 and either band 1, 2, or 5 (specified in Quality Assurance 1km)	1 km
Retrieval_Failure_Metric_16	Retrievals and other information for points that failed to retrieve via standard solution logic for retrieval using band 6 and either band 1, 2, or 5 (specified in Quality Assurance 1km)	1 km
Retrieval_Failure_Metric_1621	Retrievals and other information for points that failed to retrieve via standard solution logic for retrieval using band 6 and band 7	1 km
Retrieval_Failure_Metric_37	Retrievals and other information for points that failed to retrieve via standard solution logic for retrieval using band 20 and either band 1, 2, or 5 (specified in Quality Assurance 1km)	1 km
Scan_Start_Time	TAI time at start of scan replicated across the swath	5 km
Sensor_Azimuth	Sensor Azimuth Angle, Cell to Sensor	5 km
Sensor_Azimuth_Day	Sensor Azimuth Angle, Cell to Sensor, Day Data Only	5 km
Sensor_Azimuth_Night	Sensor Azimuth Angle, Cell to Sensor, Night Data Only	5 km
Sensor_Zenith	Sensor Zenith Angle, Cell to Sensor	5 km
Sensor_Zenith_Day	Sensor Zenith Angle, Cell to Sensor, Day Data Only	5 km
Sensor_Zenith_Night	Sensor Zenith Angle, Cell to Sensor, Night Data Only	5 km
Single_Scatter_Albedo_Ice	Ice single scatter albedo from the phase functions used to generate the forward lookup tables	—
Single_Scatter_Albedo_Liq	Liquid Water single scatter albedo from the phase functions used to generate the forward lookup tables	—
Solar_Azimuth	Solar Azimuth Angle, Cell to Sun	5 km
Solar_Azimuth_Day	Solar Azimuth Angle, Cell to Sun, Day Data Only	5 km
Solar_Azimuth_Night	Solar Azimuth Angle, Cell to Sun, Night Data Only	5 km
Solar_Zenith	Solar Zenith Angle, Cell to Sun	5 km
Solar_Zenith_Day	Solar Zenith Angle, Cell to Sun, Day Data Only	5 km
Solar_Zenith_Night	Solar Zenith Angle, Cell to Sun, Night Data Only	5 km
Spectral_Cloud_Forcing	Spectral Cloud Forcing (cloud minus clear radiance)	5 km
Statistics_1km	Statistics_1km	—
Surface_Pressure	Surface Pressure from Ancillary Data	5 km
Surface_Temperature	Surface Temperature from Ancillary Data	5 km
surface_temperature_1km	Surface Temperature for Each 1-km MODIS Pixel Interpolated from Ancillary Data	5 km
surface_temperature_1km	Surface Temperature for Each 1-km MODIS Pixel Interpolated from Ancillary Data	5 km
Latitude	Geodetic Latitude	5 km
Longitude	Geodetic Longitude	5 km

APPENDIX B. SUMMARY SDS AND QUALITY ASSURANCE (QA) ASSIGNMENTS

Mapping of Pixel Retrieval Outcome Status to SDS Assignments

SDS Names ¹ (Abbreviated Notation)	Retrieval Outcome Status																Cloud Mask 'Not Cloudy' or CSR=2	No Cloud Mask
	VNSWIR-2.1 μm Retrievals				VNSWIR-1.6 μm CER Retrievals				VNSWIR-3.7 μm CER Retrievals				1.6-2.1 μm Retrievals					
	Successful COT, CER, WP CSR=0		Successful COT, CER, WP CSR=1,3 (PCL)		Successful 1.6 μm CER CSR=0		Successful 1.6 μm CER CSR=1,3 (PCL)		Successful 3.7 μm CER CSR=0		Successful 3.7 μm CER CSR=1,3 (PCL)		Successful COT, CER, WP CSR=0		Successful COT, CER, WP CSR=1,3 (PCL)			
	Yes	No	Yes	No	Yes	No	Yes	No	Yes	No	Yes	No	Yes	No	Yes	No		
COT, CER, WP	Valid	Fill	Fill	Fill	-	-	-	-	-	-	-	-	-	-	-	-	Fill	Fill
COT_PCL, CER_PCL, WP_PCL	Fill	Fill	Valid	Fill	-	-	-	-	-	-	-	-	-	-	-	-	Fill	Fill
CER_16, WP_16	-	-	-	-	Valid	Fill	Fill	Fill	-	-	-	-	-	-	-	-	Fill	Fill
CER_16_PCL, WP_16_PCL	-	-	-	-	Fill	Fill	Valid	Fill	-	-	-	-	-	-	-	-	Fill	Fill
CER_37, WP_37	-	-	-	-	-	-	-	-	Valid	Fill	Fill	Fill	-	-	-	-	Fill	Fill
CER_37_PCL, WP_37_PCL	-	-	-	-	-	-	-	-	Fill	Fill	Valid	Fill	-	-	-	-	Fill	Fill
COT_1621, CER_1621, WP_1621	-	-	-	-	-	-	-	-	-	-	-	-	Valid	Fill	Fill	Fill	Fill	Fill
COT_1621_PCL, CER_1621_PCL, WP_1621_PCL	-	-	-	-	-	-	-	-	-	-	-	-	Fill	Fill	Valid	Fill	Fill	Fill

¹ Notation: COT = Cloud_Optical_Thickness
CER = Cloud_Effective_Radius
WP = Cloud_Water_Path

Mapping of Pixel Retrieval Outcome Status to QA Assignments

Quality_Assurance_1km Flag	Outcome Status for Attempted Retrievals (MOD35 Cloudy Pixels with CSR=0,1,3)																Cloud Mask 'Not Cloudy' or CSR=2	No Cloud Mask
	VNSWIR-2.1 μm Retrievals				VNSWIR-1.6 μm CER Retrievals				VNSWIR-3.7 μm CER Retrievals				1.6-2.1 μm Retrievals					
	Successful COT, CER, WP CSR=0		Successful COT, CER, WP CSR=1,3 (PCL)		Successful 1.6 μm CER CSR=0		Successful 1.6 μm CER CSR=1,3 (PCL)		Successful 3.7 μm CER CSR=0		Successful 3.7 μm CER CSR=1,3 (PCL)		Successful COT, CER, WP CSR=0		Successful COT, CER, WP CSR=1,3 (PCL)			
	Yes	No	Yes	No	Yes	No	Yes	No	Yes	No	Yes	No	Yes	No	Yes	No		
Retrieval Phase (3 Bits)	≥ 2	≥ 2	≥ 2	≥ 2	≥ 2	≥ 2	≥ 2	≥ 2	≥ 2	≥ 2	≥ 2	≥ 2	≥ 2	≥ 2	≥ 2	≥ 2	1	0
Multi Layer Cloud Flag (Byte 4, Bits 3,4,5)	≥ 2	≥ 2	≥ 2	≥ 2	≥ 2	≥ 2	≥ 2	≥ 2	≥ 2	≥ 2	≥ 2	≥ 2	≥ 2	≥ 2	≥ 2	≥ 2	1	0
VNSWIR-2.1 Retrieval Outcome (Byte 2, Bit 3) 0 = Failed/No Attempt 1 = Successful	1	0	0	0	-	-	-	-	-	-	-	-	-	-	-	-	0	0
VNSWIR-2.1 PCL Retrieval Outcome (Byte 8, Bit 7) 0 = Failed/No Attempt 1 = Successful	0	0	1	0	-	-	-	-	-	-	-	-	-	-	-	-	0	0
VNSWIR-1.6 Retrieval Outcome (Byte 6, Bit 3) 0 = Failed/No Attempt 1 = Successful	-	-	-	-	1	0	0	0	-	-	-	-	-	-	-	-	0	0
VNSWIR-1.6 PCL Retrieval Outcome (Byte 6, Bit 7) 0 = Failed/No Attempt 1 = Successful	-	-	-	-	0	0	1	0	-	-	-	-	-	-	-	-	0	0
VNSWIR-3.7 Retrieval Outcome (Byte 7, Bit 3) 0 = Failed/No Attempt 1 = Successful	-	-	-	-	-	-	-	-	1	0	0	0	-	-	-	-	0	0
VNSWIR-3.7 PCL Retrieval Outcome (Byte 7, Bit 7) 0 = Failed/No Attempt 1 = Successful	-	-	-	-	-	-	-	-	0	0	1	0	-	-	-	-	0	0
1.6-2.1 Retrieval Outcome (Byte 1, Bit 6) 0 = Failed/No Attempt 1 = Successful	-	-	-	-	-	-	-	-	-	-	-	-	1	0	0	0	0	0
1.6-2.1 PCL Retrieval Outcome (Byte 8, Bit 3) 0 = Failed/No Attempt 1 = Successful	-	-	-	-	-	-	-	-	-	-	-	-	0	0	1	0	0	0

 The Retrieval Phase flag contains the processed cloud phase for all cloud optical and microphysical property retrieval SDSs (including the Retrieval Failure Metric SDSs). It is repeated (and identical) for each band combination, and always immediately precedes the specific Retrieval Outcome Flags.
 The Multi Layer Cloud Flag is shared for all retrievals, though the multilayer algorithm is only run when VNSWIR-2.1 μm retrievals are successful and CSR=0.

Retrieval Failure Metric Assignments

Retrieval Band Combinations	Retrieval Outcome Status	Failure Category ¹	Retrieval Failure Metric SDS		
			COT	CER	Cost Metric (CM)
VNSWIR-2.1 μm Retrievals (Primary)			Retrieval Failure Metric		
	Successful ²	-	Fill	Fill	Fill
	Not Successful ³	Cat. 1	Valid	Max/Min	≥ 0
Cat. 3		Fill	Fill	Fill	
VNSWIR-1.6 μm CER Retrievals			Retrieval Failure Metric 16		
	Successful	-	Fill	Fill	Fill
	Not Successful	Cat. 1	Valid	Max/Min	≥ 0
Cat. 3		Fill	Fill	Fill	
VNSWIR-3.7 μm CER Retrievals			Retrieval Failure Metric 37		
	Successful	-	Fill	Fill	Fill
	Not Successful	Cat. 1	Valid	Max/Min	≥ 0
Cat. 3		Fill	Fill	Fill	
1.6-2.1 μm Retrievals			Retrieval Failure Metric 1621		
	Successful	-	Fill	Fill	Fill
	Not Successful	Cat. 1	Valid	Max/Min	≥ 0
		Cat. 2	Fill	Valid	≥ 0
Cat. 3		Fill	Fill	Fill	
All Retrieval Combinations	Cloud Mask Not Determined or "Not Cloudy", or CSR=2	-	Fill	Fill	Fill

Notes: Retrieval Failure Metric SDSs contain diagnostic information regarding optical property retrieval failures for both CSR=0 and CSR=1,3 (PCL) pixels.

Cloud retrieval phase may be obtained from the Retrieval Phase flag in the Quality_Assurance_1km SDS.

¹ Failure Categories: Cat. 1: Successful COT with CER set to max/min.
 Cat. 2: Failed COT for 1.6-2.1 μm pair, successful CER.
 Cat. 3: Failed COT and CER.

² Successful COT, CER and WP for CSR=0 or CSR=1,3 (PCL) pixels.

³ Both CSR=0 and CSR=1,3 retrieval SDSs are fill values.

The following details on cloud optical property QA bit assignments are taken from the MODIS Atmosphere Team Quality Assurance Plan, version 4.10 (23 April 2013, P. Hubanks et al.). The document is available for download at: modis-atmos.gsfc.nasa.gov/_docs/QA_Plan_C6_Master_2013_04_23.pdf. Readers should consult this link to ensure they have the most up-to-date documentation.

MODIS Atmosphere QA plan

21

Note that the *Quality_Assurance_1km* SDS in 06_L2 HDF files was expanded from 5 bytes (in Collection 005/051) to 9 bytes (in Collection 006).

Scientific Data Set (SDS): <i>"Quality_Assurance_1km"</i>			
Description: <i>Cloud Optical Property product quality and retrieval processing QA flags at 1x1 km</i>			
Length: C006 = 9 bytes (72 bits) C005/051 = 5 bytes (40 bits)			
Flag Name	Number of Bits	Bit Values	Bit Value Definitions
Primary (VNSWIR - 2.1 μm) Cloud Optical Thickness Usefulness Flag	1	0 1	Not useful Useful
Primary (VNSWIR - 2.1 μm) Cloud Optical Thickness Confidence Flag	2	0 1 2 3	No Confidence or Fill Marginal Confidence Good Confidence Very Good Confidence
Spares <i>Previously the Cloud Optical Thickness Out-of-Bounds Flag. Note: Library goes to 158.78, but there is a hard cut-off now at 150.</i>	2		
Primary (VNSWIR - 2.1 μm) Cloud Effective Radius Usefulness Flag	1	0 1	Not useful Useful
Primary (VNSWIR - 2.1 μm) Cloud Effective Radius Confidence Flag	2	0 1 2 3	No Confidence or Fill Marginal Confidence Good Confidence Very Good Confidence
Primary (VNSWIR - 2.1 μm) Cloud Water Path Usefulness Flag	1	0 1	Not useful Useful
Primary (VNSWIR - 2.1 μm) Cloud Water Path Confidence Flag	2	0 1 2 3	No Confidence or Fill Marginal Confidence Good Confidence Very Good Confidence
Cloud Retrieval Phase Flag <i>(Cloud Retrieval Phase Flag duplicated from the 3rd byte). For combining with the 1.6 - 2.1 μm Cloud Retrieval Outcome Flag (below). Needed by L3 to properly compute 1621 Cloud Fractions. (See page 25 of this Plan)</i>	3	0 1 2 3 4	Cloud Mask Undetermined or Non-Snow Land ^{n,j} Not Processed (typically clear) ^f Liquid Water Cloud Ice Cloud Undetermined Phase Cloud
1.6 - 2.1 μm Cloud Retrieval Outcome Flag <i>The Cloud Retrieval Phase Flag and 1621 Outcome Flag are read as a combined flag by L3 to properly compute 1621 Cloud Retrieval Fractions. (See page 25 of this Plan)</i>	1	0 1	Retrieval not attempted or unsuccessful ^f Retrieval successful (over ocean, snow, & ice only)
Spare	1		TBD

MODIS Atmosphere QA Plan

22

Cloud Retrieval Phase Flag <i>Primary Cloud Retrieval Phase Flag and Outcome Flag are read as a combined flag by L3 to properly compute Primary Cloud Retrieval Fractions. (See page 25 of this Plan)</i>	3	0 1 2 3 4	Cloud Mask Undetermined ^{n,f} Not Processed (typically clear) ^f Liquid Water Cloud Ice Cloud Undetermined Phase Cloud
Primary (VNSWIR - 2.1 μm) Cloud Retrieval Outcome Flag <i>Primary Cloud Retrieval Phase Flag and Outcome Flag are read as a combined flag by L3 to properly compute Primary Cloud Retrieval Fractions. (See page 25 of this Plan)</i>	1	0 1	Retrieval not attempted or unsuccessful ^f Retrieval successful
Rayleigh Correction	1	0 1	No Yes, correction was made
Atmospheric Water Vapor Correction	1	0 1	No Yes, correction was made
Band Used for Primary Optical Thickness Retrieval	2	0 1 2 3	Retrieval not attempted ^f 0.645 μm (land) 0.858 μm (water) 1.24 μm (snow / ice)
1.6 - 2.1 μm Cloud Optical Thickness Usefulness Flag	1	0 1	Not useful Useful
1.6 - 2.1 μm Cloud Optical Thickness Confidence Flag	2	0 1 2 3	No Confidence or Fill Marginal Confidence Good Confidence Very Good Confidence
1.6 - 2.1 μm Cloud Effective Radius Usefulness Flag	1	0 1	Not useful Useful
1.6 - 2.1 μm Cloud Effective Radius Confidence Flag	2	0 1 2 3	No Confidence or Fill Marginal Confidence Good Confidence Very Good Confidence
Clear Sky Restoral Type Flag	2	0 1 2 3	Not Restored Restored to clear sky via Edge Detection Restored to clear sky via Spatial Variance Restored to clear sky via 250 meter Tests
1.6 - 2.1 μm Cloud Water Path Usefulness Flag	1	0 1	Not useful Useful
1.6 - 2.1 μm Cloud Water Path Confidence Flag	2	0 1 2 3	No Confidence or Fill Marginal Confidence Good Confidence Very Good Confidence

MODIS Atmosphere QA plan

23

Primary Cloud Retrieval (VNSWIR - 2.1 μm) Multilayer Cloud & Phase Flag	3	0 1 2 3 4 5 6 7	Cloud mask undetermined ^{n,f} Not Processed (typically clear) ^f Single-Layer Liquid Water Cloud Multi-Layer Liquid Water Cloud Single-Layer Ice Cloud Multi-Layer Ice Cloud Single-Layer Undetermined Phase Cloud Multi-Layer Undetermined Phase Cloud
Primary Cloud Retrieval (VNSWIR - 2.1 μm) Outcome Flag <i>(Primary Cloud Retrieval Outcome Flag duplicated from the 3rd byte). For combining with the Primary Cloud Retrieval Multilayer Cloud & Phase Flag (above). Needed by L3 to properly compute 1L & ML Cloud Fractions.</i>	1	0 1	Retrieval not attempted or unsuccessful ^f Retrieval successful
Spare	1		TBD
Phase Difference Multilayer Test	1	0 1	No Yes
Delta Precipitable Water Multilayer Test	1	0 1	No Yes
Delta Precipitable Water at 900mb Test	1	0 1	No Yes
Tau Difference VIS-NIR Multilayer Test	1	0 1	No Yes
Pavlonis-Heidinger Multilayer Test	1	0 1	No Yes
Spares	3		TBD
VNSWIR - 1.6 μm Cloud Retrieval Phase & Outcome <i>(The Cloud Retrieval Phase Flag and Outcome Flag can be read as a "combined" flag as documented here -- or read as separate flags -- the bit structure is identical. (See page 25 of this Plan for details)</i>	4	0 1 2 3 4 10 11 12	Cloud Mask Undetermined ^{n,f} Not Processed (typically clear) ^f Failed Liquid Water Cloud Retrieval Failed Ice Cloud Retrieval Failed Undetermined Phase Cloud Retrieval Successful Liquid Water Cloud Retrieval Successful Ice Cloud Retrieval Successful Undetermined Phase Cloud Retrieval
VNSWIR - 1.6 μm PCL (Partly Cloudy) Cloud Retrieval Phase & Outcome <i>(The Cloud Retrieval Phase Flag and Outcome Flag can be read as a "combined" flag as documented here -- or read as separate flags -- the bit structure is identical. (See page 25 of this Plan for details)</i>	4	0 1 2 3 4 10 11 12	Cloud Mask Undetermined ^{n,f} Not Processed (typically clear) ^f Failed Liquid Water Cloud Retrieval Failed Ice Cloud Retrieval Failed Undetermined Phase Cloud Retrieval Successful Liquid Water Cloud Retrieval Successful Ice Cloud Retrieval Successful Undetermined Phase Cloud Retrieval

MODIS Atmosphere QA Plan

24

VNSWIR - 3.7 μm Cloud Retrieval Phase & Outcome <i>(The Cloud Retrieval Phase Flag and Outcome Flag can be read as a "combined" flag as documented here -- or read as separate flags -- the bit structure is identical. (See page 25 of this Plan for details))</i>	4	0 1 2 3 4 10 11 12	Cloud Mask Undetermined ^{n,f} Not Processed (typically clear) ^f Failed Liquid Water Cloud Retrieval Failed Ice Cloud Retrieval Failed Undetermined Phase Cloud Retrieval Successful Liquid Water Cloud Retrieval Successful Ice Cloud Retrieval Successful Undetermined Phase Cloud Retrieval
VNSWIR - 3.7 μm PCL (Partly Cloudy) Cloud Retrieval Phase & Outcome <i>(The Cloud Retrieval Phase Flag and Outcome Flag can be read as a "combined" flag as documented here -- or read as separate flags -- the bit structure is identical. (See page 25 of this Plan for details))</i>	4	0 1 2 3 4 10 11 12	Cloud Mask Undetermined ^{n,f} Not Processed (typically clear) ^f Failed Liquid Water Cloud Retrieval Failed Ice Cloud Retrieval Failed Undetermined Phase Cloud Retrieval Successful Liquid Water Cloud Retrieval Successful Ice Cloud Retrieval Successful Undetermined Phase Cloud Retrieval
1.6 - 2.1 μm PCL (Partly Cloudy) Cloud Retrieval Phase & Outcome <i>(The Cloud Retrieval Phase Flag and Outcome Flag can be read as a "combined" flag as documented here -- or read as separate flags -- the bit structure is identical. (See page 25 of this Plan for details))</i>	4	0 1 2 3 4 10 11 12	Cloud Mask Undetermined ^{n,f} Not Processed (typically clear) ^f Failed Liquid Water Cloud Retrieval Failed Ice Cloud Retrieval Failed Undetermined Phase Cloud Retrieval Successful Liquid Water Cloud Retrieval Successful Ice Cloud Retrieval Successful Undetermined Phase Cloud Retrieval
VNSWIR - 2.1 μm (Primary) PCL (Partly Cloudy) Cloud Retrieval Phase & Outcome <i>(The Cloud Retrieval Phase Flag and Outcome Flag can be read as a "combined" flag as documented here -- or read as separate flags -- the bit structure is identical. (See page 25 of this Plan for details))</i>	4	0 1 2 3 4 10 11 12	Cloud Mask Undetermined ^{n,f} Not Processed (typically clear) ^f Failed Liquid Water Cloud Retrieval Failed Ice Cloud Retrieval Failed Undetermined Phase Cloud Retrieval Successful Liquid Water Cloud Retrieval Successful Ice Cloud Retrieval Successful Undetermined Phase Cloud Retrieval

ⁿ Cloud Optical Property retrieval not attempted

^f fill values used for Cloud Optical Property retrieval

APPENDIX C. KEY ACRONYMS

AOD: Aerosol Optical Depth

C5: Collection 5 MODIS Atmosphere Team processing stream (version), begun in mid-2006

C6: Collection 6 MODIS Atmosphere Team processing stream, began in Dec. 2013 for Aqua L2 products

CALIOP: lidar instrument flow on the NASA CALIPSO mission

CHIMAERA: Cross-platform High resolution Multi-instrument AtmosphEric Retrieval Algorithms. Cloud retrieval team's development environment that simultaneously supports multiple spaceborne and airborne platforms using the same science core.

CFMIP: Cloud Feedback Modeling Intercomparison Project (<http://cfmip.metoffice.com>)

CER, r_e : Cloud Effective particle Radius

COSP: CFMIP Observation Simulator Package (<http://cfmip.metoffice.com/COSP.html>), includes the MODIS simulator.

COT, τ : Cloud Optical Thickness

CREW: Cloud Retrieval Evaluation Workshops. International Polar/GEO cloud product inter-comparison effort (www.icare.univ-lille1.fr/crew/index.php/Welcome).

CSR: Clear Sky Restoral algorithm

CTH: Cloud-Top Height

CTP: Cloud Top Pressure

CTT: Cloud-Top Temperature

CWP: Cloud Water Path (e.g., gm^{-2}); LWP: Liquid Water Path; IWP: Ice Water Path

GEWEX: Global Energy and Water Cycle Experiment (under auspices World Climate Research Programme)

GOES-R AWG: NOAA Algorithm Working Group cloud code for the GOES-R ABI imager, similar to PATMOS-x

HDF: Hierarchical Data Format. MODIS data products are in HDF4.

LAADS: Land and Atmospheres Archive and Distribution System used to distribute MODIS Atmosphere Team products

L2: Level-2 products (pixel-level, 1 km resolution at nadir for all optical property products)

L3: Level-3 products (1° aggregated/gridded for all MODIS Atmosphere Team products)

MCST: MODIS Characterization and Support Team

MOD06 /MYD06: MODIS Terra/Aqua cloud-top and optical properties Level-2 product file ID

MOD08/MYD08: MODIS Terra/Aqua Atmosphere Team Level-3 product file ID

MOD35/MYD35: MODIS Terra/Aqua cloud mask Level-2 product file ID

MODATML2/MYDATML2: MODIS Atmosphere Team joint Level-2 product file ID

MODAPS: MODIS Adaptive Processing System—processing system for MODIS atmosphere team products

MWIR: Midwave Infrared (e.g., MODIS $3.7 \mu\text{m}$ channels)

PCL: pixels identified as “partly cloudy” by the CSR algorithm (CSR values of 1 and 2)

PAF: Phase Agreement Fraction, a metric used to assess thermodynamic phase skill.

QA: Quality Assurance. Often refers to bit assignments used to qualitatively assign pixel-level retrieval accuracy or the accuracy of aggregated statistics. More generically, can refer to any approach for filtering/weighting retrieved pixels.

SDS: Science Data Set. A distinct science data set within an HDF file.

SWIR: Shortwave Infrared (e.g., MODIS 1.2, 1.6, and 2.1 μm MODIS channels)

VNIR: Visible and Near-Infrared (e.g., MODIS 0.67 and 0.86 μm channels, respectively)

VNSWIR: Refers to a retrieval using a Visible or Near-Infrared or SWIR channel as one of the channel pairs (e.g, VIS over land surfaces, NIR over ocean surfaces, 1.2 μm over snow/ice surfaces).

Cloud Product: MOD06_L2 (Terra) & MYD06_L2 (Aqua)

The MODIS Cloud product consists of a 1 km set of parameters derived from solar reflectance channels (Cloud Optical Properties and Cirrus Reflectance) and a 5 km set of parameters determined from thermal emitted channels (Cloud Top Properties).

Cloud Optical Properties

Cloud Optical Property QA flags are stored in 2 separate QA arrays (SDS's). The first SDS, *Cloud_Mask_1km*, contains Cloud Mask QA flags, which are copied from the 35_L2 Cloud Mask product. The second SDS (*Quality_Assurance_1km*) contains product quality, retrieval processing, and scene characteristic flags. Detail is provided below.

- Spatial resolution: 1 x 1 km
- Processing mode: Daytime only

Scientific Data Set (SDS): " <i>Cloud_Mask_1km</i> "			
Description: Cloud mask QA flags at 1x1 km			
Length: 2 bytes (16 bits)			
Flag Name	Number of Bits	Bit Value	Bit Value Definitions
Cloud Mask Status Flag	1	0	Undetermined ^{n.f}
		1	Determined
Cloud Mask Cloudiness Flag	2	0	Confident Cloudy (or Fill, if Status Flag = 0)
		1	Probably Cloudy
		2	Probably Clear
		3	Confident Clear
Day / Night Flag	1	0	Night ^{n.f} (or Fill, if Status Flag = 0)
		1	Day
Sunglint Flag	1	0	Yes (or Fill, if Status Flag = 0)
		1	No
Snow / Ice Flag	1	0	Yes (or Fill, if Status Flag = 0)
		1	No
Surface Type Flag	2	0	Ocean or Deep Lakes and Rivers (or Fill)
		1	Coast or Shallow Lakes and Rivers
		2	Desert
		3	Land
Heavy Aerosol Flag	1	0	Yes ^{n.f} (or Fill, if Status Flag = 0)
		1	No
Thin Cirrus Flag (<i>Based on low threshold using 1.38 μm band.</i>)	1	0	Yes (or Fill, if Status Flag = 0)
		1	No
Shadow Flag	1	0	Yes ^{n.f} (or Fill, if Status Flag = 0)
		1	No
Spares	5		TBD

APPENDIX D. CLOUD MODEL LUT SCATTERING PROPERTIES

The following six tables give the scattering properties (g , ω_0 , Q_e) for the liquid water and ice cloud models used in Collection 6. Values are shown as a function of the Look-up Table (LUT) effective radii grid points and the MODIS bands directly used in the optical retrieval algorithm. Band numbers correspond to the following nominal central wavelengths (CWL): All table values are available in the MOD06 file. The corresponding Science Data Sets (SDS) for each liquid water and ice parameter is given below.

MODIS Band No.	1	2	5	6	7	20	31
CWL (μm)	0.66	0.87	1.24	1.64	2.13	3.75	11.03

Liquid Water LUT Asymmetry Parameter (SDS: *Asymmetry_Parameter_Liq*)

Note: For liquid water retrievals, MOD06 only provides successful retrievals for $\text{CER} \geq 4 \mu\text{m}$.

Band/ CER (μm)	1	2	5	6	7	20	31
2	0.805	0.785	0.767	0.808	0.850	0.800	0.423
4	0.838	0.827	0.804	0.783	0.790	0.793	0.753
5	0.845	0.836	0.820	0.802	0.789	0.768	0.817
6	0.850	0.843	0.830	0.817	0.802	0.755	0.856
7	0.854	0.848	0.836	0.827	0.815	0.758	0.882
8	0.857	0.852	0.841	0.834	0.827	0.771	0.901
9	0.860	0.854	0.845	0.839	0.835	0.785	0.914
10	0.862	0.857	0.849	0.844	0.842	0.799	0.924
12	0.865	0.861	0.854	0.850	0.851	0.821	0.938
14	0.867	0.864	0.858	0.855	0.858	0.835	0.947
16	0.869	0.866	0.861	0.859	0.863	0.846	0.953
18	0.871	0.868	0.863	0.862	0.867	0.854	0.958
20	0.872	0.869	0.865	0.864	0.870	0.861	0.961
22	0.873	0.871	0.867	0.867	0.873	0.867	0.964
24	0.874	0.872	0.868	0.869	0.876	0.873	0.966
26	0.875	0.873	0.870	0.870	0.878	0.878	0.968
28	0.875	0.873	0.871	0.872	0.881	0.882	0.969
30	0.876	0.874	0.872	0.873	0.883	0.886	0.970

Liquid Water LUT Single Scattering Albedo (SDS: *Single_Scatter_Albedo_Liq*)

Band/ CER (μm)	1	2	5	6	7	20	31
2	1.000	1.000	1.000	0.999	0.996	0.979	0.152
4	1.000	1.000	1.000	0.998	0.991	0.967	0.295
5	1.000	1.000	0.999	0.997	0.988	0.954	0.345
6	1.000	1.000	0.999	0.996	0.986	0.941	0.384
7	1.000	1.000	0.999	0.996	0.983	0.928	0.415
8	1.000	1.000	0.999	0.995	0.981	0.918	0.439
9	1.000	1.000	0.999	0.994	0.979	0.909	0.458
10	1.000	1.000	0.999	0.994	0.976	0.900	0.473
12	1.000	1.000	0.999	0.993	0.972	0.885	0.494
14	1.000	1.000	0.998	0.992	0.968	0.871	0.506
16	1.000	1.000	0.998	0.991	0.964	0.857	0.513
18	1.000	1.000	0.998	0.990	0.960	0.845	0.516
20	1.000	1.000	0.998	0.989	0.956	0.833	0.516
22	1.000	1.000	0.998	0.988	0.953	0.821	0.515
24	1.000	1.000	0.998	0.987	0.949	0.810	0.513
26	1.000	1.000	0.997	0.986	0.945	0.799	0.511
28	1.000	1.000	0.997	0.985	0.941	0.789	0.508
30	1.000	1.000	0.997	0.983	0.938	0.780	0.506

Liquid Water LUT Extinction Efficiency (SDS: *Extinction_Efficiency_Liq*)

Band/ CER (μm)	1	2	5	6	7	20	31
2	2.291	2.403	2.531	2.977	3.252	2.587	0.375
4	2.187	2.225	2.302	2.359	2.521	3.163	0.770
5	2.160	2.194	2.257	2.310	2.374	2.825	0.966
6	2.142	2.172	2.225	2.275	2.324	2.575	1.150
7	2.128	2.155	2.202	2.246	2.296	2.449	1.319
8	2.116	2.141	2.184	2.224	2.271	2.392	1.471
9	2.107	2.131	2.169	2.205	2.250	2.361	1.607
10	2.100	2.121	2.157	2.191	2.231	2.338	1.725
12	2.089	2.107	2.138	2.168	2.203	2.301	1.916
14	2.080	2.096	2.125	2.150	2.181	2.270	2.052
16	2.073	2.088	2.114	2.137	2.165	2.245	2.145
18	2.067	2.081	2.105	2.126	2.152	2.225	2.205
20	2.063	2.076	2.098	2.118	2.141	2.209	2.240
22	2.059	2.071	2.092	2.110	2.132	2.195	2.259
24	2.056	2.067	2.086	2.104	2.124	2.184	2.266
26	2.053	2.064	2.082	2.098	2.118	2.174	2.266
28	2.050	2.061	2.078	2.093	2.112	2.165	2.261
30	2.048	2.058	2.074	2.089	2.107	2.158	2.254

Ice LUT Asymmetry Parameter (SDS: *Asymmetry_Parameter_Ice*)

Band/ CER (μm)	1	2	5	6	7	20	31
5	0.748	0.749	0.752	0.769	0.802	0.787	0.873
10	0.751	0.753	0.756	0.769	0.790	0.798	0.931
15	0.752	0.754	0.759	0.775	0.799	0.833	0.952
20	0.753	0.755	0.760	0.780	0.807	0.860	0.960
25	0.753	0.756	0.761	0.784	0.815	0.881	0.965
30	0.753	0.756	0.762	0.789	0.821	0.898	0.968
35	0.753	0.756	0.762	0.793	0.828	0.912	0.970
40	0.753	0.756	0.763	0.797	0.833	0.922	0.972
45	0.753	0.756	0.764	0.800	0.839	0.931	0.973
50	0.753	0.757	0.764	0.804	0.844	0.937	0.974
55	0.753	0.757	0.764	0.807	0.849	0.943	0.975
60	0.753	0.757	0.765	0.811	0.854	0.947	0.975

Ice LUT Single Scattering Albedo (SDS: *Single_Scatter_Albedo_Ice*)

Band/ CER (μm)	1	2	5	6	7	20	31
5	1.000	1.000	0.999	0.991	0.981	0.887	0.317
10	1.000	1.000	0.999	0.981	0.962	0.804	0.424
15	1.000	1.000	0.998	0.972	0.946	0.755	0.466
20	1.000	1.000	0.998	0.964	0.930	0.717	0.485
25	1.000	1.000	0.997	0.955	0.915	0.686	0.497
30	1.000	1.000	0.996	0.946	0.900	0.662	0.504
35	1.000	1.000	0.996	0.938	0.886	0.642	0.509
40	1.000	1.000	0.995	0.930	0.873	0.626	0.513
45	1.000	1.000	0.994	0.922	0.861	0.613	0.515
50	1.000	1.000	0.994	0.915	0.849	0.602	0.518
55	1.000	1.000	0.993	0.907	0.838	0.593	0.520
60	1.000	1.000	0.992	0.900	0.827	0.586	0.521

Ice LUT Extinction Efficiency (SDS: *Extinction_Efficiency_Ice*)

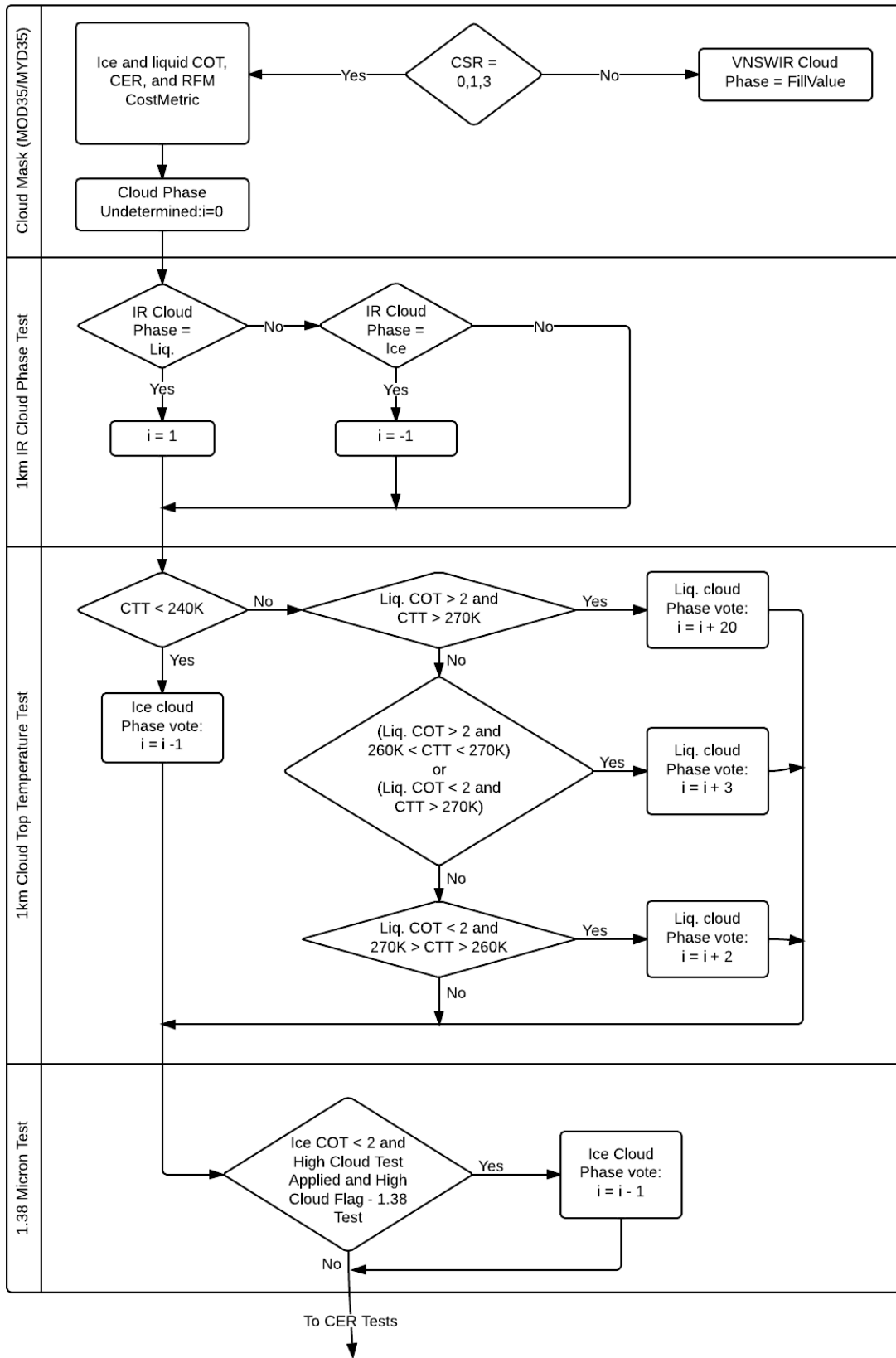
Band/ CER (μm)	1	2	5	6	7	20	31
5	2.109	2.138	2.162	2.170	2.198	2.399	1.219
10	2.065	2.086	2.107	2.128	2.100	2.199	1.601
15	2.048	2.066	2.080	2.098	2.081	2.168	1.750
20	2.039	2.054	2.065	2.080	2.067	2.141	1.819
25	2.032	2.044	2.055	2.067	2.057	2.120	1.860
30	2.027	2.038	2.048	2.058	2.049	2.105	1.885
35	2.024	2.033	2.043	2.051	2.044	2.094	1.902
40	2.021	2.029	2.038	2.046	2.039	2.085	1.913
45	2.019	2.026	2.035	2.042	2.036	2.078	1.922
50	2.017	2.024	2.032	2.039	2.033	2.072	1.929
55	2.015	2.022	2.029	2.036	2.030	2.067	1.934
60	2.014	2.020	2.027	2.034	2.028	2.062	1.939

APPENDIX E. CLOUD RETRIEVAL PHASE FLOW CHART

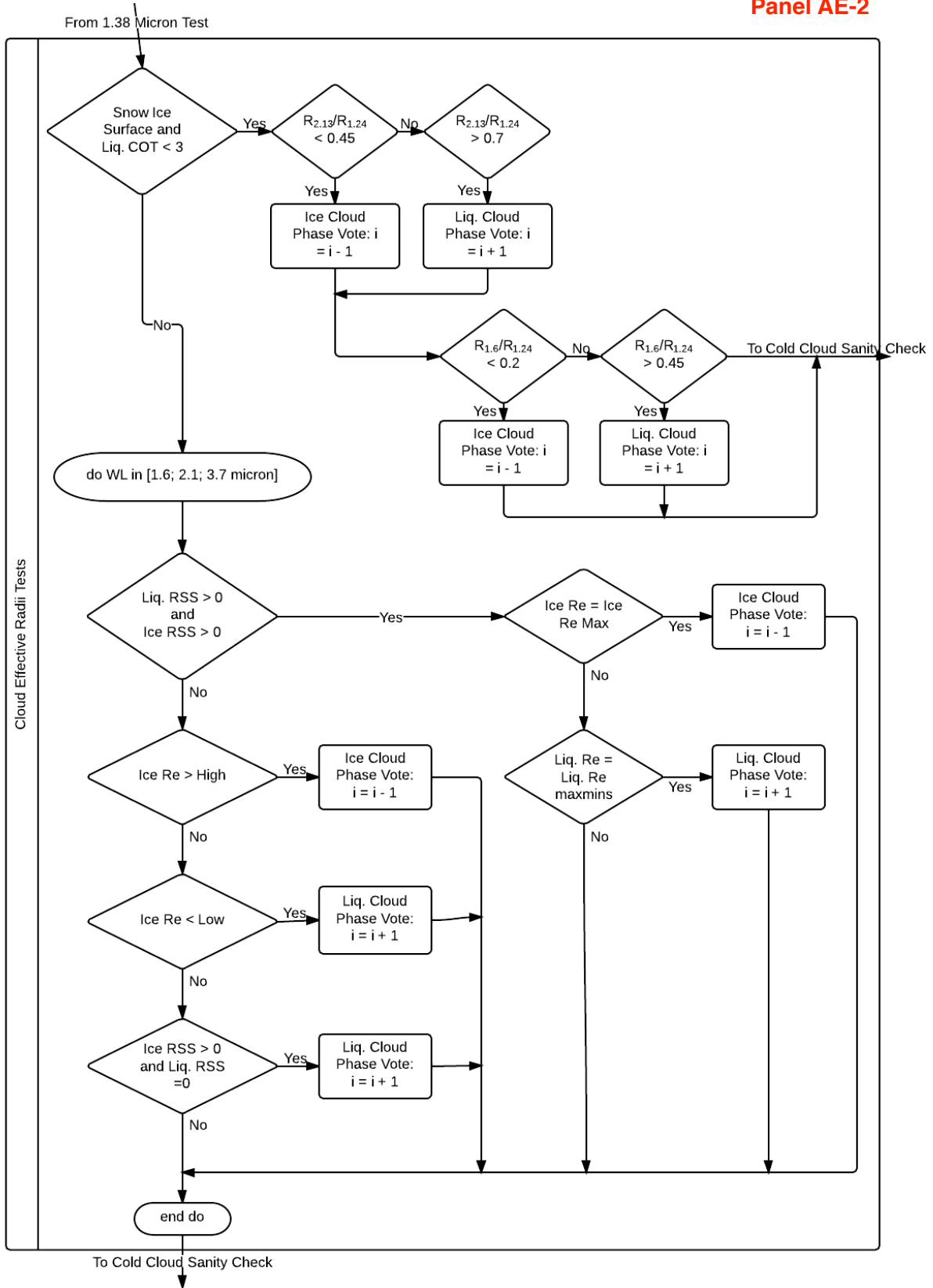
Here we summarize the MODIS C6 Cloud Retrieval Thermodynamic Phase discrimination logic flowchart (panels 1-3) and CER thresholds (panel 4) corresponding to the logic in panel 2. The new C6 phase algorithm uses a discrimination logic that includes several tests providing signed integer votes of different weights.

The four main categories of cloud phase test comprise the C6 phase algorithm (*Tri-Spectral IR Tests*, *Cloud Top Temperature Tests*, *1.38 μm Channel Test* and *Cloud Effective Radii Tests*) are shown to the left of each panel.

Panel AE-1

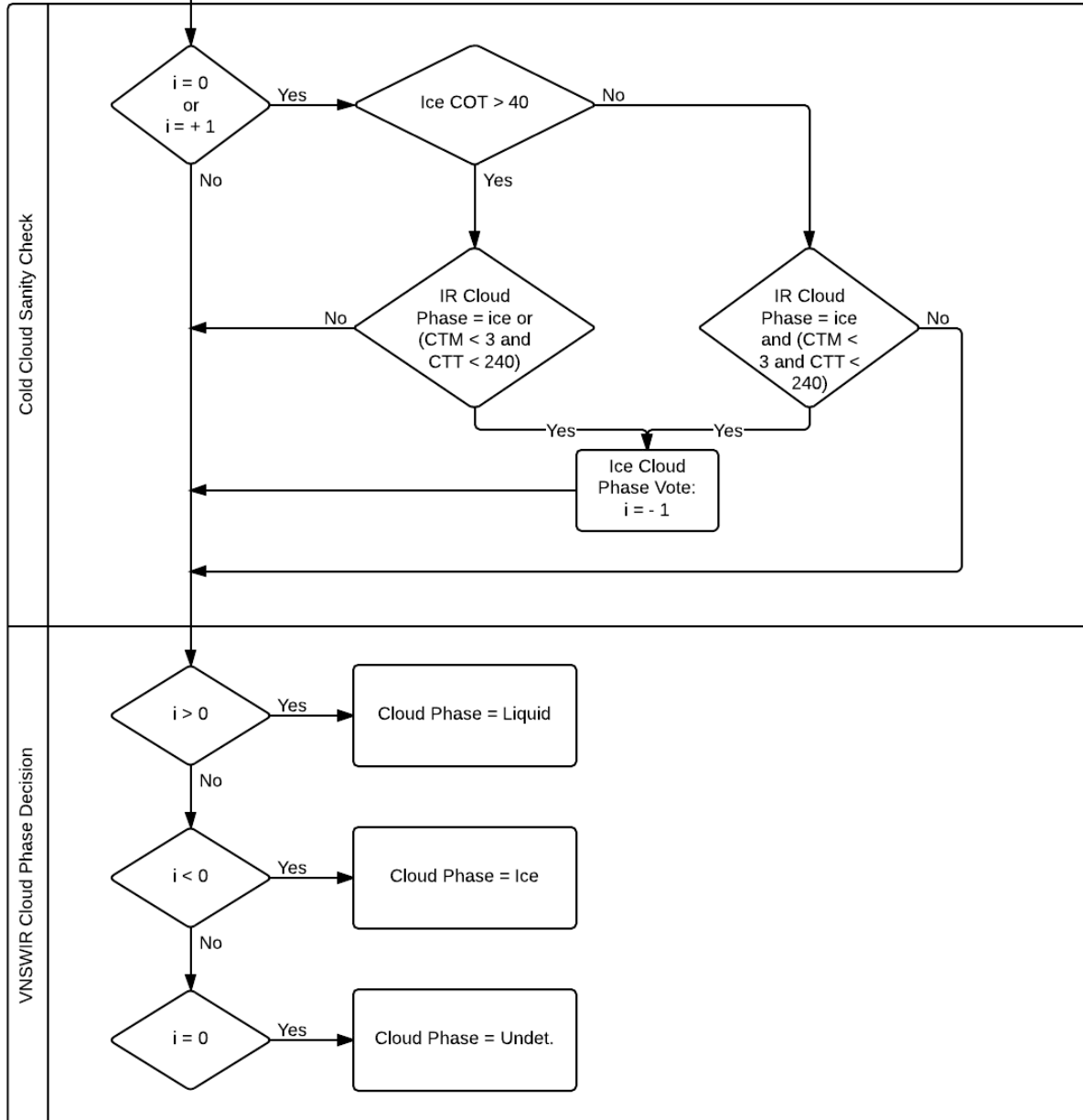


Panel AE-2



Panel AE-3

From Cloud Effective Radii Tests



Panel AE-4

MODIS Channel	CER Thresholds	SPI < 30	SPI ≥ 30
6 (1.6 μm)	Low	20 μm	20 μm
	High	30 μm	Max CER for Ice (CER > High => false???)
7 (2.1 μm)	Low	20 μm	20 μm
	High	30 μm	Max CER for Ice (CER > High => false???)
20 (3.7 μm)	Low	15 μm	15 μm
	High	25 μm	Max CER for Ice (CER > High => false???)

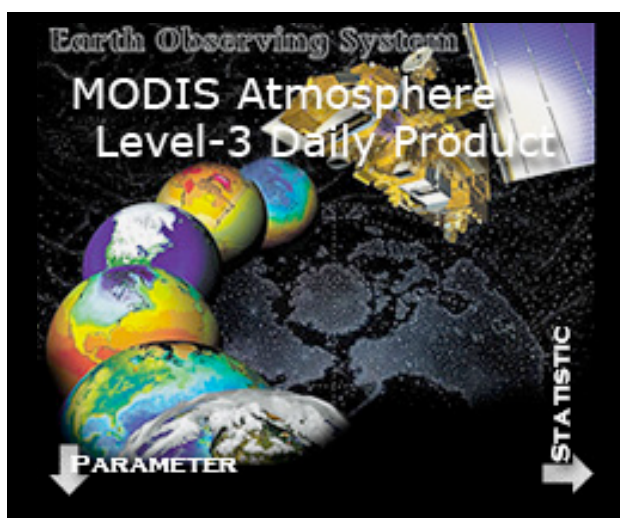
APPENDIX F. CLOUD OPTICAL/MICROPHYSICAL LEVEL-3 STATISTICS

A summary of the C6 L3 parameters cloud optical/microphysical statistical quantities is given here. A complete list of C6 Atmosphere Team L3 statistics is available on the team web site (modis-atmos.gsfc.nasa.gov/products_C006update.html). See Sect. 3 for further details.

L3 Daily Global (D3) Statistics

Collection 006 Updates (v2)

Green Shading = New Orange Shading = Changed "d" = D3 only



Mean	Standard_Deviation	Minimum	Maximum	Histogram_Counts (n)	Fraction	Pixel_Counts	Mean_Uncertainty	Log_Mean_Uncertainty	Log_Mean	Log_Standard_Deviation	JHisto_vs_Effect_Radius (nxn)	JHisto_vs_Effect_Radius_37 (nxn)	JHisto_vs_Temperature (nxn)	JHisto_vs_Emissivity (nxn)	JHisto_vs_Pressure (nxn)
------	--------------------	---------	---------	----------------------	----------	--------------	------------------	----------------------	----------	------------------------	-------------------------------	----------------------------------	-----------------------------	----------------------------	--------------------------

Cloud Optical Properties

(Primary 2.1 Retrieval)

01. Cloud_Optical_Thickness_Liquid	•	•	•	•	•			•	•	•	•			•	•
02. Cloud_Optical_Thickness_Ice	•	•	•	•	•			•	•	•	•			•	•
03. Cloud_Optical_Thickness_Undetermined	•	•	•	•						•	•				
04. Cloud_Optical_Thickness_Combined	•	•	•	•						•	•				
05. Cloud_Optical_Thickness_PCL_Liquid	•	•	•	•	•			•			•				
06. Cloud_Optical_Thickness_PCL_Ice	•	•	•	•	•			•			•				
07. Cloud_Optical_Thickness_PCL_Undetermined	•	•	•	•											
08. Cloud_Optical_Thickness_PCL_Combined	•	•	•	•											
09. Cloud_Optical_Thickness_ISCCP															•
10. Cloud_Optical_Thickness_PCL_ISCCP															•
11. Cloud_Effective_Radius_Liquid	•	•	•	•	•			•						•	•
12. Cloud_Effective_Radius_Ice	•	•	•	•	•			•						•	•
13. Cloud_Effective_Radius_Undetermined	•	•	•	•											
14. Cloud_Effective_Radius_PCL_Liquid	•	•	•	•				•							
15. Cloud_Effective_Radius_PCL_Ice	•	•	•	•				•							

APPENDIX G. SUMMARY OF HIGH-LEVEL MOD06 COLLECTION 6 EFFORTS

The following table provides a summary of the key Collection 6 MOD06 optical/microphysical algorithm development efforts. The symbol Δ denotes the main refinement activities that will continue with the proposed support; most of this work is detailed in the main body of the proposal text (see Sect. 3).

Category	Collection 5	Collection 6	Notes
Radiative Transfer			
Cloud Model: all phases	Combined discrete ordinate LUT (small COT) + asymptotic theory parameters (large COT)	Full reflectance, flux, and emissivity LUTs across retrieval space/geometry. LUT entries provided for multiple scattering component only; phase function provided in file for direct calculation of single scattering component.	<ul style="list-style-type: none"> • Single approach (LUT) => easier retrieval code maintenance. • LUT grid designed to limit median linear interpolation error to $\ll 1\%$. • Separation of single scattering component => fewer LUT grid points and interpolations during processing. • Required DISORT code mod to improve efficiency for BRDF-specified surfaces.
Δ Ice Cloud Model	Variable habit (smooth) vs. size/empirical distributions. Relatively large asymmetry parameter (g) and highly dependent on	Single habit (severely roughened aggregated columns) w/ analytic distribution (γ , $\nu_e=0.10$)	<ul style="list-style-type: none"> • Smaller g reduces COT & provides closure with non-opaque IR COT retrievals. • Nearly constant • SWIR/MWIR particle absorption decreases => larger retrieved
Surface Ancillary Datasets	Team-designed nominal seasonal gap-filled spectral albedo dataset using Terra C4 product MOD43.	New dynamic gap-filled spectral albedo dataset derived from Aqua+Terra C5 MCD43B3. Emissivity dataset from MOD06 CT product for spectral consistency.	<ul style="list-style-type: none"> • C6 albedo dataset provides higher temporal resolution than C5 (8 day interval, 16 day average). • Snow and Sea-ice spectral albedo dataset same as for C5.
Δ Incorporation of Model Error Sources	N/A	LUT includes sensitivity datasets for wind vector.	No explicit model error sources used in C5 uncertainty calculations.
Level-1 Analysis/Corrections			
Δ Band 1,2 trend detection/correction	N/A	COT monthly anomaly trend analysis	Used to justify MCST work with desert site response-vs-scan angle corrections.
Δ Aqua Band 1,2 250 m \Rightarrow 1 km aggregation	N/A	Used to improve known Aqua VNIR focal plane mis-registration w/SWIR, MWIR, and IR focal planes	Impacts Aqua COT and statistics in heterogeneous low cloud regions.

Category	Collection 5	Collection 6	Notes
Algorithm - Retrieval Science			
Retrieval channel pairs	r_e differences for VNIR-SWIR/MWIR channel pairs (relative to standard VNIR-2.1 μm).	Full retrievals reported separately for as many as 4 spectral channel pairs.	<ul style="list-style-type: none"> Doesn't filter alternate channel pair retrievals by success of standard retrieval. Allows for separate evaluation/aggregation of all channel pairs.
Cloud-Top (CT) Pressure/ Temperature	Used 5 km MOD06 CT product.	Uses new 1km MOD06 CT product. Incorporates non-unity cloud emissivity from optical retrieval into low cloud CT retrievals that use IR window channel.	
Δ Thermodynamic Phase	Used SWIR/VNIR ratio tests as a proxy for particle size that was then used to indicate phase.	SWIR/VNIR ratio tests replaced w/separate ice and liquid retrievals. Uses new tri-spectral IR phase product. Eliminated use of individual cloud mask tests. Weights applied to various tests in lieu of strict logical approach.	<ul style="list-style-type: none"> Algorithm tests/weights validated against CALIOP, POLDER products. Significant skill improvement seen for most regions (e.g., land, ocean, snow/ice) though still limited by available spectral bands.
Δ Misc.	N/A	Numerous science and code infrastructure performance improvements.	<ul style="list-style-type: none"> Improved processing efficiency. Easier code maintenance, porting to other sensors.
Algorithm - Pixel Quality Assessment (QA)/Filtering			
Δ Updated 'Clear Sky Restoral' (CSR) algorithm	N/A	Improve discrimination between heavy aerosol (smoke/dust) and glint from low uniform cloud population.	Added explicit aerosol model tests. Replaced height/phase discrimination test w/CT 'method' flags.
Pixels identified as not-overcast and/or cloudy FOV by CSR algorithm	Do not retrieve CSR-identified pixels	Attempt retrievals on CSR-identified pixels and, if successful, write results to separate dataset (SDS).	Separate SDS allows for analysis of CSR population w/out need to read/interpret QA assignments.
Failed Retrieval Metrics ('failure' defined as the simultaneous COT, missing outside of LUT space)	No failure metrics reported	The following metrics are reported: nearest COT, nearest 2D measurement point to nearest LUT solution point.	Allow users to understand failure mode (e.g., large small COT) for cloudy FOVs not meeting 1D fwd. model assumptions. Potentially useful for radiative studies, comparison with other observational datasets, and high resolution LES models.
Multilayer cloud detection	<i>Wind et al. [2010]</i>	Updated multilayer detection using additional tests from <i>Pavolonis and Heidinger (2004)</i> .	

Category	Collection 5	Collection 6	Notes
Retrieval Confidence QA	2-bit assignment	Not actively assigned. Superseded by pixel-level uncertainty SDS.	QA assignments confusing to users, lack of consistency across products. L3 users directed to "Uncertainty of Mean" SDS derived from pixel-level uncertainties.
Sub-pixel Heterogeneity	N/A	Bands 1 & 2 250 m reflectance heterogeneity included in MOD35 and MOD06 dataset.	Heterogeneity partial predictor for marine liquid water cloud spectral
Algorithm - Pixel Level Uncertainty			
Instrument Calibration	Combined with model error sources and fixed at 5% relative	Uses L1B scene-dependent pixel-level spectral uncertainty indices (improved for C6)	Reduces combined uncertainty in many cases.
^Δ Model Errors		See LUT above for details.	
^Δ 3. Error Sources	Not included	Accounts for effective cloud and surface emissivity and retrieved dependence on ancillary water vapor field.	More realistic (larger) 3.7 μm channel uncertainties.